UNIVERSITY OF CALGARY

Modelling, Simulation and Identification of Induction Machines in Continuous and Discrete Time

by

Juntao Pan

A THESIS

SUBMITTED TO THE FACULTY OF GRADUATE STUDIES

IN PARTIAL FULFILMENT OF THE REQUIREMENTS FOR THE

DEGREE OF MASTER OF SCIENCE

DEPARTMENT OF ELECTRICAL AND COMPUTER ENGINEERING

CALGARY, ALBERTA

January, 2004

UNIVERSITY OF CALGARY

FACULTY OF GRADUATE STUDIES

The undersigned certify that they have read, and recommend to the Faculty of Graduate Studies for acceptance, a thesis entitled "Modelling, Simulation and Identification of Induction Machines in Continuous and Discrete Time" submitted by Juntao Pan in partial fulfillment of the requirements for the degree of Master of Science.

Supervisor, Dr. D. Westwick
Department of Electrical and Computer Engineering

Co-supervisor, Dr. E.P. Nowicki
Department of Electrical and Computer Engineering

Dr. O.P. Malik
Department of Electrical and Computer Engineering

Dr. B. R. Young
Department of Chemical and Petroleum Engineering

21 JAN 04
Date

Abstract

Field orientation control, sometimes called vector control, is applied in the control of induction machines to obtain high performance dynamic responses. The key to field orientation control is knowing the instantaneous magnitude and direction of the rotor flux. The magnitude and direction of the rotor flux can either be measured directly with sensors in the direct field orientation control method or be estimated in the indirect field orientation control method. However the performance of the indirect field orientation control method is sensitive to variations in motor parameters such as the rotor resistance and the magnetizing inductance. Unfortunately motor parameters vary greatly with temperature, frequency and current amplitude.

In this thesis a novel method of using a subspace identification method to estimate the rotor flux directly is presented. Simulations of field orientation control with both open loop and closed loop control schemes are first carried out and the sensitivity of field orientation control to the variations in motor parameters is studied. Furthermore the saturation effect in induction machines is taken into consideration. All of the models of induction machines are discretized in order that the identification algorithms can be implemented with a digital signal processor. Finally a subspace identification method for linear parameter-varying (LPV) systems is used to identify the rotor flux of the induction machine. Positive results have been obtained, indicating the potential of the subspace identification method in field orientation control of induction machines.

Acknowledgments

The thesis would have been impossible without the assistance of many people. First I would like to thank Dr. E.P. Nowicki and Dr. David T. Westwick, my supervisors, for their constant support, advice and encouragement throughout the course of my study. Actually, they started providing support even before I came to Canada by sending me many helpful materials for this project. Under their guidance in research, I have learnt a lot, not only from their substantial academic concepts and wide knowledge in their areas, but from their personalities, their patience and understanding in the face of problems. I believe I will benefit from the experience for the rest of my life.

My gratitude should also be extended to Dr. Vincent Verdult. Without his generosity of sharing the toolbox of nonlinear system identification with me, it would take much longer time to complete this thesis. I also very much appreciate the help from Dr. Chris Macnab in obtaining discretized models and Ed Evanik who installed the motor drive in the lab.

I am deeply grateful to all the support staff in the department, the secretaries, the IT management team, for their excellent work to make this thesis happen. For those friends who helped in many ways, I also express my sincere gratitude.

Finally I would like to thank my wife, Sunny Xiao, for her tireless support and understanding through the challenges of this work.

To my parents
and
my beloved wife

Contents

List of Tables

List of Figures

List of Symbols

AC	Alternating Current
B'	magnetic flux density
CSI	Current Source Inverter
C_e, C_e^{-1}	Transformation from stationary two-phase d-q to synchronous frame $d^e - q^e$ and its inverse
DC	Direct Current
DSP	Digital Signal Processor
E_a	back emf
FOC	Field Orientation Control
H	magnetic field intensity
I_a	armature current of DC motor
I_m, I_s, I_r	steady state magnetizing current, stator current and rotor current
$\overline{I_M}$	magnetizing current phasor
$\overline{I_T}$	torque current phasor
$\overline{I}_s$	phasor of three-phase stator current
J_m	inertia coefficient
L	inductance
LPV	Linear Parameter-Varying
L_{ls}	stator leakage inductance
L_{lr}	rotor leakage inductance

L_m	mutual inductance
L_r	self rotor inductance
L_s	self stator inductance
MIMO	Multiple Input, Multiple Output
MOESP	MIMO Output-Error State Space
N	number of columns in a Hankel matrix
N_c	number of conductor turns
N_m	the number of samples of input and output
PEM	Prediction-Error Method
R_a	armature resistance
SMI	Subspace Model Identification
SVD	Singular Value Decomposition
T, T^{-1}	transformation from three-phase a-b-c to two-phase d-q and its inverse
V	armature terminal voltage of DC motor
VAF	Variance-Accounted-For
VSI	Voltage Source Inverter
V_m	measurement noise
U, u	input signal
Y, y	output signal without noise
Z	output signal with measurement noise
d	stationary direct axis
d^e	synchronous rotating direct axis

$e_{\omega d}$	rotor speed electromagnetic force of d-axis
$e_{\omega q}$	rotor speed electromagnetic force of q-axis
f_c	Coulomb friction coefficient
f_v	viscous friction coefficient
i_{as}, i_{bs}, i_{cs}	three-phase sinusoidal AC currents
i_{dr}	rotor current of d-axis
i_{ds}	stator current of d-axis
i'_{ds}, i'_{qs}	two-phase of sinusoidal AC current with a phase difference of 90 degrees
i_m	magnetizing current
i_{qr}	rotor current of q-axis
i_{qs}	stator current of q-axis
mmf	magnetomotive force
n	system order
p	differential operator
p'	pole pairs
q	stationary quadrature axis
q^e	synchronous rotating quadrature axis
r_r	rotor resistance
r_s	stator resistance
s	slip

t_c	friction torque
t_m	induction machine electromagnetic torque
t_r	load torque
v_{ds}	stator voltage of d-axis
v_{qs}	stator voltage of q-axis
x	state vector of state space model
δ	the angle of magnetizing current vector to the reference axis
ϕ	magnetic flux of one turn
ϕ_f	flux produced by the field winding
ζ	time-varying parameter vector
λ	flux linkage
λ_a	air gap flux linkage
λ_{ds}	stator flux linkage of d-axis
λ_{dr}	rotor flux linkage of d-axis
λ_m	magnetizing flux linkage
λ_{qr}	rotor flux linkage of q-axis
λ_{qs}	stator flux linkage of q-axis
μ	core permeability
μ_0	permeability of air
τ_r	induction machine rotor time constant

ω_r	angular velocity of rotor
ω_s	synchronous frame angular velocity
ω_{sl}	slip angular velocity
$\backslash$	pseudo inverse operation in MATLAB
$\otimes$	Kronecker product
$\odot$	Khatri-Rao product

Chapter 1

Introduction

1.1 Induction Motor

Energy is an important concept in an economic context. The mean energy consumption per capita in a country is an indicator of its state of technical development [24]. Electricity is a common form of energy due to its relatively efficient generation, low-loss transportation and flexible conversion into a final form.

Among the possible final forms of energy, mechanical energy is of the most importance. It is estimated that about 60% of the electricity generated in an industrial country is eventually converted to mechanical energy [24]. Electric drives play an important role in the conversion of electricity into mechanical energy. One of the most common types of industrial drives is the induction motor drive.

The induction motor has many advantages in comparison with other electric motors, e.g. cost, robustness, maintenance freedom, power density, and hence has wide application in industry. The induction motor was, and is, widely used in installations where no speed regulation is required since it was once difficult to adjust the speed of an induction motor. DC machine drives dominated variable speed drive applications for many decades. With research and development of semiconductor power devices and intensive research work in variable speed AC drives, the performance of the induction motor in variable speed applications has improved rapidly. With the development of field orientation control in the early 70s, the performance of induction motor drives became comparable to, or even better, than that of DC machine drives [6].

1.2 Field Orientation Control

The reason that DC motors have high performance in motion control is that a separately excited DC motor permits the separate control of torque and flux. The linearity of the system makes a DC motor easier to control than an AC motor. However, the mechanical commutation of the DC machine causes higher failure rates, even with frequent maintenance. Furthermore, commutation sparks constrain a DC motor from being applied in hazardous environments or in high power applications (i.e. megawatt level). In order to improve the performance of an induction motor in motion control, a principle, similar to that of separate excitation, was applied to induction motor control and is referred to as field orientation control [6].

Field orientation control, sometimes called vector control, is based on a vector transformation from a stationary reference frame to a rotating reference frame and vice versa when necessary. As its name implies, the principle of field orientation control is to establish a synchronous reference frame such that the d-axis (i.e. direct axis) coincides with the orientation of the total rotor flux linkage of the machine. In this frame, stator currents are decoupled into two orthogonal components: the torque component along the q-axis (i.e. quadrature axis) and the flux component along the d-axis. This decoupling permits the direct control of shaft torque while keeping the flux magnitude constant. In other words, the induction motor can be controlled like a separately excited DC motor. The key to the implementation of field orientation control is how to obtain the information about the instantaneous direction of the rotor flux vector. In general, there are two generic approaches. The first one is to utilize direct sensing of the air gap flux by the use of Hall probes, search coils or other measurement devices [29]. This technique is accurate and insensitive to variations in motor parameters. However it is expensive, intrusive and introduces sensor reliability issues. The second method is an indirect approach where the rotor flux is estimated from stator currents, stator voltages and/or rotor velocity. This approach uses a parameter model of the induction machine to predict the rotor flux with the available measurements and is therefore sensitive to variations in motor parameters such as the rotor resistance and the magnetizing inductance. Unfortunately motor parameters vary greatly with temperature, frequency and current amplitude. Therefore in order to achieve the same performance as the direct method, motor parameters must be estimated accurately and instantaneously.

1.3 System Identification

A system model can be determined from physical principles or by system identification or by a combination of these approaches. System identification has the virtue of being nearly instantaneous in some cases. According to the definition of Zadeh, system identification is the determination, on the basis of input and output, of a model within a specified class of models, to which the system under test is equivalent [9].

Referring to Fig. 1.1, system identification is the process of determining the model of the target system, the structure, order, and the corresponding parameters, from measurements of the inputs, *U,* and outputs, *Z,* of the system, where the outputs, *Z,* are often contaminated by measurement noise, V_m. However if the structure of the model is well known, for example our system is an induction motor, what is needed might be to estimate some parameters within the model, which is called parameter estimation. According to Eykhoff [9], parameter estimation is defined as the experimental determination of values of parameters that govern dynamic and/or non-linear behavior, assuming that the structure of the process model is known. In this thesis, a subspace identification method is applied to estimate the values of rotor flux directly in order to obtain better performance from an induction machine in motion control applications.

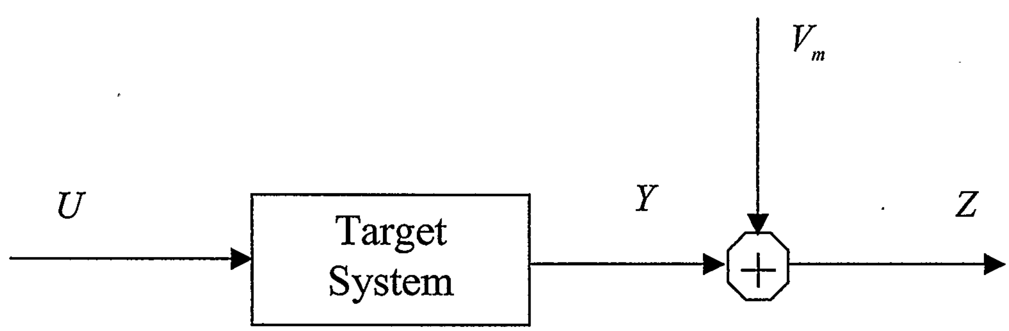

Fig. 1.1 Concept of System Identification

1.4 Thesis Organization

This thesis is composed of eight chapters that present the identification of an induction machine so that the performance of field orientation control can be improved by reducing the impact of machine parameter variation. Chapter 2 is dedicated to the introduction of the induction machine models that are going to be used in this thesis. The model taking saturation into consideration is presented to introduce even more non-linearity into the induction machine model.

In Chapter 3 the basic concepts of field orientation control of an induction machine are explained, including the two axes d-q theory, matrix transformations and field orientation control principles. The influences of variations of primary parameters will be discussed in Chapter 6.

In Chapter 4, the fundamental concepts of system identification are introduced and an identification method for a linear parameter-varying (LPV) model is presented.

In order to apply the identification algorithms in the simulation of an induction machine, the model should be discretized to accelerate the simulation and to facilitate final implementation (e.g. using a microcontroller). What is discussed in Chapter 5 is the discretization of induction machine models, both with and without saturation. Discretization of an LPV system is also discussed.

In Chapter 6, computer simulations of a 1 kW induction machine are developed. The results of simulating different models of induction machines are compared to theoretical calculations to validate the models. Field orientation controllers are incorporated into the simulations.

Chapter 7 discusses the several steps that we employed for identification of rotor flux. The corresponding identification results are presented and explained.

Discussions and a conclusion are provided in Chapter 8 together with requirements for future work. The contributions of this thesis are also discussed in Chapter 8.

Chapter 2

Mathematical Models of an Induction Machine

In this chapter, some fundamentals of induction machines are first introduced such as torque generation and the effects of saturation. Then mathematical models, both with and without saturation effects, are described. Although these models include nonlinear terms, the nonlinearities can be represented by an appropriate choice of time-varying linear terms. Therefore a special linear parameter-varying model is presented to describe induction machines. Since identification methods for linear parameter-varying models are available, it makes good preparation for the identification of induction machine dynamics.

2.1 Elementary Induction Machines

When three-phase alternating current is supplied directly to the stator in a two-pole induction machine, a rotating magnetic field of the same frequency is established. By induction, i.e. transformer action, AC voltages are induced in the rotor along with alternating currents. With the interaction between the rotating magnetic field and currents in the rotor, electromagnetic torque is produced in the rotor, thus providing torque to the load that may be connected to the rotor shaft. Depending on the load torque, the shaft rotates at a frequency that is slightly less than the rotation frequency of the magnetic field. This frequency difference is referred to as the slip frequency. The frequency of the voltages and currents induced in the rotor windings is the slip frequency. If an induction machine has more than two poles, the magnetic field rotates at a frequency equal to the three-phase frequency divided by the number of pole pairs.

There are two basic types of rotors used in induction machines. A wound rotor carries a polyphase winding similar to, and wound with the same number of poles, as the stator. The terminals of the rotor winding are connected to insulated slip rings mounted on the shaft. Carbon brushes that contact these rings make the rotor terminals available external to the machine. Another, much more commonly used, kind of rotor is called the squirrel-cage rotor. It has a winding consisting of conducting bars embedded in slots in the rotor iron and short-circuited at each end by conducting rings. Since induction motors with squirrel-cage rotors have many outstanding advantages, such as extreme simplicity and ruggedness, they are extensively used in industry [11]. Therefore we chose this kind of induction machine as the object of our research.

2.2 Saturation in Induction Machines

The stator and rotor of an induction machine are composed largely of high-permeability magnetic material that is normally called the core. The core is excited by a winding carrying current to produce a magnetic field in it. Since the stator and rotor cores have a much larger permeability, μ, than that of surrounding air, μ_0, the magnetic flux is confined almost entirely to the core materials and the air gap between the stator and rotor.

As a current is applied to the stator winding, a corresponding magnetic field intensity, H, is generated. The relationship between the magnetic field intensity, H, and magnetic flux density, B', is a property of the material in which the field exists, and may be approximated by

$$B' = \mu \mathrm{H} \tag{2-1}$$

where μ is the permeability. The magnetic flux, ϕ, crossing a surface, S, is the surface integral of the normal component of B', given by

$$\phi = \int_S B' da \tag{2-2}$$

Therefore through the use of magnetic materials with high permeability, it is possible to obtain large magnetic flux densities with relatively low levels of magnetizing force. Since magnetic forces and energy densities increase with increasing flux density, this effect plays a large role in the performance of energy conversion devices like induction machines.

Ferromagnetic materials are the most common magnetic materials used by far in the construction of induction machines [11]. They are composed of a large number of magnetic domains. When the material is not magnetized, the domain magnetic moments are randomly oriented and the net resulting magnetic flux in the material is zero. When an external magnetizing force is applied to the material, the domain magnetic moments tend to align with the applied magnetic field. Thus the dipole magnetic moments add to the applied field, resulting in a much larger value of flux density than would exist from the magnetizing force alone. The larger the applied field is, the more magnetic moments are aligned with the applied field. Eventually all of them become aligned, at which point they cannot contribute to increasing the magnetic flux density any further and the material is said to be saturated.

Due to saturation, the effective permeability, μ, which is equal to ratio of magnetic flux density to the applied magnetizing force, is not linear with respect to the applied magnetizing force, H. A typical $B'-H$ curve for a magnetic material is shown in Fig. 2-1. Notice that with increasing magnetic field intensity, *H,* the curve begins to flatten out as the material becomes magnetically saturated.

When saturation is taken into account, the inductance *L*, which is defined as

$$L = \frac{\lambda}{i} \tag{2-3}$$

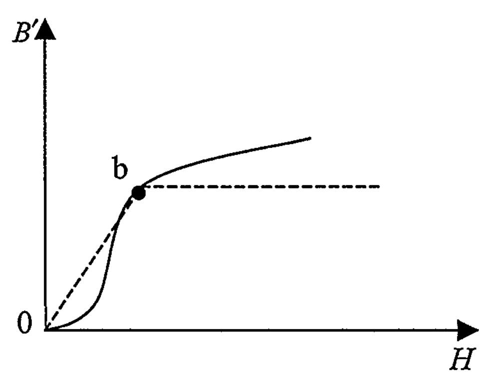

Fig. 2-1 $B'-H$ curve for a magnetic material; B' is the magnetic flux density and *H* is the magnetic field intensity, also referred to as the magnetizing force.

is no longer constant due to the nonlinear dependence of flux density on the magnetic conditions in the core. Note that λ is referred to as flux linkage and is defined as

$$\lambda = N_c \phi \tag{2-4}$$

where N_c is the number of conductor turns.

In other words, to the right of the point marked b in Fig. 2-1, the magnetic flux will not increase with the increasing current i at the same rate as it does to the left of the point b. However the effects of the nonlinear magnetic characteristics of the core material can often be approximated by some sort of empirical linear relation, yielding solutions of acceptable engineering accuracy. When the induction machine is working below point b in Fig. 2-1, L is considered to be constant. Beyond point b, L will vary as the current increases, so that the magnetic flux linkage, λ, no longer increases linearly. Note that an induction machine operating under rated conditions has values of B' and H corresponding to point b, i.e., at the "knee" of the $B'-H$ curve.

In this thesis, the $B'-H$ curve is approximated by the dashed line in Fig. 2-1 in order to take saturation into account in a relatively simple manner.

2.3 Mathematical Model of an Induction Machine without Saturation

For an induction machine with a balanced three-phase supply, the two axis or d-q, theory [15] is normally used for dynamic modeling. According to this theory, variables and parameters are expressed in orthogonal direct (d) and quadrature (q) axis components. The d-q axis representation of an induction machine is shown in Fig. 2-2.

In the induction machine representation of Fig. 2-2, the stator and rotor are abstracted into symmetrical windings d_s, q_s and d_r, q_r. The d-q axes are fixed on the stator. Since

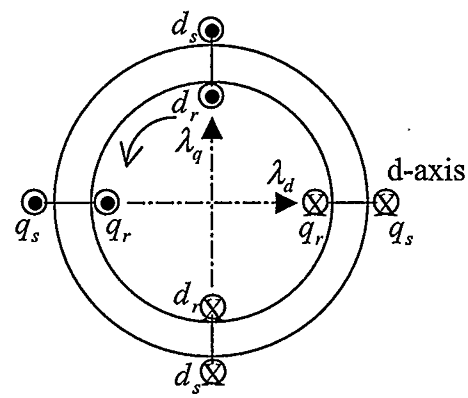

Fig. 2-2 Induction machine in d-q axis representation

the rotor currents are rotating synchronously relative to the d-q axes, they are pseudo static currents.

In Fig. 2-2, λ_d , λ_q are the magnetic flux linkages linking the d and q axis windings respectively. The positive directions of flux linkage, current and electromagnetic force are indicated by the arrows. The angular velocity of the rotor is denoted by ω_r, where counter-clockwise rotation corresponds to a positive value of ω_r.

The mathematical model of a squirrel cage induction machine can be expressed in differential equations as follows [32]

$$v_{ds} = i_{ds} r_s + p\lambda_{ds} \tag{2-5}$$

$$v_{qs} = i_{qs} r_s + p\lambda_{qs} \tag{2-6}$$

$$0 = i_{dr} r_r + p\lambda_{dr} + e_{\omega d} \quad (2\text{-}7)$$

$$0 = i_{qr} r_r + p\lambda_{qr} + e_{\omega q} \quad (2\text{-}8)$$

where v_{ds} - d-axis component of stator voltage

v_{qs} - q-axis component of stator voltage

r_s - stator resistance

r_r - rotor resistance

p - differential operator

i_{ds} - d-axis component of stator current

i_{qs} - q-axis component of stator current

λ_{ds} - d-axis component of stator flux linkage

λ_{qs} - q-axis component of stator flux linkage

i_{dr} - d-axis component of rotor current

i_{qr} - q-axis component of rotor current

λ_{dr} - d-axis component rotor of flux linkage

λ_{qr} - q-axis component rotor of flux linkage

$e_{\omega d}$ - d-axis component of rotor velocity electromagnetic force

$e_{\omega q}$ - q-axis component of rotor velocity electromagnetic force

The speed electromotive force, i.e. the induced voltage, can be expressed as

$$e_{\omega d} = \omega_r \lambda_{qr} \quad (2\text{-}9)$$

$$e_{\omega q} = -\omega_r \lambda_{dr} \tag{2-10}$$

The flux linkages can be expressed in terms of inductances and currents as

$$\lambda_{ds} = L_s i_{ds} + L_m i_{dr} \tag{2-11}$$

$$\lambda_{qs} = L_s i_{qs} + L_m i_{qr} \tag{2-12}$$

$$\lambda_{dr} = L_m i_{ds} + L_r i_{dr} \tag{2-13}$$

$$\lambda_{qr} = L_m i_{qs} + L_r i_{qr} \tag{2-14}$$

where L_s - self stator inductance

L_r - self rotor inductance

L_m - mutual inductance

$$L_s = L_{ls} + L_m \tag{2-15}$$

$$L_r = L_{lr} + L_m \tag{2-16}$$

where L_{ls} - stator leakage inductance

L_{lr} - rotor leakage inductance

Substituting (2-9) to (2-14) into (2-5) to (2-8) yields a mathematical model of the induction machine that may be expressed in matrix form as

$$\begin{bmatrix} v_{ds} \\ v_{qs} \\ 0 \\ 0 \end{bmatrix} = \begin{bmatrix} r_s + L_s p & 0 & L_m p & 0 \\ 0 & r_s + L_s p & 0 & L_m p \\ L_m p & \omega L_m & r_r + L_r p & \omega_r L_r \\ -\omega L_m & L_m p & -\omega_r L_r & r_r + L_r p \end{bmatrix} \begin{bmatrix} i_{ds} \\ i_{qs} \\ i_{dr} \\ i_{qr} \end{bmatrix} \tag{2-17}$$

Note that if L_m, L_s and L_r are kept constant then saturation is neglected in this model.

If rotor flux linkages λ_{dr} and λ_{qr} are used as the states to replace the rotor current i_{dr} and i_{qr}, the mathematical model becomes [2]

$$\begin{bmatrix} v_{ds} \\ v_{qs} \\ 0 \\ 0 \end{bmatrix} = \begin{bmatrix} r_s + \frac{L_m^2 r_r}{L_r^2} + (L_s - \frac{L_m^2}{L_r})p & 0 & -\frac{L_m}{L_r \tau_r} & -\frac{L_m \omega_r}{L_r} \\ 0 & r_s + \frac{L_m^2 r_r}{L_r^2} + (L_s - \frac{L_m^2}{L_r})p & \frac{L_m \omega_r}{L_r} & -\frac{L_m}{L_r \tau_r} \\ -\frac{L_m}{\tau_r} & 0 & \frac{1}{\tau_r} + p & \omega_r \\ 0 & -\frac{L_m}{\tau_r} & -\omega_r & \frac{1}{\tau_r} + p \end{bmatrix} \begin{bmatrix} i_{ds} \\ i_{qs} \\ \lambda_{dr} \\ \lambda_{qr} \end{bmatrix} \qquad (2\text{-}18)$$

where $\tau_r = \frac{L_r}{r_r}$ is the rotor time constant of the induction machine

The mechanical equation may be expressed as

$$\dot{\omega}_r = -\frac{\omega_r}{\tau_m} + b_m(t_m - t_r - t_c) \qquad (2\text{-}19)$$

where the dot denotes the differential operation (ie $\dot{\omega}_r = p\omega_r$)

$$\tau_m = \frac{J_m}{f_v} \qquad (2\text{-}20)$$

J_m - inertia coefficient, Nms^2

f_v - viscous friction coefficient, Nms

$$b_m = \frac{p'}{J_m} \qquad (2\text{-}21)$$

p' - pole pairs

$$t_m = \tfrac{3}{2} p' \frac{L_m}{L_r}(i_{qs}\lambda_{dr} - i_{ds}\lambda_{qr}) \text{ - motor torque} \qquad (2\text{-}22)$$

$$t_c = f_c \operatorname{sgn}(\omega) \text{ - friction torque, } N.m \tag{2-23}$$

f_c - Coulomb friction coefficient, Nm

t_r - load torque, $N.m$

Equation (2-19) is typically what is employed by machine designers and researchers for torque considerations. In some analyses, one or more of the friction terms may be neglected. We will employ (2-18) with and without saturation as well as (2-19) neglecting the friction torque and taking no load torque into consideration.

2.4 Mathematical Model of an Induction Machine with Saturation

In the mathematical model of section 2.3, linear magnetic conditions are assumed. When saturation of the main flux path is taken into account, this assumption is no longer valid. The effects of saturation on the performance of electrical machines have been discussed in many papers in the literature [5,10,12,34,35,36,37,38,40]. The importance of saturation and of the existence of the intersaturation effect, sometimes called cross-saturation, have been presented [41]. The cross-saturation effect involves saturation in one axis affecting saturation in the other and vice versa, so that the saturation effects introduce coupling terms between the two axes [7]. Due to cross-saturation, some parameters in the mathematical model of an induction machine have to be modified and additional terms introduced. For example the stator (and rotor) self-inductances in orthogonal axes are no longer equal. In this thesis, the generalized equations of the induction machine in [25] are used to take cross-saturation into account. Here is the starting model in [7]

$$\begin{bmatrix} v_{ds} \\ v_{qs} \\ 0 \\ 0 \end{bmatrix} = \begin{bmatrix} r_s + L_{ds}p & L_{2s}p & (L_o + L_{2c})p & L_{2s}p \\ L_{2s}p & r_s + L_{qs}p & L_{2s}p & (L_o - L_{2c})p \\ (L_o + L_{2c})p & L_{2s}p + \omega_r L_m & r_r + L_{dr}p & L_{2s}p + \omega_r L_r \\ L_{2s}p - \omega_r L_m & (L_o - L_{2c})p & L_{2s}p - \omega_r L_r & r_r + L_{qr}p \end{bmatrix} \begin{bmatrix} i_{ds} \\ i_{qs} \\ i_{dr} \\ i_{qr} \end{bmatrix} \tag{2-24}$$

where $$L_o = (L + L_m)/2 \tag{2-25}$$

$$L_2 = (L - L_m)/2 \tag{2-26}$$

$$L_{2c} = L_2 \cos 2\delta \tag{2-27}$$

$$L_{2s} = L_2 \sin 2\delta \tag{2-28}$$

$$L = \frac{d|\lambda_m|}{d|i_m|} \tag{2-29}$$

$$L_m = \frac{\lambda_m}{i_m} \tag{2-30}$$

$$\lambda_m = L_m i_m \text{ - magnetizing flux linkage} \tag{2-31}$$

$$i_m = i_s + i_r \text{ - magnetizing current} \tag{2-32}$$

$$L_{ds} = L_{ls} + (L_o + L_{2c}) \tag{2-33}$$

$$L_{qs} = L_{ls} + (L_o - L_{2c}) \tag{2-34}$$

δ - the angle of magnetizing current vector to the reference axis

Note that L is a dynamic inductance while L_m is a static inductance and the equations given above are in a static reference frame fixed on the stator.

In this saturated model of the induction machine, the currents are chosen as the state variables in order that the cross-saturation effect can be fully explained both physically and mathematically. In order to integrate the saturated model into the model presented in the previous section, rotor currents should be replaced by rotor fluxes. A unified main flux saturation model in d-q axis form of induction machines can be found in [25]. The model with stator currents and rotor fluxes as the state variables is as below [25]

$$[v_{dq}] = [A]\frac{d[x_{dq}]}{dt} + [B][x_{dq}] \tag{2-35}$$

where
$$[v_{dq}] = [v_{ds} \quad v_{qs} \quad 0 \quad 0]^T \tag{2-36}$$

$$[x_{dq}] = [i_{ds} \quad i_{qs} \quad \lambda_{dr} \quad \lambda_{qr}]^T \tag{2-37}$$

$$[A] = \begin{bmatrix} L_l - \frac{L_{lr}^2}{L_{dd}} & -\frac{L_{lr}^2}{L_{dq}} & 1-\frac{L_{lr}}{L_{dd}} & -\frac{L_{lr}}{L_{dq}} \\ -\frac{L_{lr}^2}{L_{dq}} & L_l - \frac{L_{lr}^2}{L_{qq}} & -\frac{L_{lr}}{L_{dq}} & 1-\frac{L_{lr}}{L_{qq}} \\ 0 & 0 & 1 & 0 \\ 0 & 0 & 0 & 1 \end{bmatrix} \tag{2-38}$$

$$[B] = \begin{bmatrix} r_s & 0 & 0 & 0 \\ 0 & r_s & 0 & 0 \\ -r_r\frac{L_m}{L_r} & 0 & \frac{r_r}{L_r} & \omega_r \\ 0 & -r_r\frac{L_m}{L_r} & -\omega_r & \frac{r_r}{L_r} \end{bmatrix} \tag{2-39}$$

where
$$L_l = L_{ls} + L_{lr} \tag{2-40}$$

$$(\frac{1}{L_{dd}}) = (\frac{1}{\Lambda'})\cos^2\delta + (\frac{1}{\Lambda})\sin^2\delta \tag{2-41}$$

$$(\frac{1}{L_{qq}}) = (\frac{1}{\Lambda})\cos^2\delta + (\frac{1}{\Lambda'})\sin^2\delta \tag{2-42}$$

$$(\frac{1}{L_{dq}}) = (\frac{1}{\Lambda'} - \frac{1}{\Lambda})\cos\delta\sin\delta \tag{2-43}$$

$$\cos\delta = \frac{\lambda_d}{\lambda} \tag{2-44}$$

$$\sin\delta = \frac{\lambda_q}{\lambda} \tag{2-45}$$

$$\lambda = \lambda_r + L_{lr} i_s \tag{2-46}$$

$$\lambda_d = \lambda_{dr} + L_{lr} i_{ds} = (L_{lr} + L_m) i_{dm} \tag{2-47}$$

$$\lambda_q = \lambda_{qr} + L_{lr} i_{qs} = (L_{lr} + L_m) i_{qm} \tag{2-48}$$

$$\Lambda = \frac{\lambda}{i_m} = L_{lr} + L_m \tag{2-49}$$

$$\Lambda' = \frac{d\lambda}{di_m} = L_{lr} + L \tag{2-50}$$

Note that equations (2-29) and (2-30) are still applied in this model. In the derivation of the two saturated models, it is assumed that saturation affects only the main flux path. Therefore leakage fluxes L_{ls} and L_{lr} are constant in this case. Actually these two saturated models are equivalent. The proof of the equivalence is presented in Appendix A.

2.5 Bilinear Model of Induction Machines

A bilinear state-space system representation is a nonlinear extension of a linear system. In this system the evolution of the state does not only depend on the input and state, but also on the product between the input and state [42]. With this extension a bilinear system is more general than a linear system while less complex than general nonlinear systems, and is thus relatively easy to analyze.

In simulations of an induction machine, the rotor velocity is normally taken as one of the state variables. Therefore combining equations (2-18) and (2-19) and rearranging, we can obtain the induction machine model as below

$$\begin{bmatrix} \dot{i}_{ds} \\ \dot{i}_{qs} \\ \dot{\lambda}_{dr} \\ \dot{\lambda}_{qr} \\ \dot{\omega}_r \end{bmatrix} = \begin{bmatrix} -\frac{r_s + \frac{L_m^2}{L_r} r_r}{L_s - \frac{L_m^2}{L_r}} & 0 & \frac{\frac{L_m}{L_r \tau_r}}{L_s - \frac{L_m^2}{L_r}} & 0 & 0 \\ 0 & -\frac{r_s + \frac{L_m^2}{L_r} r_r}{L_s - \frac{L_m^2}{L_r}} & 0 & \frac{\frac{L_m}{L_r \tau_r}}{L_s - \frac{L_m^2}{L_r}} & 0 \\ \frac{L_m}{\tau_r} & 0 & -\frac{1}{\tau_r} & 0 & 0 \\ 0 & \frac{L_m}{\tau_r} & 0 & -\frac{1}{\tau_r} & 0 \\ 0 & 0 & 0 & 0 & -\frac{1}{\tau_m} \end{bmatrix} \begin{bmatrix} i_{ds} \\ i_{qs} \\ \lambda_{dr} \\ \lambda_{qr} \\ \omega_r \end{bmatrix} + \begin{bmatrix} \frac{1}{L_s - \frac{L_m^2}{L_r}} & 0 \\ 0 & \frac{1}{L_s - \frac{L_m^2}{L_r}} \\ 0 & 0 \\ 0 & 0 \\ 0 & 0 \end{bmatrix} \begin{bmatrix} v_{ds} \\ v_{qs} \end{bmatrix} +$$

$$\begin{bmatrix} \frac{\frac{L_m}{L_r} \omega_r \lambda_{qr}}{L_s - \frac{L_m^2}{L_r}} \\ -\frac{\frac{L_m}{L_r} \omega_r \lambda_{dr}}{L_s - \frac{L_m^2}{L_r}} \\ -\omega_r \lambda_{qr} \\ \omega_r \lambda_{dr} \\ \frac{3}{2} p' b_m \frac{L_m}{L_r} (i_{qs} \lambda_{dr} - i_{ds} \lambda_{qr}) - b_m t_c \end{bmatrix}. \tag{2-51}$$

This model structure can be expressed as follows

$$\dot{x} = Ax + F(x \otimes x) + Bu \tag{2-52}$$

$$y = Cx + Du \tag{2-53}$$

where $\otimes$ denotes the Kronecker product whose definition will be presented in Chapter 4, $x \in IR^n$ is the state, $u \in IR^m$ is the input including two stator voltages in d-q axes and $y \in IR^l$ is the output.

However we do not have an identification technology for this structure. Therefore the rotor velocity will be regarded as an input variable during the identification of the induction machine model, although it cannot be changed independently of other inputs. It is still practical since the rotor speed can be measured and stored for a period of time for the purpose of identification.

The induction model (2-18) can then be changed into this form as follows by taking the rotor velocity as one of the input variables

$$\begin{bmatrix} \dot{i}_{ds} \\ \dot{i}_{qs} \\ \dot{\lambda}_{dr} \\ \dot{\lambda}_{qr} \end{bmatrix} = \begin{bmatrix} -\frac{r_s + \frac{L_m^2}{L_r} r_r}{L_s - \frac{L_m^2}{L_r}} & 0 & \frac{\frac{L_m}{L_r \tau_r}}{L_s - \frac{L_m^2}{L_r}} & 0 \\ 0 & -\frac{r_s + \frac{L_m^2}{L_r} r_r}{L_s - \frac{L_m^2}{L_r}} & 0 & \frac{\frac{L_m}{L_r \tau_r}}{L_s - \frac{L_m^2}{L_r}} \\ \frac{L_m}{\tau_r} & 0 & -\frac{1}{\tau_r} & 0 \\ 0 & \frac{L_m}{\tau_r} & 0 & -\frac{1}{\tau_r} \end{bmatrix} \begin{bmatrix} i_{ds} \\ i_{qs} \\ \lambda_{dr} \\ \lambda_{qr} \end{bmatrix} + \begin{bmatrix} \frac{1}{L_s - \frac{L_m^2}{L_r}} & 0 \\ 0 & \frac{1}{L_s - \frac{L_m^2}{L_r}} \\ 0 & 0 \\ 0 & 0 \end{bmatrix} \begin{bmatrix} v_{ds} \\ v_{qs} \end{bmatrix} +$$

$$\begin{bmatrix} \frac{\frac{L_m}{L_r} \omega_r \lambda_{qr}}{L_s - \frac{L_m^2}{L_r}} \\ -\frac{\frac{L_m}{L_r} \omega_r \lambda_{dr}}{L_s - \frac{L_m^2}{L_r}} \\ -\omega_r \lambda_{qr} \\ \omega_r \lambda_{dr} \end{bmatrix} \qquad (2\text{-}54)$$

By studying the model representation of the induction machine above, we can determine that bilinear models can be applied to represent the induction machine quite well if rotor velocity is taken as one input. Therefore the induction machine model can be described as a continuous-time bilinear system, expressed by the following two equations

$$\dot{x} = Ax + F(u \otimes x) + Bu \tag{2-55}$$

$$y = Cx + Du \tag{2-56}$$

With thorough investigation of the induction machine model, we can show that the only non-linear term in the time derivative of the state contains the product of rotor velocity and the state. To simplify the analysis even further, linear parameter-varying (LPV) models [42] are applied to obtain simpler representation of the induction machine.

The general LPV system can be represented as

$$\dot{x} = A_0 x + [A_1, A_2, \ldots, A_s](\zeta \otimes x) + B_0 u + [B_1, B_2, \ldots, B_s](\zeta \otimes u) \tag{2-57}$$

$$y = Cx + Du \tag{2-58}$$

where $\zeta \in IR^s$ is the time-varying parameter vector.

The general LPV system can be easily modified to represent an induction machine model by setting

$$A = A_0$$

$$B = B_0$$

$$[A_1, A_2, \ldots, A_s] = F$$

$$[B_1, B_2, \ldots, B_s] = 0$$

$$\zeta = \omega_r$$

Then equations (2-57) and (2-58) become

$$\dot{x} = Ax + F\omega_r x + Bu \tag{2-59}$$

$$y = Cx + Du \tag{2-60}$$

2.6 Chapter Summary

In this chapter, induction machine models with and without saturation are reviewed from the literature [2, 25] and implemented in this project, while the LPV model of induction machines is developed in this thesis. In Chapter 5, these models are discretized for identification purposes and to assist implementation in the vector control of an induction machine using a microprocessor.

Chapter 3

Analysis of Field Orientation Control

In this chapter we give an overview of field orientation control, including the principles of vector transformation, descriptions of the characteristics of field orientation control in both steady state and under transient conditions and two basic methods of implementing field orientation control. The advantages and disadvantages of the two implementations are presented and discussed. Especially the prime disadvantage of the indirect method, namely sensitivity to parameter variation, which provides the motivation of this thesis, is discussed.

3.1 DC Machine Torque Control

Before discussing field orientation control in an induction machine, it is worthwhile to first discuss the torque control principle used in DC machines. Indeed before field orientation control theory was established by Blaschke in the 1970s [6], DC machines dominated electromechanical systems requiring fast response and four quadrant operation with good performance near zero speed [1]. DC machines have a proportional relationship between the armature current and shaft torque providing a direct means of achieving torque control.

A DC machine consists of a stationary field structure and a rotating armature winding supplied through a commutator and brushes. The commutator is used to reverse the direction of the armature winding currents as the coils pass the brush position so that the armature current distribution is roughly fixed in space for any rotor position.

Fig. 3.1 shows the steady state armature equivalent circuit and the spatial representation of field and armature currents. V is the armature terminal voltage and R_a is the armature resistance. As illustrated in Fig. 3.1, the field flux and armature magnetomotive force (mmf) are always in a mutually perpendicular orientation. This ensures that the field flux

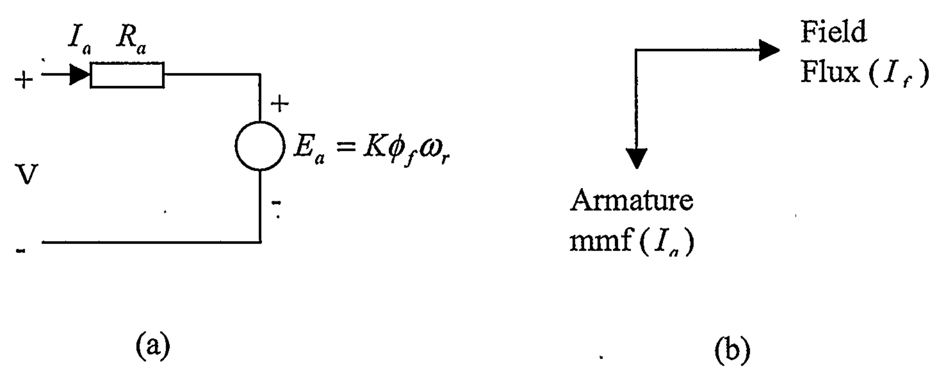

Figure 3.1 DC machine model;
(a) armature model (b) spatial current representation

is basically unaffected by the armature current. Two results come from the electromagnetic interaction between the field flux and the armature mmf. One is an induced voltage proportional to rotor velocity, given by

$$E_a = K_v\phi_f\omega_r \tag{3-1}$$

Another is an electromagnetic torque proportional to the armature current given by

$$T_e = K_t\phi_f I_a \tag{3-2}$$

In mks units, the proportionality constants are equal, i.e., $K_v = K_t = K$. E_a is the emf; ϕ_f is the flux produced by the field winding located in the stator; ω_r is the angular velocity of the rotor and I_a is armature current. The speed is normally adjusted by maintaining a fixed field flux while varying the armature voltage. Normally, adjustable torque operation in the DC machine can be obtained by controlling the armature current since with a constant field flux, the torque is almost directly proportional to armature current. A feedback current regulator is usually used to accomplish the torque adjustment. Hence the torque is proportional to the current reference.

In the DC machine, the separate field excitation system ensures a constant value of the field flux and the commutator ensures the orthogonal spatial angle between the flux and the armature MMF. That makes torque control in a DC machine relatively easy. For induction machines, it is much more complex to achieve both a constant field flux and an orthogonal spatial angle between the flux and armature MMF. Thus the control mechanisms are more difficult to understand than these in a DC motor.

3.2 Vector Transformation in Induction Machine Torque Control

3.2.1 Principle of vector transformation for induction machine field orientation control

Neglecting friction terms, the basic electromechanical motion equation followed by all rotational electromechanical systems is

$$t_m - t_r = J_m \dot{\omega} \tag{3-3}$$

where t_m is the electromagnetic torque

t_r is the load torque

J_m is the inertia coefficient

$\dot{\omega}$ is the angular acceleration

From the above equation, we can see that controlling the dynamic performance of a system requires controlling the dynamic torque of that system ($t_m - t_r$). In cases where the characteristics of t_r are known, the problem becomes controlling electromagnetic torque t_m.

The electromagnetic torque of an induction machine is

$$t_m = K_t \lambda_a I_r \cos\varphi_r \tag{3-4}$$

where K_t is the torque constant

λ_a is the air gap flux linkage

I_r is the rotor current

$\cos\varphi_r$ is the power factor of rotor circuit

Since the air gap flux linkage is generated by the excitation current

$$I_m = I_s + I_r \tag{3-5}$$

where I_s is the stator current

I_r is the rotor current transformed to stator circuit

λ_a is not independent of I_r. Therefore these two variables cannot be controlled independently. Moreover both the air gap flux linkage, λ_a, and the rotor current, I_r, are generated essentially by the stator. That means two variables have to be controlled within a single control loop. In this case, the two control processes influence each other, causing system oscillation or lengthening dynamic response time. In addition, stator currents can be denoted by time vectors while the air gap flux linkage is a rotating space vector. Since a vector has both magnitude and angle components, both must be controlled. In order to improve the dynamic performance of an induction machine, it is useful to transform the controlled variables from vectors to scalars first. Then the same method of torque control used in a DC motor can be applied to control torque in an induction machine. Among the principles of an induction machine, the generation of rotating flux linkage is the most important. Thus any transformation of stator currents has to be based on such a condition that it generates an identical rotating flux linkage. The three phase stator windings of an induction machine can be abstracted into static a-b-c coordinates. Applying three-phase sinusoidal AC currents distributed symmetrically in time, i_{as}, i_{bs} and i_{cs}, we can obtain a rotating flux linkage with the same angular velocity as the AC currents $\omega_s = 2\pi f_s$, displayed in Figure 3.2 (a), (d).

Similarly two-phase stator windings d and q, with a phase difference of 90 degree in space, can also be abstracted into static d-q coordinates, applying two phases of sinusoidal AC current with a phase difference of 90 degrees, i.e., i'_{ds}, i'_{qs}, to generate a rotating flux linkage as in Figure 3.2 (b), (e). If the two sets of windings generate exactly the same rotating flux linkages λ, they can be called equivalent windings.

In Figure 3.2 (c), (f), two orthogonal windings M and T are supplied with DC currents I_{Ms}, I_{Ts} respectively, so that they generate a flux linkage, λ_s, that is static relative to the windings. If the windings M and T rotate at the synchronous velocity $\omega_s = 2\pi f_s$, then the flux linkage λ_s will also rotate at the synchronous velocity. The windings M and T are normally abstracted to the M-T coordinate system. As long as λ_s is the same as λ, the rotating DC windings M-T are equivalent to the static AC windings.

In terms of generating the rotating flux linkage, the three sets of windings in Figure 3.2 are equivalent. Therefore there must be a relationship between the AC currents i_{as}, i_{bs}, i_{cs} and i'_{ds}, i'_{qs} and DC currents I_{Ms}, I_{Ts} so that they all generate the same rotating

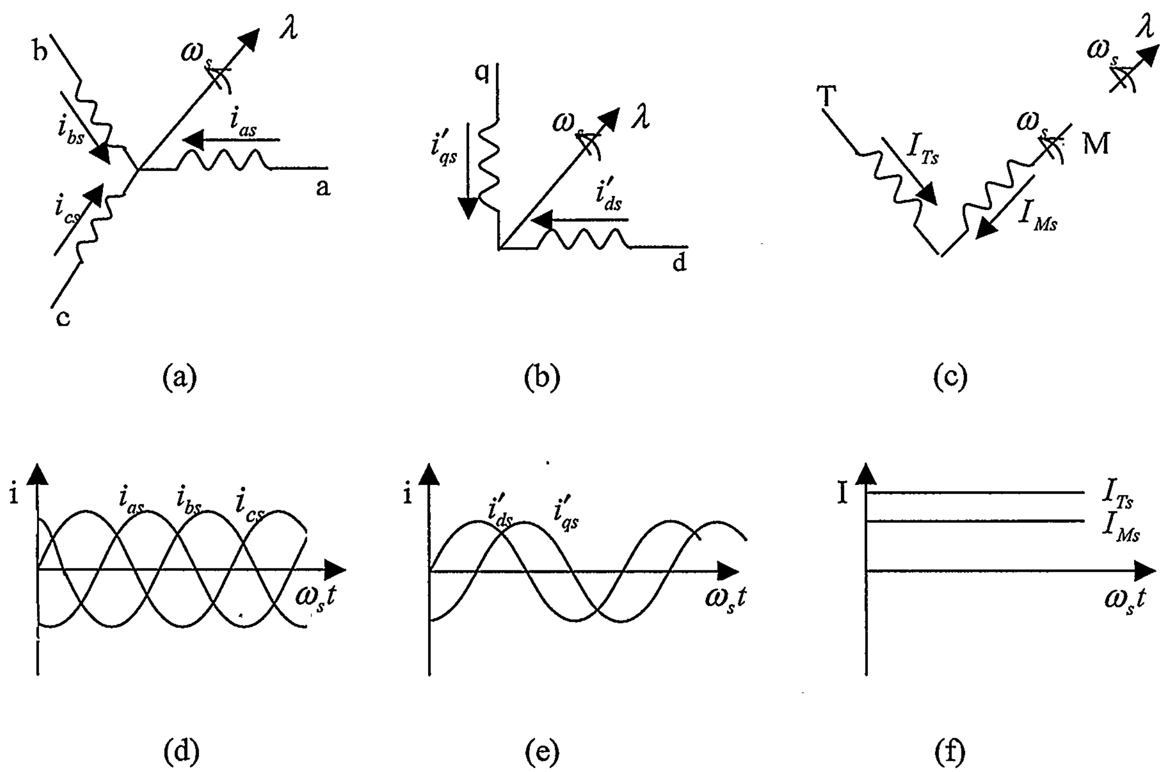

Figure 3.2 static 3-phase AC, static 2-phase AC and rotating DC equivalent windings

flux linkage. The relationship is called the vector transformation. In other words, for a given i_{as}, i_{bs}, i_{cs}, there must be a corresponding i'_{ds}, i'_{qs} and an I_{Ms}, I_{Ts} that all generate the same rotating flux linkage and vice versa. Hence I_{Ms}, I_{Ts} can be controlled completely through i_{as}, i_{bs}, i_{cs}.

In Figure 3.2 (c), the flux linkage λ_s is generated only by the current I_{Ms} in M-T coordinates if we align the direction of λ_s with the M-axis of the M-T coordinate system. I_{Ts} is only responsible for the generation of electromagnetic torque. Therefore in M-T coordinates, the induction machine is made equivalent to the DC motor where the M winding acts as the excitation winding in the DC motor and the T winding acts as the armature winding. The control of electromagnetic torque can be achieved by controlling the equivalent scalars, i.e. DC currents I_{Ms}, I_{Ts} through the vector transformation from i_{as}, i_{bs}, i_{cs}. In order to complete the transformation from i_{as}, i_{bs}, i_{cs} to I_{Ms}, I_{Ts} for control purposes and further to transform the adjusted I_{Ms}, I_{Ts} back to i_{as}, i_{bs}, i_{cs} to drive the induction machine, a coordinate transformation of vector quantities and the corresponding inverse transformation have to be utilized. That is why this kind of control system is called vector control. Normally in the coordinate transformation, the direction of rotor flux linkage, λ_r, is used as the M-axis of the rotating M-T coordinate system. In this coordinate system, equivalent stator currents comprise two orthogonal DC currents. One is the excitation current, I_{Ms}, aligned with the direction of rotor flux linkage, λ_r.

The other is the torque current, I_{Ts}, perpendicular to I_{Ms}. Hence this control method is also called field-orientation vector control or simply vector control.

3.2.2 Coordinate Transformation

As indicated in section 2.3, the d-q axes, or two-axis, theory is normally used for dynamic modeling and analysis of an induction machine with a balanced three-phase supply. Actually all the models presented in Chapter 2 are based on the d-q axis theory. In this theory, variables and parameters are expressed in orthogonal axes with direct (d) and quadrature (q) components in either stationary or rotating reference frames. In the stationary reference frame the d-q axes are fixed on the stator and denoted as d and q respectively. For rotating cases, normally the speed is chosen the same as the rotor magnetic field to transform the AC variables in the stationary reference into DC ones (for steady state) and thus simplify the model of the induction machine. This synchronous rotating reference frame is the same as the M-T coordinates presented in section 3.2.1. In this frame, d-q axes are commonly denoted by d^e and q^e.

In this section, the principles of coordinate transformation are presented, including the transformation from three-phase coordinates, a-b-c, to two-phase coordinates, d-q, which are stationary with respect to the a-b-c system and the transformation from stationary d-q coordinates to synchronous rotating d-q coordinates, d^e, q^e.

3.2.3 Transformations between different coordinates

The phasor (time-vector) diagrams of the three-phase and two-phase systems are shown in Fig. 3.3, while the space vector diagrams and windings are shown in Fig. 3.4

According to the principle of rotating magnetic field generation in induction machines, the phase sequences of the a-b-c and d-q currents should be *a, b, c* and *d, q* respectively as in Fig. 3.3 if counterclockwise rotating magnetic fields are to be established, i.e. from winding *a* to *b* in Fig.3.4 (a) and from winding *d* to *q* in Fig. 3.4 (b).

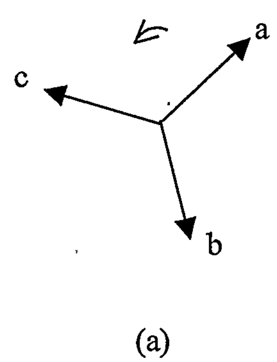

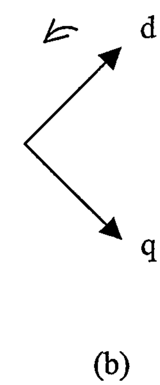

Fig. 3.3 (a) Three-phase (b) two-phase phasor diagrams

Let the a-phase winding axis be coincident with the d-phase winding axis as in Fig. 3.4. The principle of variable transformation is illustrated further in Fig. 3.5. Assuming that axes a and d have zero initial inclination when $t = 0$, the mathematical transformation for stator currents between three-phase coordinates a-b-c and the d-q two-phase frame fixed on the stator is given by

$$I_{dqs} = T\, I_{abcs} \tag{3-6}$$

Where

$$I_{dqs} = [i_{ds}, i_{qs}]^T$$

$$I_{abcs} = [i_{as}, i_{bs}, i_{cs}]^T$$

$$T = \tfrac{2}{3}\begin{bmatrix} 1 & \cos(\tfrac{2\pi}{3}) & \cos(\tfrac{4\pi}{3}) \\ 0 & \sin(\tfrac{2\pi}{3}) & \sin(\tfrac{4\pi}{3}) \end{bmatrix} \tag{3-7}$$

or conversely

$$I_{abcs} = T^{-1} I_{dqs} \tag{3-8}$$

where

$$T^{-1} = \begin{bmatrix} 1 & 0 \\ \cos(\tfrac{2\pi}{3}) & \sin(\tfrac{2\pi}{3}) \\ \cos(\tfrac{4\pi}{3}) & \sin(\tfrac{4\pi}{3}) \end{bmatrix} \tag{3-9}$$

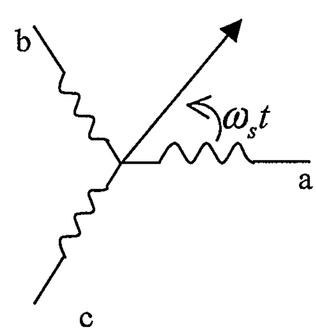

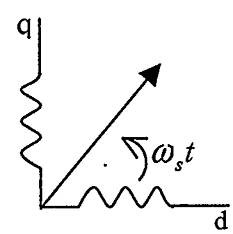

Fig. 3.4 (a) Three-phase (b) two-phase space vector diagrams

Transformation from stationary two-phase d-q to synchronous frame $d^e - q^e$

The transformation between the d-q frame and $d^e - q^e$ synchronous one is given by [48]

$$I_{dqs}^e = C_e I_{dqs} \tag{3-10}$$

where

$$I_{dqs}^e = [i_{ds}^e, i_{qs}^e]^T$$

$$I_{dqs} = [i_{ds}, i_{qs}]^T$$

$$C_e = \begin{bmatrix} \cos\varphi & \sin\varphi \\ -\sin\varphi & \cos\varphi \end{bmatrix} \tag{3-11}$$

or conversely

$$I_{dqs} = C_e^{-1} I_{dqs}^e \tag{3-12}$$

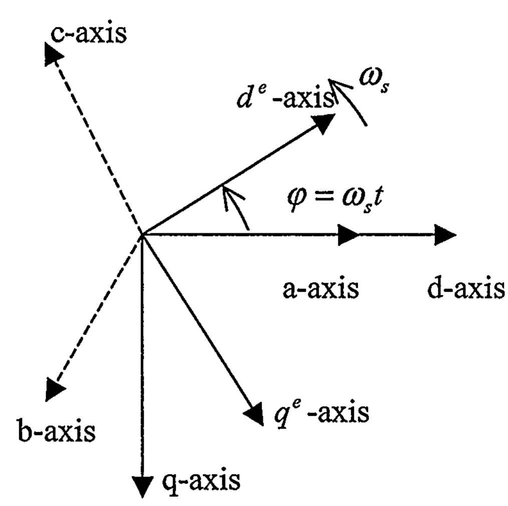

Fig. 3.5 The principle of variable transformations

where

$$C_e^{-1} = \begin{bmatrix} \cos\varphi & -\sin\varphi \\ \sin\varphi & \cos\varphi \end{bmatrix} \tag{3-13}$$

and φ is the instantaneous angle of the $d^e - axis$ with respect to the d-axis.

Therefore the most important aspect of the transformation from the stationary two-phase d-q to the synchronous frame, $d^e - q^e$, is to find the parameter φ. In field orientation control of induction machines discussed in the next section, φ is the direction of the rotor flux.

3.3 Field Orientation Control

3.3.1 Principle of Induction Machine Field Orientation Control

As stated previously, with the help of vector transformation from a stationary reference frame to a rotating reference frame, stator currents are decoupled into two orthogonal components: the torque component and the magnetizing component. Then the torque can be controlled in proportion to the torque component of the stator current while keeping the flux constant. The principle of field-orientation control of induction machines can be interpreted further by examining the equivalent circuit and phasor diagram, c.f. Fig. 3-6 and Fig. 3-7.

The three-phase stator current of an induction machine is represented by a phasor $\overline{I_s}$. It is decoupled into two orthogonal components: torque current $\overline{I_T}$ and magnetizing current

$\overline{I_M}$ as shown in the equivalent circuit in Fig. 3.6. In the equivalent circuit, $\overline{I_M}$ is transformed to the part of the stator current that is responsible for the generation of rotor flux. That is why there are some parameters in addition to the magnetizing inductance and rotor resistance.

For field orientation control of an induction machine, normally the magnetizing current $\overline{I_M}$ is maintained constant to keep the rotor flux constant. The torque current $\overline{I_T}$ is controlled according to the torque requirement. In the stator current phasor diagram in Fig. 3.7, $\overline{I_{s1}}$ corresponds to a small torque while $\overline{I_{s2}}$ corresponds to a large one.

As a consequence of the fact that the voltage across the magnetizing reactance and the voltage across the equivalent rotor resistance are equal (see Fig. 3.6), the following equation can be obtained.

$$\omega_s \frac{L_m^2}{L_r} I_M = \frac{L_m^2}{L_r^2} \frac{r_r}{s} I_T \tag{3-14}$$

where s is the slip

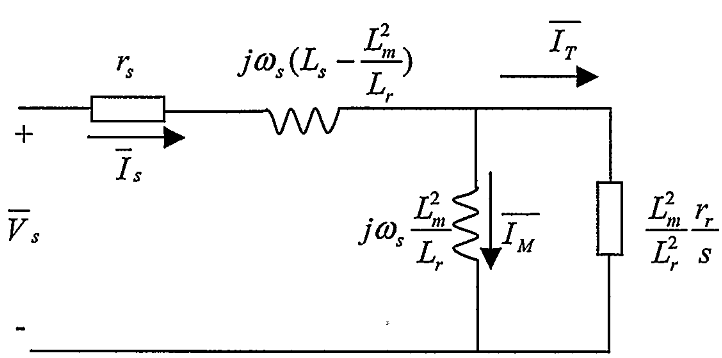

Fig. 3.6 Induction Machine Equivalent Circuit Without Rotor Leakage Flux

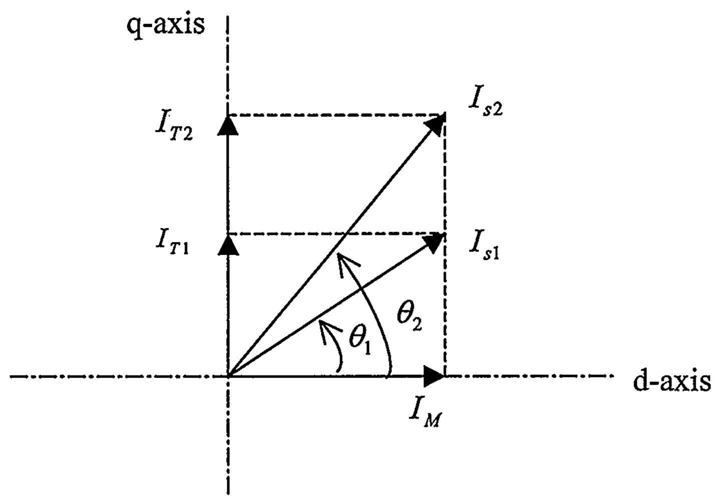

Fig. 3.7 Phasor Diagram Showing Torque and Magnetizing Components of Stator Current

Thus the slip angular frequency is

$$\omega_{sl} = s\omega_s = \frac{r_r I_T}{L_r I_M} \tag{3-15}$$

For an induction machine the stator current and the slip frequency determine the torque completely and the current components I_T and I_M specify both rotor flux and torque. Once I_T and I_M are chosen, the corresponding slip frequency is determined so as to yield the proper torque and flux. This is the basis of field orientation control of an induction machine and is discussed in more detail next.

The technique discussed above is a means of steady state control. The same concepts can also be applied for transient conditions. In order to analyze the transient conditions of an induction machine, a two-axis model in the synchronous reference frame rotating at a speed corresponding to the stator excitation frequency, ω_s, is obtained by the appropriate coordinate transformations, discussed in section 3.2, as follows. The superscript e is used to denote the variables in the synchronous reference frame [32].

$$v_{ds}^e = r_s i_{ds}^e + p\lambda_{ds}^e - \omega_s \lambda_{qs}^e \tag{3-16}$$

$$v_{qs}^e = r_s i_{qs}^e + p\lambda_{qs}^e + \omega_s \lambda_{ds}^e \tag{3-17}$$

$$0 = r_r i_{dr}^e + p\lambda_{dr}^e - \omega_{sl} \lambda_{qr}^e \tag{3-18}$$

$$0 = r_r i_{qr}^e + p\lambda_{qr}^e + \omega_{sl} \lambda_{dr}^e \tag{3-19}$$

$$\lambda_{ds}^e = L_s i_{ds}^e + L_m i_{dr}^e \tag{3-20}$$

$$\lambda_{qs}^e = L_s i_{qs}^e + L_m i_{qr}^e \tag{3-21}$$

$$\lambda_{dr}^e = L_m i_{ds}^e + L_r i_{dr}^e \tag{3-22}$$

$$\lambda_{qr}^e = L_m i_{qs}^e + L_r i_{qr}^e \tag{3-23}$$

$$t_m = \tfrac{3}{2} p' \frac{L_m}{L_r} (i_{qs}^e \lambda_{dr}^e - i_{ds}^e \lambda_{qr}^e) \tag{3-24}$$

In field orientation control of an induction machine, the stator currents should be oriented in phase and in quadrature with the rotor flux linkage. This is accomplished by choosing ω_s to be the instantaneous speed of the rotor flux linkage and fixing the phase of the reference system so that the rotor flux linkage is completely along the d-axis. As a result,

$$\lambda_{qr}^e = 0 \tag{3-25}$$

Applying (3-25) in (3-16) to (3-23), the following equations can be obtained for field orientation control of an induction machine in the synchronous reference frame

$$i_{ds}^{e} = \frac{(1+\tau_r p)\lambda_{dr}^{e}}{L_m} \tag{3-26}$$

$$i_{qs}^{e} = -\frac{L_r}{L_m} i_{qr}^{e} = \frac{\lambda_{dr}^{e}\tau_r}{L_m}\omega_{sl} \tag{3-27}$$

$$i_{dr}^{e} = -\frac{\lambda_{dr}^{e} p}{r_r} \tag{3-28}$$

$$i_{qr}^{e} = -\frac{\lambda_{dr}^{e}}{r_r}\omega_{sl} \tag{3-29}$$

$$t_m = \tfrac{3}{2} p \frac{L_m}{L_r} i_{qs}^{e} \lambda_{dr}^{e} \tag{3-30}$$

The slip angular frequency can be represented with the stator currents

$$\omega_{sl} = \frac{\tfrac{r_r}{L_r} L_m i_{qs}^{e}}{\lambda_{dr}^{e}} = \frac{1+\tau_r p}{\tau_r}\frac{i_{qs}^{e}}{i_{ds}^{e}} \tag{3-31}$$

Based on these equations, the torque production in field orientation control of induction machine is illustrated in Fig. 3.8.

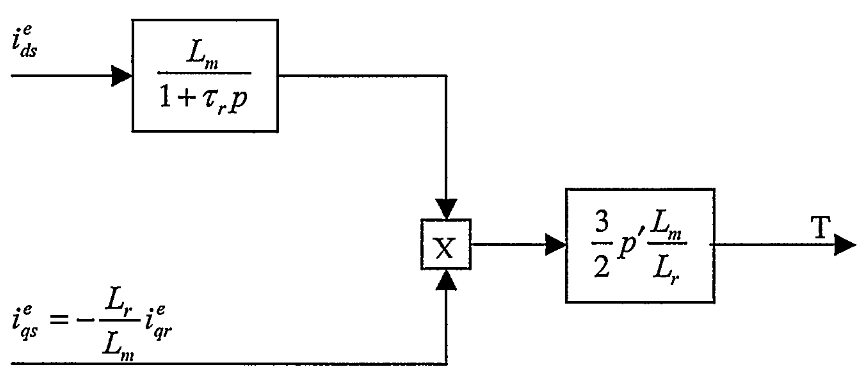

Fig. 3.8 Torque Production For Field Orientation in Terms of Currents

3.3.2 Implementation of Field Orientation Control in Induction Machines

As indicated above, the implementation of field orientation control for induction machines can be carried out starting with a vector transformation provided the angle of the rotor flux is known. There are two basic approaches to obtain the flux magnitude and the angle θ_{rf}, namely

1) The direct method where the rotor flux linkage is determined with direct magnetic field measurements.
2) The indirect method where the rotor flux linkage is calculated using the slip relation in field orientation control.

Direct Field Orientation Control

For direct field orientation control, the magnitude and direction of rotor flux linkages are determined by sensing the air gap flux density, B', with flux sensing coils or Hall elements as shown in Fig. 3-9 [1].

In Fig. 3-9, the asterisk is used to denote the command variables. In this thesis, PI controllers are normally applied for the speed or torque controller as well as the field flux controller [28]. The vector transformation block has been introduced in section 3.2. Many kinds of inverter are available such as the Voltage Source Inverter (VSI) and the Current Source Inverter (CSI) [29]. In the flux calculation block, a correction for rotor leakage flux is carried out following equations (3-32) and (3-33) below, which were obtained from equations (2-13) to (2-16) and (2-31), (2-32).

$$\lambda_{dr} = \frac{L_r}{L_m}\lambda_{dm} - L_{lr}i_{ds} \tag{3-32}$$

$$\lambda_{qr} = \frac{L_r}{L_m}\lambda_{qm} - L_{lr}i_{qs} \tag{3-33}$$

In principle the direct method is inherently the most desirable control scheme since it uses feedback control and direct sensing of the regulated variable, hence it is essentially insensitive to variations in machine parameters. The only machine parameters required are the rotor leakage inductance, L_{lr}, which is essentially a constant value independent of temperature or flux level, and L_r / L_m which is only moderately affected by saturation of the main flux paths in the machine. However this method suffers from high cost and

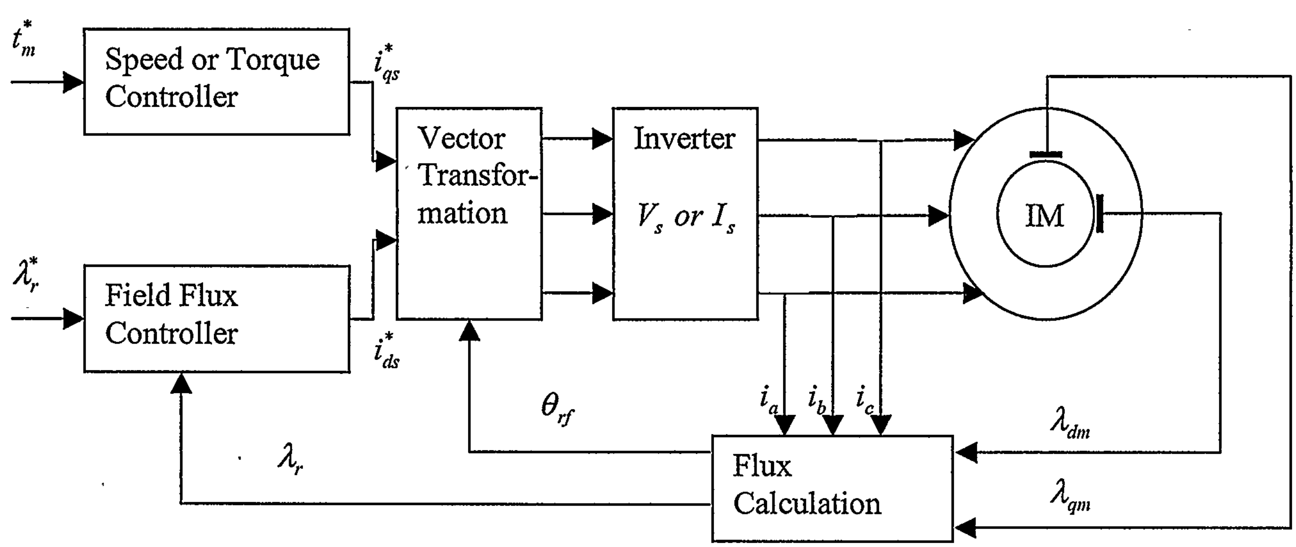

Fig. 3.9 Block diagram of direct field orientation control

the unreliability of the flux measurement. Moreover the special mechanical work required to place the sensing element in the machine makes the approach even more impractical [29].

Indirect Field Orientation Control

Indirect field orientation control utilizes the slip relation (3-31) as part of the controller and does not require a direct measurement of the rotor field. That means satisfying the slip relation is a necessary and sufficient condition to produce field orientation, i.e. if the slip relation is satisfied, i_{ds}^{e} must be aligned with the rotor flux.

Fig. 3.10 illustrates the slip relation in block diagram form. Note that the figure is for transient conditions and in steady state the diagram agrees with the steady state form of the slip relation given in equation (3-15). The block diagram of the indirect method is shown in Fig. 3.11.

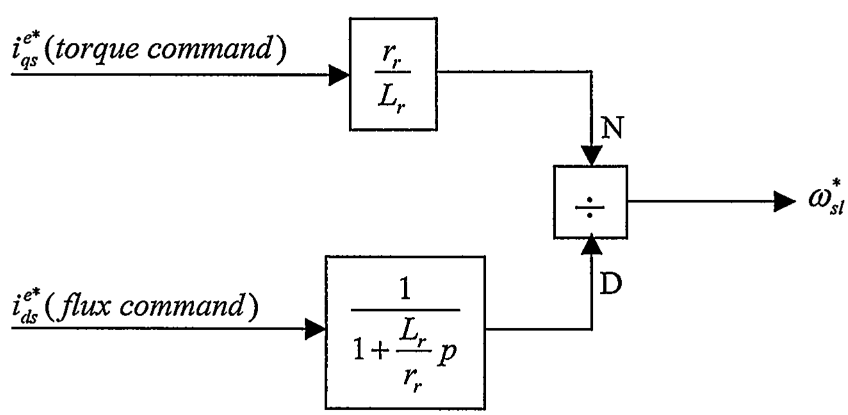

Fig. 3.10 Slip Calculator For Indirect Field Orientation Control

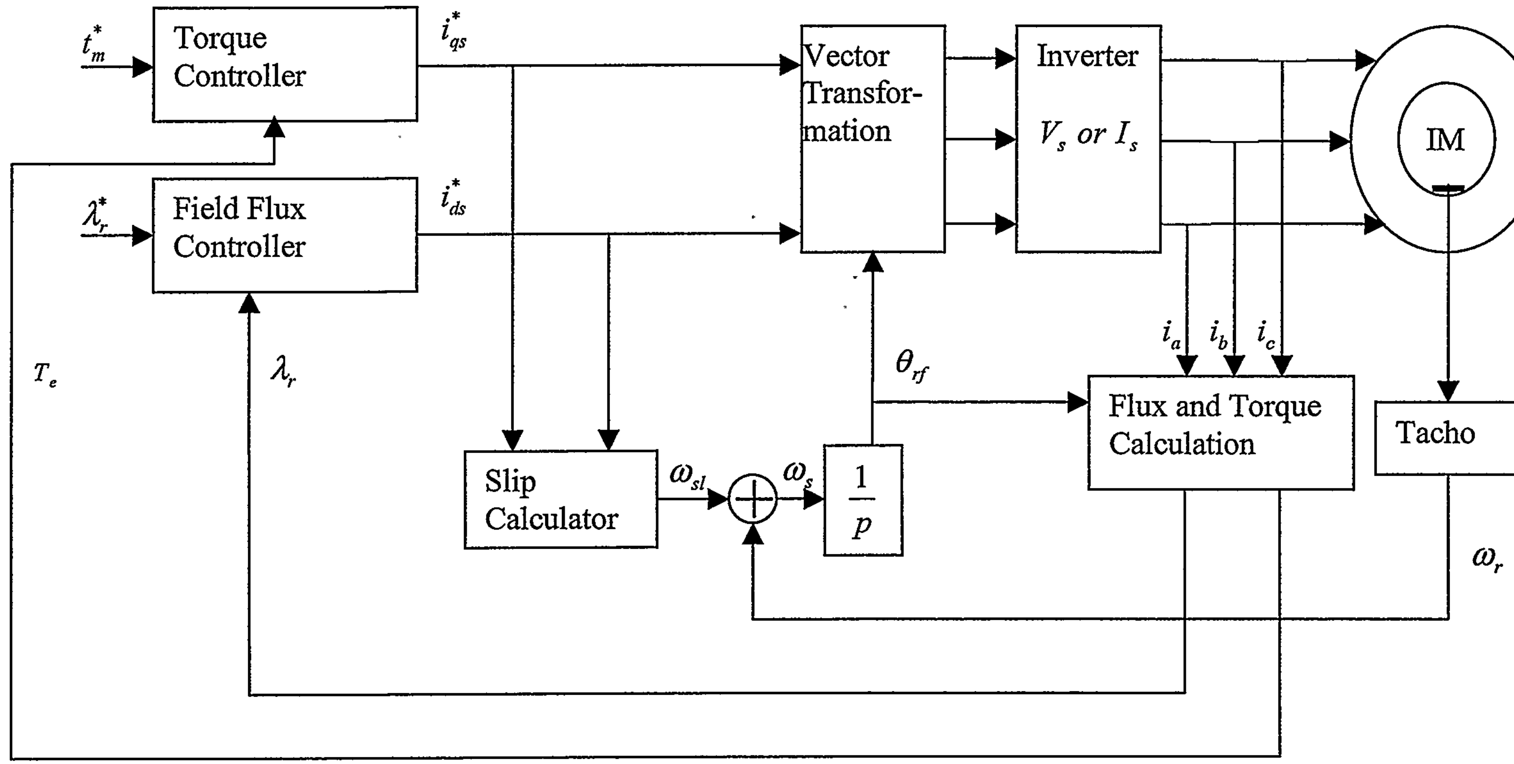

Fig.3.11 Block diagram of indirect field orientation control

The torque controller block and the field flux controller block in Fig. 3.11 are the torque and flux regulating loops that are the optional parts of the control system. Sometimes the torque regulating loop can be replaced by the speed loop, in which case the rotor velocity, ω_r, will be needed as a feedback signal to compare it with the command speed. If an open loop approach is used to control an induction machine, then the torque and flux feedback are not required. Models of field orientation control with open loop control and with closed loop control of rotor speed are given in Appendix B.

In the slip calculator of Fig. 3.10, the major limitation of indirect field orientation control is clearly illustrated. The rotor time constant $\tau_r = L_r / r_r$ directly affects the computed slip. If values of L_r / r_r used to compute the slip are different from the actual ones, the resulting slip will be in error and correct field orientation will not be achieved. Unfortunately motor parameters change widely with temperature, frequency and current amplitude, especially the resistances, which vary dramatically with temperature. Consequently the control gains are not set accurately, leading to saturation or underexcitation of the induction machine [13]. Thus the dynamic performance of the machine will deteriorate.

Much effort has been put into parameter identification methods for induction machines [3,8,13,14,18,19,20,21,30,36], basically focusing on identifying the resistances of the stator or rotor, or identifying the rotor time constant, τ_r. Many methods were introduced to update the identified parameters in field orientation control and so to improve dynamic performance. In this thesis, a novel approach is introduced to identify rotor flux using subspace identification methods [16]. The background on subspace identification is given in the next chapter.

Field Orientation Control Using Voltage as the Controlled Variable

Since the induction machine model that is used in this thesis employs the stator voltage equations and indirectly controls the currents by controlling induction machine terminal voltages, the voltage equations will be decoupled in order to use voltage as the control variable.

Rewriting the stator equations given in (3-16) and (3-17) to represent them in terms of rotor flux, and solving the equations from (3-20) to (3-23) yields

$$\lambda_{ds}^{e} = (L_s - \frac{L_m^2}{L_r})\, i_{ds}^{e} + \frac{L_m}{L_r}\lambda_{dr}^{e} = L_s^{'} i_{ds}^{e} + \frac{L_m}{L_r}\lambda_{dr}^{e} \tag{3-34}$$

$$\lambda_{qs}^{e} = (L_s - \frac{L_m^2}{L_r})\, i_{qs}^{e} + \frac{L_m}{L_r}\lambda_{qr}^{e} = L_s^{'} i_{qs}^{e} + \frac{L_m}{L_r}\lambda_{qr}^{e} \tag{3-35}$$

Then the stator voltage equations in terms of rotor flux linkages are

$$v_{ds}^{e} = (r_s + L_s^{'} p)\, i_{ds}^{e} + \frac{L_m}{L_r} p\lambda_{dr}^{e} - \omega_s (L_s^{'} i_{qs}^{e} + \frac{L_m}{L_r}\lambda_{qr}^{e}) \tag{3-36}$$

$$v_{qs}^{e} = (r_s + L_s^{'} p)\, i_{qs}^{e} + \frac{L_m}{L_r} p\lambda_{qr}^{e} + \omega_s (L_s^{'} i_{ds}^{e} + \frac{L_m}{L_r}\lambda_{dr}^{e}) \tag{3-37}$$

Now new voltage variables are defined to relate the currents directly in the following equations

$$v_{ds}^{e'} = (r_s + L_s' p)\, i_{ds}^e = v_{ds}^e - \frac{L_m}{L_r} p\lambda_{dr}^e + \omega_s (L_s' i_{qs}^e + \frac{L_m}{L_r} \lambda_{qr}^e) \tag{3-38}$$

$$v_{qs}^{e'} = (r_s + L_s' p)\, i_{qs}^e = v_{qs}^e - \frac{L_m}{L_r} p\lambda_{qr}^e - \omega_s (L_s' i_{ds}^e + \frac{L_m}{L_r} \lambda_{dr}^e) \tag{3-39}$$

Referring to equations (3-38) and (3-39), the "primed" voltages can be obtained through a PI controller as long as the command currents are known. Then the stator voltages are derived from equations (3-38) and (3-39) to control the stator currents as commanded.

For a field orientation system, the decoupling equations become simpler since $\lambda_{qr}^e = 0$ and the equations are as follows

$$v_{ds}^{e'} = (r_s + L_s' p)\, i_{ds}^e = v_{ds}^e - \frac{L_m}{L_r} p\lambda_{dr}^e + \omega_s L_s' i_{qs}^e \tag{3-40}$$

$$v_{qs}^{e'} = (r_s + L_s' p)\, i_{qs}^e = v_{qs}^e - \omega_s (L_s' i_{ds}^e + \frac{L_m}{L_r} \lambda_{dr}^e) \tag{3-41}$$

A diagram incorporating stator voltage decoupling is given in Fig. 3-12 to provide "a big picture" that illustrates where the decoupling is implemented in the field orientation control scheme. In the MatLab Simulink models provided in Apendix B, the decoupling is completed primarily within S-functions.

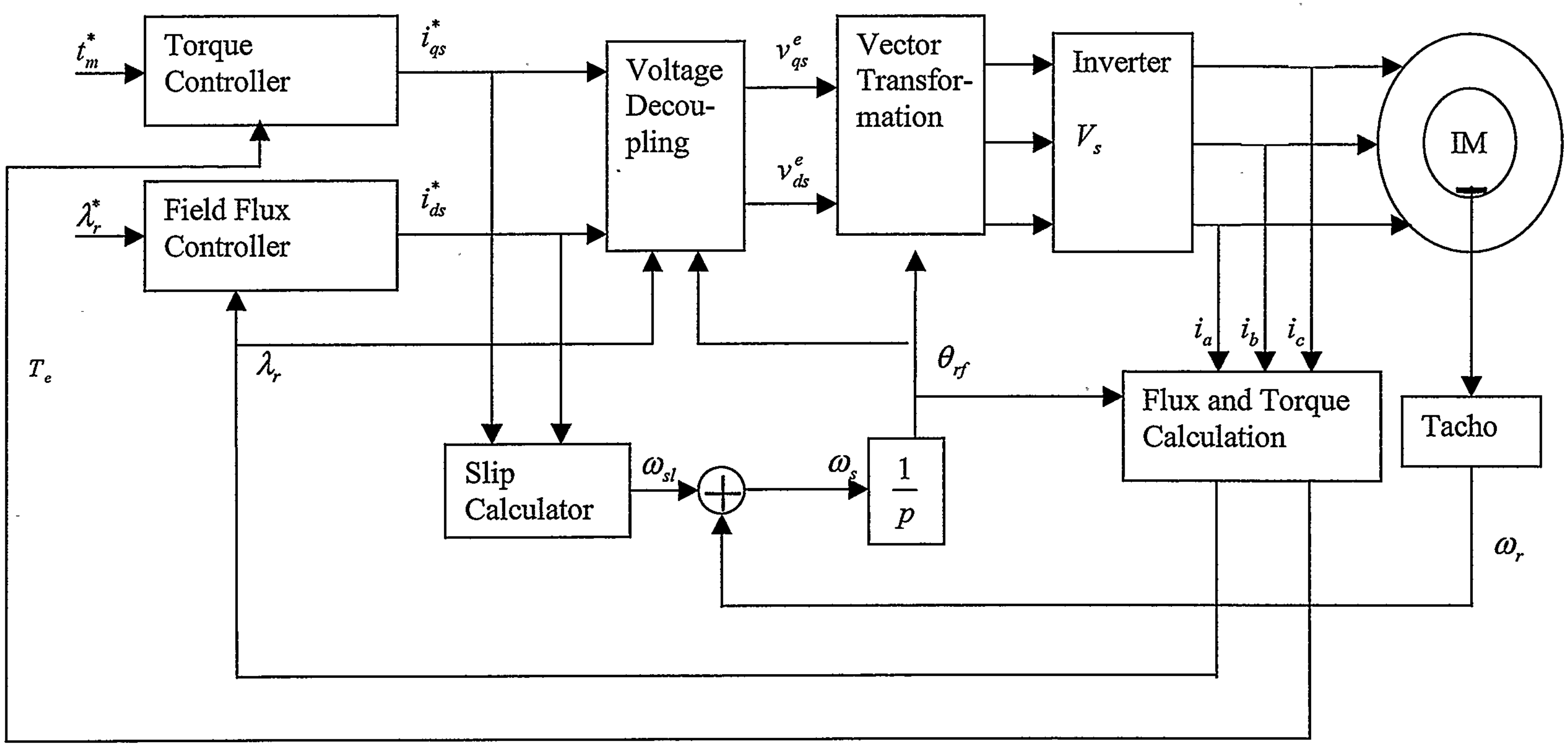

Fig.3.12 Block diagram of indirect field orientation control with stator voltage decoupling

3.4 Chapter Summary

In this chapter, the principle of FOC is introduced first. Two basic methods of implementing FOC are presented, illustrating the advantages and the disadvantages of both methods. The disadvantage of the indirect method, sensitivity to variations of induction machine parameters, provides the motivation of identifying the rotor flux with a subspace identification method that will be introduced in the next chapter.

Chapter 4

System Identification

In this chapter we start by presenting an overview of system identification. Then the basic principles of subspace model identification are discussed to provide a basis for discussions on identification of linear parameter-varying systems. Our work, presented in the following chapters makes use of the linear parameter-varying representation.

4.1 Introduction

Many engineering applications require an accurate model to describe the dynamic behavior of the system under consideration, especially for applications that employ automatic control. The fundamental approach to find a model is to derive it from physical principles. Naturally, in depth knowledge from one or more specialists is required, sometimes resulting in extremely complicated models, which may or may not be practical. Aside from the sophistication of the required model, in the case of a novel application a time consuming investigative procedure may be necessary. However in some cases, particularly for large systems with poorly understood components and/or varying parameters, it may be practically impossible to obtain a model only based on analysis of the fundamental principles.

Another way to develop a model is through system identification, as defined in Chapter 1 [9,26]. The aim of system identification is to directly estimate the model of the system under consideration based on input and output data. Although physical principles are not necessarily used directly to model the system, fundamental principles are still very important for selecting the appropriate inputs to generate required measurements and for model selection and model validation.

Normally four steps are involved in system identification [26]. First, a set of candidate models is selected within which it is expected that at least one will be suitable. Second, appropriate inputs are designed to excite the dynamic behavior of the system to be modeled. Then input and output signals are recorded from identification experiments carried out with the selected inputs. In the third step, an identification method is selected to estimate the parameters. The evaluation of model quality is based on how well the models are able to reproduce the recorded data. Finally the validity of the identified models is assessed in terms of how the models relate to the measured data, prior knowledge and their intended use. A separate data set from the one used for identification should be employed for the validation purpose. If the models first obtained do not pass the model validation tests, the procedure has to be repeated with revision of various steps until a model or models that meet the specified criteria are found.

In many engineering applications, linear time-invariant models often provide acceptable accuracy. Therefore a considerable body of theory has been developed for the identification of linear systems. In particular two methods are popular. One is known as the Prediction-Error Method (PEM), and is based on parameter optimization in a maximum likelihood framework [26]. The prediction of $\hat{y}(k)$ at time step k-1 is the minimum variance estimate of the output $y(k)$ based on the (unknown) model parameters, the present input $u(k)$, the past values of the input $u(j)$ and the output $y(j)$ for $j < k$. The prediction error is the difference between the measured output and that predicted by the model $y(k) - \hat{y}(k)$. The prediction error is used to create a cost-function, which is then minimized by tuning the model parameters.

The other popular method, recently developed, is Subspace Model Identification [16,45,46,47] which is based on the state space realization algorithm developed first by Kalman and Ho [17] and later improved by Kung [22] who incorporated the Singular Value Decomposition (SVD). In subspace model identification, the order of the target system can be obtained with much more ease than in the PEM framework. No explicit cost-function needs to be optimized and the solution is based on geometrical properties of signal spaces. An overview of MIMO Output-Error State Space (MOESP), one of the subspace model identification algorithms, will be presented to provide some background about subspace model identification algorithms. More details can be found elsewhere [16].

Although linear models have many advantages, they still have their limitations since most real systems involve nonlinear characteristics. Reviewing the model of an induction machine as given by (2-51), we can obviously see a nonlinear term involving the product of rotor speed and rotor flux. Therefore identification methods for nonlinear systems have to be used to identify rotor fluxes directly. An identification algorithm for bilinear systems is introduced in Section 4.3 [42], but first some background on subspace model identification is needed.

4.2 Subspace Model Identification

In this section, a subspace model identification algorithm, known as MIMO Output-Error State Space (MOESP), is presented [45]. The advantage of the MOESP algorithm is that it can be applied to a wide variety of models in a unified manner. First, the state space realization algorithm that is the basis of MOESP is illustrated. Then the ordinary MOESP approach, denoted OM-MOESP, is explained.

State Space Realization Algorithm

This algorithm is used to construct a minimal state space model from a given impulse response. In the algorithm, no particular parameterization of the state space model is used, and no optimization of a parametric model is needed. Instead it uses geometrical properties of the system and specially structured of matrices, to obtain a model.

The state space realization problem can be defined as follows.

Consider a linear system described by the following state space equations [4]

$$x(k+1) = Ax(k) + Bu(k) \tag{4-1}$$

$$y(k) = Cx(k) + Du(k) \tag{4-2}$$

with $x(k) \in R^n, y(k) \in R^l$ and $u(k) \in R^m$. The system matrices *A, B, C* and *D* are of appropriate dimensions. A set of impulse response parameters $L_k \in R^{l \times m}, k \in [0, 2i-1]$ is assumed to be available. The parameter *i* equals the number of block rows in the Hankel Matrix M_i defined from L_k. This parameter should be larger than the system order *n*.

$$M_i = \begin{bmatrix} L(1) & L(2) & \cdots & L(i) \\ L(2) & L(3) & \cdots & L(i+1) \\ \vdots & \vdots & \ddots & \vdots \\ L(i) & L(i+1) & \cdots & L(2i-1) \end{bmatrix} \tag{4-3}$$

The state space realization problem is to calculate the system order, *n,* and the system matrices, A_T, B_T, C_T and D_T, where the additional subscript T refers to the determination of the system matrices up to a similarity transformation that does not alter the input output behavior of the system.

According to Theorem 2.1 in [16], two results can be obtained

1. The minimal order, *n*, of the system is equal to rank(M_i).
2. M_i can be factored into

$$M_i = \Gamma_{T_i} \Psi_{T_i} \tag{4-4}$$

with

$$\Gamma_{T_i} = \begin{bmatrix} C_T \\ C_T A_T \\ \vdots \\ C_T A_T^{i-1} \end{bmatrix}$$

$$\Psi_{T_i} = \begin{bmatrix} B_T & A_T B_T & \cdots & A_T^{i-1} B_T \end{bmatrix}$$

which are the extended observability matrix and the extended controllability matrix of an equivalent state space description, respectively. The factorization of M_i can be performed through singular value decomposition.

If matrices Γ_{T_i} and Ψ_{T_i} are calculated, the state space matrices can be extracted from them. First Construct U_1 from the top $(i\ \text{-}1)*l$ rows of Γ_{T_i} and U_2 from the lower $(i\ \text{-}1)*l$ rows. Then the matrix A_T can be obtained with linear regression as follows.

$$\begin{bmatrix} C_T \\ C_T A_T \\ \vdots \\ C_T A_T^{i-2} \end{bmatrix} A_T = \begin{bmatrix} C_T A_T \\ C_T A_T^2 \\ \vdots \\ C_T A_T^{i-1} \end{bmatrix} \quad \text{or} \quad U_1 A_T = U_2 \tag{4-5}$$

So $$A_T = (U_1^T U_1)^{-1} U_1^T U_2 \tag{4-6}$$

or $$A_T = U_1 \backslash U_2 \tag{4-7}$$

where \ is the notation used by MATLAB to denote multiplication by the pseudo inverse (4-6). Then the matrix B_T is read from the first m columns of Ψ_{T_i} , C_T corresponds to the upper l rows of Γ_{T_i}, and D_T is equal to $L(0)$.

Ordinary MOESP Algorithm

This algorithm identifies the state space matrices of a system from measurements of its inputs and outputs rather than through the use of the impulse response as employed in the state space realization algorithm. Although in practice measurements are always contaminated with noise, we present the identification problem in the noise-free case to illustrate the basic principle of the MOESP family of subspace identification algorithms. More elaborate identification problems are discussed elsewhere [16,47].

The noise-free identification problem is illustrated through reference to Fig. 4.1. Suppose the input and output data-set, $\{u(k),\ y(k)\}$, $k \in [0, N_m - 1]$ with $u(k) \in R^m$ and $y(k) \in R^l$ of a system described by the state space equations (4-1) and (4-2) are known. Assume that the system is minimal and stable and that the number of samples is much larger than the order of the system ($N_m >> n$). Also assume that the input is persistently exciting of sufficient order to permit the identification [16].

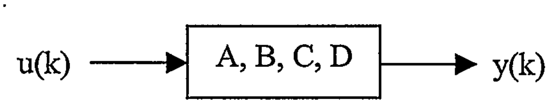

Fig. 4.1 Schematic representation of the noise-free model

As in the state space realization problem, the noise-free identification problem includes calculating the system order, *n*, and the system matrices A_T, B_T, C_T and D_T, where the additional index T refers to the determination of the system matrices up to a similarity transformation.

As indicated above, the number of samples of input and output is N_m, with $u(k) \in R^m$, $k \in [0, N_m - 1]$. The output of the system can be represented as follows

$$
\begin{aligned}
y(0) &= Cx(0) + Du(0) \\
y(1) &= Cx(1) + Du(1) \\
&= CAx(0) + CBu(0) + Du(1) \\
y(2) &= CA^2x(0) + CABu(0) + CBu(1) + Du(2) \\
&\vdots \\
y(k) &= CA^kx(0) + CA^{k-1}Bu(0) + \cdots + CBu(k-1) + Du(k)
\end{aligned}
\tag{4-8}
$$

With N = N_m - i +1 this can be transformed into the following matrix form

$$
\begin{bmatrix} y(0) & y(1) & \cdots & y(N-1) \\ y(1) & y(2) & \cdots & y(N) \\ \vdots & \vdots & \ddots & \vdots \\ y(i-1) & y(i) & \cdots & y(N+i-2) \end{bmatrix} = \begin{bmatrix} C \\ CA \\ \vdots \\ CA^{i-1} \end{bmatrix} \begin{bmatrix} x(0) & x(1) & \cdots & x(N-1) \end{bmatrix}
$$

$$
+ \begin{bmatrix} D & 0 & \cdots & 0 \\ CB & D & \cdots & 0 \\ \vdots & \vdots & \ddots & \vdots \\ CA^{i-2}B & CA^{i-3}B & \cdots & D \end{bmatrix} \begin{bmatrix} u(0) & u(1) & \cdots & u(N-1) \\ u(1) & u(2) & \cdots & u(N) \\ \vdots & \vdots & \ddots & \vdots \\ u(i-1) & u(i) & \cdots & u(N+i-2) \end{bmatrix} \tag{4-9}
$$

This equation is called the data equation, and relates all the measured data in one equation. The input and output matrices are again Hankel matrices. A shorthand notation is normally used to represent a Hankel matrix. Take the Hankel matrix constructed from the output $y(k)$ as an example.

$$Y_{i,j,N} = \begin{bmatrix} y(i) & y(i+1) & \cdots & y(i+N-1) \\ y(i+1) & y(i+2) & \cdots & y(i+N) \\ \vdots & \vdots & \ddots & \vdots \\ y(i+j-1) & y(i+j) & \cdots & y(i+j+N-2) \end{bmatrix} \tag{4-10}$$

where the three subscripts of $Y_{i,j,N}$ denote

i – the index in the left upper entry of $Y_{i,j,N}$

j – the number of rows

N – the number of columns

A two-subscript notation is used to denote a row-vector constructed from $x(k)$.

$$X_{i,N} = \begin{bmatrix} \bar{x}(i) & \bar{x}(i+1) & \cdots & \bar{x}(i+N-1) \end{bmatrix} \tag{4-11}$$

where i – the starting index

N – the length of vector

The data equation (4-9) can be transformed into a condensed form as

$$Y_{0,i,N} = \Gamma_i X_{0,N} + H_i U_{0,i,N} \tag{4-12}$$

where

$$\Gamma_i = \begin{bmatrix} C \\ CA \\ \vdots \\ CA^{i-1} \end{bmatrix} \quad \text{and} \quad H_i = \begin{bmatrix} D & 0 & \cdots & 0 \\ CB & D & \cdots & 0 \\ \vdots & \vdots & \ddots & \vdots \\ CA^{i-2}B & CA^{i-3}B & \cdots & D \end{bmatrix} \tag{4-13}$$

The initial goal of the identification is to estimate the state space matrices A and C. From the state space realization algorithm introduced above, we know that the matrices A and C are easily estimated as long as the matrix Γ_i is known.

In the data equation (4-12), there are two terms required to construct the output of a system. The past input is accumulated in the state of the system. Both the state and the present input build up corresponding vector spaces. These two vector spaces form the output vector space in a particular way characterized by the target system. The process of subspace identification is to find that particular combination in terms of the state space matrices. MOESP tries to find the mapping from the state to the output, i.e. matrices A and C. Therefore the second term in the data equation (4-12), which is the contribution to the output from the input, has to be eliminated first.

In order to remove the input term from the output, a method called orthogonal projection is used. It involves the right multiplication of the output with an orthogonal projection matrix, $\Pi^{\perp}_{U_{0,i,N}}$, that projects the output onto the orthogonal complement of $U_{0,i,N}$.

The orthogonal projection matrix can be determined by

$$\Pi^{\perp}_{U_{0,i,N}} = I - U^T_{0,i,N}(U_{0,i,N}U^T_{0,i,N})^{-1}U_{0,i,N} \tag{4-14}$$

Obviously $U_{0,i,N}\Pi^{\perp}_{U_{0,i,N}} = 0$.

In order to insure that $\Pi^{\perp}_{U_{0,i,N}}$ exists, $U_{0,i,N}U^T_{0,i,N}$ has to be full rank. This will be guaranteed if the input is persistently exciting of order i or greater [16].

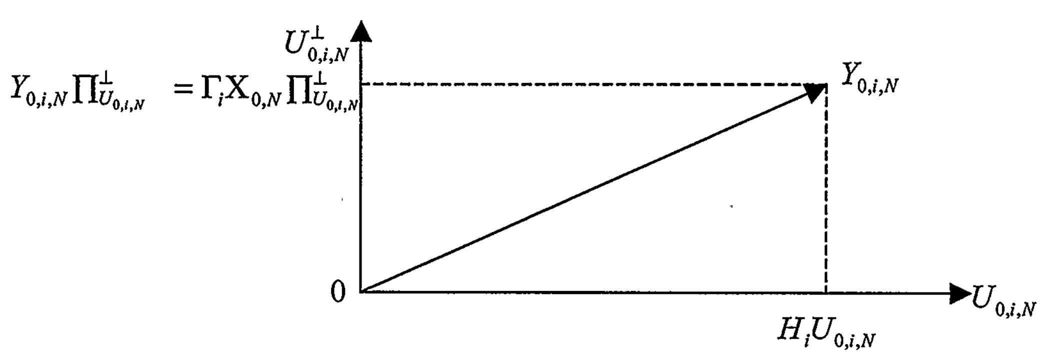

Fig. 4.2 Orthogonal Projection of the output

After the orthogonal projection onto the output, we obtain

$$Y_{0,i,N}\Pi^{\perp}_{U_{0,i,N}} = \Gamma_i X_{0,N}\Pi^{\perp}_{U_{0,i,N}} \tag{4-15}$$

from which Γ_i can be obtained from the column-space.

Actually the orthogonal projection can also be done by QR factorization as follows

$$\begin{bmatrix} U_{0,i,N} \\ Y_{0,i,N} \end{bmatrix} = \begin{bmatrix} R_{11} & 0 \\ R_{21} & R_{22} \end{bmatrix} \begin{bmatrix} Q_1 \\ Q_2 \end{bmatrix} \tag{4-16}$$

where $U_{0,i,N} \in R^{mi\times N}$ and $Y_{0,i,N} \in R^{li\times N}$. Q_1 is of the same size as $U_{0,i,N}$ and Q_2 as $Y_{0,i,N}$. Correspondingly, $R_{11} \in R^{mi\times mi}, R_{21} \in R^{li\times mi}$ and $R_{22} \in R^{li\times li}$.

According to Theorem 2.2 in [16], with the QR factorization (4-16), the following holds

$$R_{22} = \Gamma_i X_{0,N} Q_2^T \tag{4-17}$$

Then performing the singular value decomposition on R_{22}, we obtain

$$R_{22} = U\Sigma V^T \tag{4-18}$$

The number of non-zero singular values is the order of the system, n. The column-space of R_{22} is equal to the first n columns of U, which is equivalent to Γ_{T_i} in the state space realization algorithm. Therefore A_T and C_T can be calculated in a similar manner. Construct U_1 from the top $(i\ \text{-}1)*l$ rows of Γ_{T_i} and U_2 from the lower $(i\ \text{-}1)*l$ rows. Then,

$$C_T = \text{the upper } l \text{ rows of } \Gamma_{T_i}$$

$$A_T = U_1 \backslash U_2$$

Unfortunately, due to the influence of the input term in (4-12), B_T and D_T cannot be found directly as in the state space realization algorithm. Therefore new methods need to be developed to do that. Here only the method to estimate B_T, D_T and the initial state for the noise-free identification problem will be introduced, while other details are found in [16].

The output $y(k)$ of a system described by (4-1) and (4-2) can be rewritten as

$$y(k) = CA^k x(0) + \sum_{\tau=0}^{k-1} CA^{k-1-\tau} Bu(\tau) + Du(k) \tag{4-19}$$

Let $\otimes$ denote the Kronecker product of a matrix $\Phi \in R^{p\times q}$ and $\Psi \in R^{m\times n}$, defined as

$$\Phi \otimes \Psi = \begin{bmatrix} \phi_{11}\Psi & \phi_{12}\Psi & \cdots & \phi_{1q}\Psi \\ \phi_{21}\Psi & \phi_{22}\Psi & \cdots & \phi_{2q}\Psi \\ \vdots & \vdots & \ddots & \vdots \\ \phi_{p1}\Psi & \phi_{p2}\Psi & \cdots & \phi_{pq}\Psi \end{bmatrix} \tag{4-20}$$

and let vec($\cdot$) denote the vector containing the columns of the matrix ($\cdot$) on top of each other. Using this notation, (4-19) becomes

$$y(k) = CA^k x(0) + \left[\sum_{\tau=0}^{k-1} u(\tau)^T \otimes CA^{k-1-\tau}\right] vec(B) + \left[u(k)^T \otimes I_l\right] vec(D) \tag{4-21}$$

If the following matrices are defined

$$Y_{0,N,1} = \begin{bmatrix} y(0) \\ y(1) \\ \vdots \\ y(N-1) \end{bmatrix} \qquad \Gamma_N = \begin{bmatrix} C \\ CA \\ \vdots \\ CA^{N-1} \end{bmatrix} \tag{4-22}$$

$$\rho = \begin{bmatrix} 0 \\ u(0)^T \otimes C \\ \vdots \\ \sum_{\tau=0}^{N-2} u(\tau)^T \otimes CA^{N-2-\tau} \end{bmatrix} \qquad \eta = \begin{bmatrix} u(0)^T \otimes I_l \\ u(1)^T \otimes I_l \\ \vdots \\ u(N-1)^T \otimes I_l \end{bmatrix} \tag{4-23}$$

$$\beta = \mathrm{vec}(B) \qquad \delta = \mathrm{vec}(D)$$

then (4-21) can be rewritten as

$$Y_{0,N,1} = \begin{bmatrix} \Gamma_N & \rho & \eta \end{bmatrix} \begin{bmatrix} x_0 \\ \beta \\ \delta \end{bmatrix} \tag{4-24}$$

Then the coefficients of B, D and x_0 can be calculated by solving (4-24) as a linear regression:

$$\begin{bmatrix} x_0 \\ \beta \\ \delta \end{bmatrix} = \begin{bmatrix} \Gamma_N & \rho & \eta \end{bmatrix} \backslash Y_{0,N,1} \tag{4-25}$$

In practice, the true values of matrices A and C are not available. Therefore only their estimates, $\hat{A}_T$ and $\hat{C}_T$, can be used to estimate the matrices $\hat{B}_T$ and $\hat{D}_T$ and $\hat{x}_{0_T}$ to within the same similarity transformation as A_T and C_T.

The subspace identification algorithms have been implemented in the toolbox SMI2.0 by B. Haverhamp [16]. In section 7.1, SMI2.0 is used to verify the model of induction machines.

4.3 LPV State Space System Identification

As shown in sections 2.3-2.5, nonlinearities are involved in models of induction machines. Therefore identification algorithms for nonlinear systems have to be used to identify rotor fluxes directly either with PEM methods and or with subspace identification methods. There are two approaches to determine the structure of a nonlinear model. The first approach is to choose a relatively simple structure for which the corresponding identification method is computationally attractive. However, this represents a limited class of nonlinear systems due to its simple structure. Linear models, bilinear models, Hammerstein models and Wiener models are examples of this approach. The second approach is to choose the model structure that can represent a large class of nonlinear systems. The disadvantage is that the corresponding identification algorithms are complicated. Examples of this approach are sigmoidal neural networks, radial basis function networks, local linear model structures, Takagi-Sugeno fuzzy models and hinging hyperplanes models. Reviewing the model structure of the induction machine, we choose a bilinear state space model to identify rotor fluxes directly. Since bilinear systems are one kind of multivariable linear parameter-varying (LPV) system, subspace identification of an LPV system will be presented first.

4.3.1 Introduction to Subspace Identification of LPV Models

A linear parameter-varying (LPV) system can be described by state equations with the following structure [43], that is an extension of the state space model in innovation form

$$x_{k+1} = A\begin{bmatrix} x_k \\ \zeta_k \otimes x_k \end{bmatrix} + B\begin{bmatrix} u_k \\ \zeta_k \otimes u_k \end{bmatrix} + K\begin{bmatrix} e_k \\ \zeta_k \otimes e_k \end{bmatrix} \tag{4-26}$$

$$y_k = Cx_k + Du_k + e_k \tag{4-27}$$

where $\otimes$ denotes the Kronecker product, $x_k \in R^n$ represents the unknown state, $u_k \in R^m$ is the input, $y_k \in R^l$ is the output, $\zeta_k \in R^s$ is the time-varying parameter vector (s is the number of the elements in the time-varying parameter vector) and $e_k \in R^l$ is a white noise disturbance signal that is independent of u_k and ζ_k. The identification objective is to determine the matrices *A, B, C, D* and *K* given measurements of the input u_k, the output y_k and the parameter vector ζ_k.

It can be seen that by taking the parameter vector ζ_k equal to the input u_k and setting all columns of the matrix B to zero except the first m columns, the LPV model (4-26) and (4-27) will become a bilinear system model. Therefore the LPV identification method presented below is easily modified for the identification of a bilinear system.

A major problem with subspace identification methods for both bilinear and LPV systems is the huge dimension of the data matrices involved. The number of rows in the data matrices grows exponentially with the order of the system. In [42], an approach that selected a subset of the most dominant rows from the data matrices was introduced to solve the dimensionality problem. In this way the identified LPV model is an approximate one. Then a nonlinear optimization algorithm can be applied to improve the initial model estimate provided by subspace identification of the LPV system. In section 4.3.2, subspace identification of an LPV system is presented

4.3.2 LPV Subspace Identification Method

The following matrix partitions need to be defined before further derivation [42]

$$A = [A_0, A_1, A_2, \cdots A_s]$$

$$B = [B_0, B_1, B_2, \cdots B_s]$$

$$K = [K_0, K_1, K_2, \cdots K_s]$$

$$\overline{A}_i := A_i - K_i C, \quad \overline{B}_i := B_i - K_i D$$

where A, B, C, D, K are the matrices used in (4-26) and (4-27), $B_i \in R^{n \times m}$, $K_i \in R^{n \times l}$ for $i = 0,1,2, \ldots, s$.

The Khatri-Rao product, denoted by the symbol, $\odot$, will be used extensively in the derivation. It is a column-wise Kronecker product for two matrices that have an equal number of columns. Let $M \in R^{p \times q}$ and $N \in R^{r \times q}$ be two matrices, then the Khatri-Rao product of them equals

$$\mathrm{M} \odot \mathrm{N} = [m_1 \otimes n_1 \quad m_2 \otimes n_2 \quad \cdots \quad m_q \otimes n_q] \tag{4-28}$$

where m_i and n_i ($i = 1,2, \ldots, q$) are the columns of the matrices M and N respectively.

More matrix partitions are defined below [44]

$$P_k := [\zeta_k \quad \zeta_{k+1} \quad \cdots \quad \zeta_{k+N-1}] \in R^{s \times N}$$

$$X_k := [x_k \quad x_{k+1} \quad \cdots \quad x_{k+N-1}] \in R^{n \times N}$$

$$X_{j|j} := \begin{bmatrix} X_j \\ P_j \odot X_j \end{bmatrix} \in R^{(s+1)n \times N}$$

$$X_{k+j|j} := \begin{bmatrix} X_{k+j-1|j} \\ P_{k+j} \odot X_{k+j-1|j} \end{bmatrix} \in R^{((s+1)^{k+1})n \times N}$$

$$Y_k := \begin{bmatrix} y_k & y_{k+1} & \cdots & y_{k+N-1} \end{bmatrix} \in R^{l \times N}$$

$$Y_{j|j} := \begin{bmatrix} Y_j \\ P_j \odot Y_j \end{bmatrix} \in R^{(s+1)l \times N}$$

$$Y_{k+j|j} := \begin{bmatrix} Y_{k+j} \\ P_{k+j} \odot Y_{k+j} \\ Y_{k+j-1|j} \\ P_{k+j} \odot Y_{k+j-1|j} \end{bmatrix} \in R^{((s+1)^{k+1}-1)l(s+1)/s \times N}$$

The matrices U_k and E_k are defined similarly to Y_k while $U_{k+j|j}$ and $E_{k+j|j}$ are defined similarly to $Y_{k+j|j}$. Note that the recursion in the definitions of $X_{k+j|j}$, $Y_{k+j|j}$, $U_{k+j|j}$ and $E_{k+j|j}$ leads to very large matrices whose rows increase exponentially with the order of the system. Also,

$$\gamma_{j|j} := Y_j \in R^{\ell \times N}$$

$$\gamma_{k+j|j} := \begin{bmatrix} Y_{k+j} \\ \gamma_{k+j-1|j} \end{bmatrix} \in R^{(k+1)\ell \times N}$$

$$\widetilde{P}_{j|j} := P_j \in R^{s \times N}$$

$$\widetilde{P}_{k+j|j} := \begin{bmatrix} \widetilde{P}_{k+j-1|j} \\ P_{k+j,1} \\ P_{k+j,1} \odot \widetilde{P}_{k+j-1|j} \\ \vdots \\ P_{k+j,s} \\ P_{k+j,s} \odot \widetilde{P}_{k+j-1|j} \end{bmatrix} \in R^{((s+1)^{k+1}-1) \times N}$$

where $P_{k,i}$ denotes the ith row of P_k. Then the relation between $X_{k+j|j}$ and $\widetilde{P}_{k+j|j}$ is as follows

$$X_{k+j|j} = \begin{bmatrix} X_j \\ \widetilde{P}_{k+j|j} \odot \quad X_j \end{bmatrix} \tag{4-29}$$

Based on these defined matrices, the data equations for an LPV system representation can be formulated as below according to Lemma 1 and Lemma 2 in [44].

For the LPV system of (4-26), (4-27), the state data equations are

$$X_{k+j} = \overline{\Delta}_k^x X_{k+j-1|j} + \overline{\Delta}_k^u U_{k+j-1|j} + \overline{\Delta}_k^y Y_{k+j-1|j} \tag{4-30}$$

where $\overline{\Delta}_1^x := [\overline{A}_0, \overline{A}_1, \ldots, \overline{A}_s]$

$$\overline{\Delta}_k^x := [\overline{A}_0 \overline{\Delta}_{k-1}^x, \overline{A}_1 \overline{\Delta}_{k-1}^x, \ldots, \overline{A}_s \overline{\Delta}_{k-1}^x]$$

$$\overline{\Delta}_1^u := [\overline{B}_0, \overline{B}_1, \ldots, \overline{B}_s]$$

$$\overline{\Delta}_k^u := [\overline{\Delta}_1^u, \overline{A}_0 \overline{\Delta}_{k-1}^u, \overline{A}_1 \overline{\Delta}_{k-1}^u, \ldots, \overline{A}_s \overline{\Delta}_{k-1}^u]$$

$$\overline{\Delta}_1^y := [\overline{K}_0, \overline{K}_1, \ldots, \overline{K}_s]$$

$$\overline{\Delta}_k^y := [\overline{\Delta}_1^y, \overline{A}_0 \overline{\Delta}_{k-1}^y, \overline{A}_1 \overline{\Delta}_{k-1}^y, \ldots, \overline{A}_s \overline{\Delta}_{k-1}^y]$$

and the output data equations are

$$Y_{k+j|j} = H_k^x X_{k+j-1|j} + H_k^u U_{k+j-1|j} + H_k^e E_{k+j-1|j} + G_k^u U_{k+j} + G_k^e E_{k+j} \tag{4-31}$$

where $H_1^x := \begin{bmatrix} CA_0 & CA_1 & \cdots & CA_s \\ C & 0 & \cdots & 0 \end{bmatrix}$

$$H_k^x := \begin{bmatrix} CA_0 \Delta_{k-1}^x & CA_1 \Delta_{k-1}^x & \cdots & CA_s \Delta_{k-1}^x \\ H_{k-1}^x & 0 & \cdots & 0 \end{bmatrix}$$

$$\Delta_1^x := [A_0, A_1, \ldots, A_s]$$

$$\Delta_k^x := [A_0\Delta_{k-1}^x, A_1\Delta_{k-1}^x, \ldots, A_s\Delta_{k-1}^x]$$

$$H_1^u := \begin{bmatrix} CB_0 & CB_1 & \cdots & CB_s \\ D & 0 & \cdots & 0 \end{bmatrix}$$

$$H_k^u := \begin{bmatrix} CB_0 & CB_1 & \cdots & CB_s & CA_0\Delta_{k-1}^u & CA_1\Delta_{k-1}^u & \cdots & CA_s\Delta_{k-1}^u \\ G_{k-1}^u & 0 & \cdots & 0 & H_{k-1}^u & 0 & \cdots & 0 \end{bmatrix}$$

$$\Delta_1^u := [B_0, B_1, \ldots, B_s]$$

$$\Delta_k^u := [\Delta_1^u, A_0\Delta_{k-1}^u, A_1\Delta_{k-1}^u, \ldots, A_s\Delta_{k-1}^u]$$

$$H_1^e := \begin{bmatrix} CK_0 & CK_1 & \cdots & CK_s \\ I_\ell & 0 & \cdots & 0 \end{bmatrix}$$

$$H_k^e := \begin{bmatrix} CK_0 & CK_1 & \cdots & CK_s & CA_0\Delta_{k-1}^e & CA_1\Delta_{k-1}^e & \cdots & CA_s\Delta_{k-1}^e \\ G_{k-1}^e & 0 & \cdots & 0 & H_{k-1}^e & 0 & \cdots & 0 \end{bmatrix}$$

$$\Delta_1^e := [K_0, K_1, \ldots, K_s]$$

$$\Delta_k^e := [\Delta_1^e, A_0\Delta_{k-1}^e, A_1\Delta_{k-1}^e, \ldots, A_s\Delta_{k-1}^e]$$

$$G_k^u := \begin{bmatrix} D \\ 0 \end{bmatrix}, \qquad G_k^e := \begin{bmatrix} I_\ell \\ 0 \end{bmatrix}$$

Based on the data equations for system (4-26) and (4-27), let

$$W_{j,0} := \begin{bmatrix} U_{j-1|0} \\ Y_{j-1|0} \end{bmatrix} \qquad \text{and} \qquad Z_{k,j,0} := \begin{bmatrix} U_{k+j} \\ U_{k+j-1|j} \\ \widetilde{P}_{k+j-1|j} \odot W_{j,0} \end{bmatrix},$$

then according to Lemma 4 in [44], the following QR factorization can be made

$$\begin{bmatrix} W_{j,0} \\ Z_{k,j,0} \\ \gamma_{k+j|j} \end{bmatrix} = \begin{bmatrix} R_{11} & 0 & 0 \\ R_{21} & R_{22} & 0 \\ R_{31} & R_{32} & R_{33} \end{bmatrix} \begin{bmatrix} Q_1 \\ Q_2 \\ Q_3 \end{bmatrix} \tag{4-32}$$

Under the assumption that the matrix

$$\lim_{N\to\infty} \frac{1}{\sqrt{N}} \begin{bmatrix} W_{j,0} \\ Z_{k,j,0} \end{bmatrix} \tag{4-33}$$

has full row rank, the noise e_k is non-zero, the pair (A_0,C) is observable and there exists a $j > n$ such that $\overline{\Delta}_j^x X_{j-1|0} = 0$, we have

$$\lim_{N\to\infty} \frac{1}{\sqrt{N}} \Gamma_k X_j = \lim_{N\to\infty} \frac{1}{\sqrt{N}} \overline{R}(:,1:n_w) W_{j,0} \quad w.p.1 \tag{4-34}$$

where $\Gamma_k := H_k^x(:,1:n)$

$$\overline{R} := \frac{1}{\sqrt{N}} [R_{31}, R_{32}] \left(\frac{1}{\sqrt{N}} \begin{bmatrix} R_{11} & 0 \\ R_{21} & R_{22} \end{bmatrix} \right)^{-1}$$

n_w is the total number of rows in $W_{j,0}$

w.p.1 means 'with probability 1'

The state sequence can be calculated as the row space of the right hand side of (4-34). With singular value decomposition

$$\overline{R}(:,1:n_w) W_{j,0} = [U_1 \quad U_2] \begin{bmatrix} \Sigma_1 & 0 \\ 0 & \Sigma_2 \end{bmatrix} \begin{bmatrix} V_1^T \\ V_2^T \end{bmatrix} \tag{4-35}$$

where $\Sigma_1 \in R^{n\times n}$, the state sequence can be estimated as

$$\hat{X}_j = \Sigma_1^{-1/2} V_1^T \tag{4-36}$$

If the noise is not excessive, the singular values in Σ_1 will be much bigger than those in Σ_2. Hence the order of the system, *n*, can be determined from the gap in the singular values. Then the system matrices can be estimated up to a similarity transformation by linear regression as follows

$$[\hat{C},\hat{D}] = Y_j [\hat{X}_j^T \quad U_j^T] \left(\begin{bmatrix} \hat{X}_j \\ U_j \end{bmatrix} [\hat{X}_j^T \quad U_j^T] \right)^{-1} \tag{4-37}$$

$$\hat{E}_j = Y_j - [\hat{C},\hat{D}] \begin{bmatrix} \hat{X}_j \\ U_j \end{bmatrix} \tag{4-38}$$

$$[\hat{A},\hat{B},\hat{K}] = \hat{X}_{j+1} \Theta_j^T (\Theta_j \Theta_j^T)^{-1} \tag{4-39}$$

where $\Theta_j^T = [\hat{X}_{j|j}^T, U_{j|j}^T, \hat{E}_{j|j}^T]$

$$\hat{X}_{j|j} := \begin{bmatrix} \hat{X}_j \\ P_j \odot \hat{X}_j \end{bmatrix}, \qquad \hat{E}_{j|j} := \begin{bmatrix} \hat{E}_j \\ P_j \odot \hat{E}_j \end{bmatrix}$$

Now the system matrices can be estimated with a subspace identification method. However the number of rows in the matrices $W_{j,0}$ and $Z_{k,j,0}$ increases exponentially with the order of the system. In order to compute the QR factorization, the amount of memory required is excessive as compared to that available in present day desktop computers. Table 4-1 gives the number of rows for the data matrices $W_{j,0}$ and $Z_{k,j,0}$ as a function of block size k and of the system dimensions for a square system with three time-varying parameters ($\zeta_k \in R^3$) [44].

Therefore the method above is impractical without any modification. A method of selecting the most dominant rows of the data matrices is proposed in [42] to overcome the dimension problem with subspace identification of an LPV system. Also an efficient implementation of the selection algorithm is introduced to process the data matrices row by row instead of building the formation of the complete matrices. Even with these modifications, it still takes a couple of days to perform the identification algorithm on an induction machine model, a fourth-order system with two inputs and two outputs, using a server with four 900MHz SPARC III processors and 4GB memory that is available in the department of electrical engineering of University of Calgary.

Table 4-1 Total number of rows in the matrices $W_{j,0}$ and $Z_{k,j,0}$; s=3,m=1,k=j-1, from [42]

	$l=1$	$l=2$	$l=3$	$l=4$	$l=5$
$k=2$	168	336	504	672	840
$k=3$	2712	5424	8136	10848	13560
$k=4$	43608	87216	130824	174432	218040
$k=5$	698712	1397424	2096136	2794848	3493560

Thus far, we have illustrated how to estimate the system matrices of an LPV system with the subspace identification method. However the estimated model can only be used as an initial model since some errors are introduced in the process of subspace identification. One obvious error source is the selection of the most dominant rows of the data matrices used in the QR factorization. Further optimization of the initial estimated model is needed to identify a more accurate model of the system. A nonlinear optimization method is presented in [42] to identify the LPV model using a local gradient search.

Comparing the LPV representation of (4-26) and (4-27) and the model of a bilinear system, (2-55) and (2-56), it is straightforward to extend the identification method for an LPV system discussed above, to the identification of a bilinear system. Taking the parameter vector ζ_k equal to the input u_k and the matrices $B_1, B_2,..., B_s$ and $K_1, K_2,..., K_s$ equal to zero, we obtain a bilinear system

$$x_k = A_0 x_k + [A_1, A_2,..., A_s](u_k \otimes x_k) + B_0 u_k + K_0 e_k \tag{4-40}$$

$$y_k = Cx_k + Du_k + e_k \tag{4-41}$$

Correspondingly the data matrices $Y_{k+j|j}$ become

$$Y_{j|j} = Y_j \in R^{\ell \times N}$$

$$Y_{k+j|j} = \begin{bmatrix} Y_{k+j} \\ Y_{k+j-1|j} \\ U_{k+j} \odot Y_{k+j-1|j} \end{bmatrix} \in R^{((s+1)^{k+1}-1)\ell/s \times N}$$

Similar modifications must be made to the matrix $U_{k+j|j}$. Also the same selection algorithm to reduce the rows in the data matrices can be applied in subspace identification for bilinear systems.

All of the operations discussed in this section, including identification, row selection and optimization algorithms have been recently incorporated into a Matlab toolbox by V. Verdult. Dr. Verdult kindly provided the author with a pre-release copy of this toolbox.

4.4 Chapter Summary

This chapter reviewed subspace identification methods for linear and LPV systems, based primarily on the work of Haverkamp [16] and Verdult [42]. Modified version of these methods will be used to identify the dynamics of a simulated induction machine in Chapter 7, which will also present our modifications. First discussions are presented on our induction motor discretization and modelling approaches in chapters 5 and 6 respectively.

Chapter 5

Model Discretization

In the literature, models of induction machines are almost always presented as continuous-time models. However the identification methods discussed in the previous chapter are based on a discrete-time system representation. Therefore we present in this chapter our own discrete time induction motor model. This is necessary for the purpose of system identification and flux estimation using the LPV approach since we must verify that the discrete-time model also has the LPV structure. Furthermore, the eventual controller implementation on a microprocessor will be facilitated by using a discrete-time model.

5.1 Introduction

In order to employ the subspace methods discussed in the previous chapter, a discrete-time induction machine model is needed. Also due to the advantages of decision-making capability and flexibility offered by digital control systems, induction machine drives are usually implemented with microprocessor control. For a discrete-time control system, signals can change only at discrete instants of time corresponding to the times at which some physical measurement is performed or the times at which the memory of a digital computer is read or written [33].

According to [27], suppose there is a continuous nonlinear system described as follows

$$\dot{x} = A(t)x + B(t)u + g(t) \tag{5-1}$$

where A(t), B(t) are the time-varying matrixes

g(t) incorporates all nonlinear terms

For discretization, the above expression needs to be integrated from time $t = t_1$ to $t = t_2$, where $t_2 - t_1 = h$ is the time step. Without losing generality, let $t_1 = kh, t_2 = (k+1)h$. Rewriting equation (5-1) as

$$\dot{x} = A(t_1)x + (A(t) - A(t_1))x + B(t)u + g(t) \tag{5-2}$$

Pre-multiplying by $\exp(-A(t_1)t)$ and defining $\Delta A = A(t) - A(t_1)$, then

$$e^{-A(t_1)t}\dot{x} - e^{-A(t_1)t}A(t_1)x = e^{-A(t_1)t}(\Delta Ax + B(t)u + g(t)) \tag{5-3}$$

$$\frac{de^{-A(t_1)t}x}{dt} = e^{-A(t_1)t}(\Delta Ax + B(t)u + g(t)) \tag{5-4}$$

Integrating the left hand side of (5-4) gives

$$\int_{t_1}^{t_2} \frac{de^{-A(t_1)t}x}{dt} d\tau = e^{-A(t_1)t}x(t)\Big|_{t_1}^{t_2} = e^{-A(t_1)t_2}x(t_2) - e^{-A(t_1)t_1}x(t_1) \tag{5-5}$$

Integrating and multiplying both sides of (5-4) by $\exp(A(t_1)t_2)$ gives

$$x(t_2) - e^{A(t_1)(t_2 - t_1)}x(t_1) = \int_{t_1}^{t_2} e^{A(t_1)(t_2-\tau)}(\Delta A(\tau)x + B(\tau)u + g(\tau))d\tau \tag{5-6}$$

Now substitute $t_1 = kh, t_2 = (k+1)h$ and denote $x_k = x(kh), A_k = A(kh)$. From (5-6) this gives

$$x_{k+1} = e^{hA_k}x_k + \int_{kh}^{(k+1)h} e^{A_k((k+1)h-\tau)}(\Delta A(\tau)x + B(\tau)u + g(\tau))d\tau \tag{5-7}$$

Defining $\Delta B(t) = B(t) - B_k$ gives

$$x_{k+1} = e^{hA_k} x_k + \int_{kh}^{(k+1)h} e^{A_k((k+1)h-\tau)} d\tau B_k u + \int_{kh}^{(k+1)h} e^{A_k((k+1)h-\tau)} (\Delta A(\tau)x + \Delta B(\tau)u + g(\tau))d\tau \tag{5-8}$$

$$= A_{d,k} x_k + B_{d,k} u + \int_{kh}^{(k+1)h} e^{A_k((k+1)h-\tau)} (\Delta A(\tau)x + \Delta B(\tau)u + g(\tau))d\tau$$

where $A_{d,k} = e^{hA_k}$ is the discrete time state transition matrix [4,27], and

$B_{d,k} = \int_{kh}^{(k+1)h} e^{A_k((k+1)h-\tau)} d\tau B_k$ is the discrete time B matrix mapping inputs to states

5.2 Discretization of the Induction Machine Model without Saturation

Adding angular speed ω as a state and re-arranging equation (2-18), (2-19) into the form of (5-1), we obtain

$$\begin{bmatrix} \dot{i}_{ds} \\ \dot{i}_{qs} \\ \dot{\lambda}_{dr} \\ \dot{\lambda}_{qr} \\ \dot{\omega}_r \end{bmatrix} = \begin{bmatrix} -\frac{r_s + \frac{L_m^2}{L_r} r_r}{L_s - \frac{L_m^2}{L_r}} & 0 & \frac{\frac{L_m}{L_r \tau_r}}{L_s - \frac{L_m^2}{L_r}} & 0 & 0 \\ 0 & -\frac{r_s + \frac{L_m^2}{L_r} r_r}{L_s - \frac{L_m^2}{L_r}} & 0 & \frac{\frac{L_m}{L_r \tau_r}}{L_s - \frac{L_m^2}{L_r}} & 0 \\ \frac{L_m}{\tau_r} & 0 & -\frac{1}{\tau_r} & 0 & 0 \\ 0 & \frac{L_m}{\tau_r} & 0 & -\frac{1}{\tau_r} & 0 \\ 0 & 0 & 0 & 0 & -\frac{1}{\tau_m} \end{bmatrix} \begin{bmatrix} i_{ds} \\ i_{qs} \\ \lambda_{dr} \\ \lambda_{qr} \\ \omega_r \end{bmatrix} + \begin{bmatrix} \frac{1}{L_s - \frac{L_m^2}{L_r}} & 0 \\ 0 & \frac{1}{L_s - \frac{L_m^2}{L_r}} \\ 0 & 0 \\ 0 & 0 \\ 0 & 0 \end{bmatrix} \begin{bmatrix} v_{ds} \\ v_{qs} \\ 0 \\ 0 \\ 0 \end{bmatrix} +$$

$$\begin{bmatrix} \frac{\frac{L_m}{L_r} \omega_r \lambda_{qr}}{L_s - \frac{L_m^2}{L_r}} \\ -\frac{\frac{L_m}{L_r} \omega_r \lambda_{dr}}{L_s - \frac{L_m^2}{L_r}} \\ -\omega_r \lambda_{qr} \\ \omega_r \lambda_{dr} \\ \frac{3}{2} b_m p' \frac{L_m}{L_r} (\lambda_{dr} i_{qs} - \lambda_{qr} i_{ds}) - b_m t_c \end{bmatrix} \tag{5-9}$$

Since in this model A_k and B_k are constant, $\Delta A(\tau), \Delta B(\tau)$ are equal to 0. By denoting A_k and B_k as A and B, equation (5-8) becomes

$$x_{k+1} = e^{hA}x_k + \int_{kh}^{(k+1)h} e^{A((k+1)h-\tau)}d\tau B + \int_{kh}^{(k+1)h} e^{A((k+1)h-\tau)}g(\tau)d\tau \tag{5-10}$$

The discretized A matrix A_d can be obtained by taking a Taylor approximation

$$A_d = e^{hA} \approx I + hA + \tfrac{h^2A^2}{2} + \tfrac{h^3A^3}{6} \tag{5-11}$$

However, for the discretized B matrix $B_d = \int_{kh}^{(k+1)h} e^{A((k+1)h-\tau)}d\tau B$, calculation of the integral is required. This can be accomplished as follows. Suppose the curve in Fig. 5.1 represents the function of e^{At}. First order estimation of the integral includes two parts. One is the shaded rectangular area and the other is the triangular area above the rectangle.

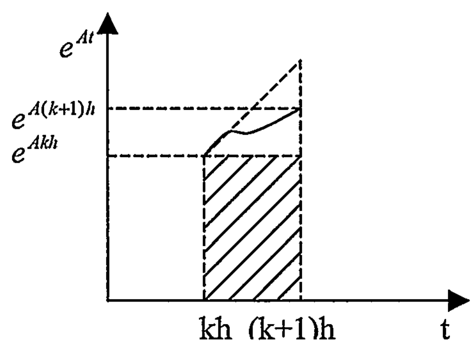

Fig. 5.1 Calculation of the integral

The area of the rectangle is he^{hA} and the area of the triangule is $\frac{1}{2}h^2(-Ae^{hA})$. Therefore the 1st order approximation of the integral becomes

$$\int_{kh}^{(k+1)h} e^{A((k+1)h-\tau)}d\tau \approx he^{hA} + \tfrac{1}{2}h^2(-Ae^{hA}) = he^{hA}(I - \tfrac{hA}{2}) \tag{5-12}$$

The same type of approximation is applied to the last integral in equation (5-10) and gives

$$\int_{kh}^{(k+1)h} e^{A((k+1)h-\tau)}g(\tau)d\tau \approx he^{hA}g(kh) + \tfrac{1}{2}h^2(g(kh)(-Ae^{hA}) + e^{hA}(\frac{\partial g(\tau)}{\partial \omega}\dot{\omega} + \frac{\partial g(\tau)}{\partial \lambda}\dot{\lambda}) \tag{5-13}$$

where the derivative of $g(t)$, $\frac{dg}{dt} = \frac{\partial g(\tau)}{\partial \omega}\dot{\omega} + \frac{\partial g(\tau)}{\partial \lambda}\dot{\lambda}$. Differentiating the nonlinear term in equation (5-9), we obtain

$$\frac{dg}{dt} = \begin{bmatrix} \dfrac{\frac{L_m}{L_r}\lambda_{qr}}{L_s - \frac{L_m^2}{L_r}}\dot{\omega}_r + \dfrac{\frac{L_m}{L_r}\omega_r}{L_s - \frac{L_m^2}{L_r}}\dot{\lambda}_{qr} \\ -\dfrac{\frac{L_m}{L_r}\lambda_{dr}}{L_s - \frac{L_m^2}{L_r}}\dot{\omega}_r - \dfrac{\frac{L_m}{L_r}\omega_r}{L_s - \frac{L_m^2}{L_r}}\dot{\lambda}_{dr} \\ -\lambda_{qr}\dot{\omega}_r - \omega_r\dot{\lambda}_{qr} \\ \lambda_{dr}\dot{\omega}_r + \omega_r\dot{\lambda}_{dr} \\ \frac{3}{2}b_m p'\frac{L_m}{L_r}(i_{qs}\dot{\lambda}_{dr} + \lambda_{dr}\dot{i}_{qs} - \lambda_{qr}\dot{i}_{ds} - i_{ds}\dot{\lambda}_{qr}) \end{bmatrix} \tag{5-14}$$

The derivatives in (5-14) can be approximately calculated with the difference of the corresponding variables between current values and previous ones divided by the sampling period h.

5.3 Discretization of the Induction Machine Model with Saturation

The model of the induction machine with saturation (2-35) to (2-39) can be rewritten as

$$\dot{x} = A^{-1}\bar{v} - A^{-1}Bx$$

$$= A^{-1}\bar{v} - A^{-1}B_1x - A^{-1}B_2x \tag{5-15}$$

where $B = B_1 + B_2$ (5-16)

$$B_1 = \begin{bmatrix} r_s & 0 & 0 & 0 \\ 0 & r_s & 0 & 0 \\ -r_r\frac{L_m}{L_r} & 0 & \frac{r_r}{L_r} & 0 \\ 0 & -r_r\frac{L_m}{L_r} & 0 & \frac{r_r}{L_r} \end{bmatrix}, \qquad B_2 = \begin{bmatrix} 0 & 0 & 0 & 0 \\ 0 & 0 & 0 & 0 \\ 0 & 0 & 0 & \omega_r \\ 0 & 0 & -\omega_r & 0 \end{bmatrix} \tag{5-17}$$

and $\bar{v} = [v_{ds} \quad v_{qs} \quad 0 \quad 0]^T$. Adding ω_r as one of the state variables gives

$$\dot{x} = \begin{bmatrix} A^{-1} & 0 \\ 0 & 0 \end{bmatrix}\begin{bmatrix} \bar{v} \\ 0 \end{bmatrix} - \begin{bmatrix} A^{-1}B_1 & 0 \\ 0 & \frac{1}{\tau_m} \end{bmatrix} x - \begin{bmatrix} A^{-1}B_2x' \\ \frac{3}{2}b_m p'\frac{L_m}{L_r}(\lambda_{dr}i_{qs} - \lambda_{qr}i_{ds}) - b_m t_c \end{bmatrix} \tag{5-18}$$

where x' is the previous state vector with 4 states. Therefore the last term of (5-18) is the nonlinear part of the model. Substituting for B_2 and x' in the last term of (5-18) gives,

$$g(t) = \begin{bmatrix} \omega_r A^{-1}(1,4)\lambda_{dr} - \omega_r A^{-1}(1,3)\lambda_{qr} \\ \omega_r A^{-1}(2,4)\lambda_{dr} - \omega_r A^{-1}(2,3)\lambda_{qr} \\ \omega_r A^{-1}(3,4)\lambda_{dr} - \omega_r A^{-1}(3,3)\lambda_{qr} \\ \omega_r A^{-1}(4,4)\lambda_{dr} - \omega_r A^{-1}(4,3)\lambda_{qr} \\ \frac{3}{2}b_m p'\frac{L_m}{L_r}(\lambda_{dr}i_{qs} - \lambda_{qr}i_{ds}) - b_m t_c \end{bmatrix} \tag{5-19}$$

Then the derivative of g(t) is

$$dg = \begin{bmatrix} \dot{\omega}_r A^{-1}(1,4)\lambda_{dr} + \omega_r A^{-1}(1,4)\dot{\lambda}_{dr} - \dot{\omega}_r A^{-1}(1,3)\lambda_{qr} - \omega_r A^{-1}(1,3)\dot{\lambda}_{qr} \\ \dot{\omega}_r A^{-1}(2,4)\lambda_{dr} + \omega_r A^{-1}(2,4)\dot{\lambda}_{dr} - \dot{\omega}_r A^{-1}(2,3)\lambda_{qr} - \omega_r A^{-1}(2,3)\dot{\lambda}_{qr} \\ \dot{\omega}_r A^{-1}(3,4)\lambda_{dr} + \omega_r A^{-1}(3,4)\dot{\lambda}_{dr} - \dot{\omega}_r A^{-1}(3,3)\lambda_{qr} - \omega_r A^{-1}(3,3)\dot{\lambda}_{qr} \\ \dot{\omega}_r A^{-1}(4,4)\lambda_{dr} + \omega_r A^{-1}(4,4)\dot{\lambda}_{dr} - \dot{\omega}_r A^{-1}(4,3)\lambda_{qr} - \omega_r A^{-1}(4,3)\dot{\lambda}_{qr} \\ \frac{3}{2}b_m p'\frac{L_m}{L_r}(\lambda_{dr}\dot{i}_{qs} + \dot{\lambda}_{dr}i_{qs} - \lambda_{qr}\dot{i}_{ds} - \dot{\lambda}_{qr}i_{ds}) \end{bmatrix} \tag{5-20}$$

5.4 Discretization of the LPV Induction Machine Model

In order to discretize the LPV model of the induction machine (2-59), simply take the term $F\omega_r x$ as g(t) and obtain

$$x_{k+1} = e^{hA}x_k + \int_{kh}^{(k+1)h} e^{A((k+1)h-\tau)}d\tau B + \int_{kh}^{(k+1)h} e^{A((k+1)h-\tau)}F\omega_r x d\tau \tag{5-21}$$

where the third term can be derived with the same method introduced previously to obtain

$$\int_{kh}^{(k+1)h} e^{A((k+1)h-\tau)}F\omega_r x d\tau = he^{hA}\omega_{rk}Fx_k + \tfrac{1}{2}h^2(w_{rk}Fx_k A(-e^{hA}) + e^{hA}(\dot{\omega}_{rk}Fx_k + \omega_{rk}F\dot{x}_k)) \tag{5-22}$$

where F is constant and derivatives of ω_k and x_k can be obtained in the same way as introduced in section 5.2.

5.5 Chapter Summary

In this chapter, the induction machine models introduced in Chapter 2 are discretized for identification purposes as well as for the eventual implementation of the identification algorithms with a microprocessor.

Chapter 6

Modelling and Simulation

The underlying research for this thesis progressed in several stages. First continuous-time induction machine models were simulated and verified. Then Field Orientation Control (FOC) of the induction machine was designed and tested based on the simulation model of the induction machine. In the simulation of FOC, two control methods were applied: open loop and closed loop. The impacts of variations in the parameters of the induction machine on the performance of the FOC system were also studied, providing the motivation of this project. The third stage was to take account of saturation effects in the induction machine model. The next stage was the discretization of the induction machine models both with and without saturation, as well as the discretization of the induction machine LPV model used as a candidate model to identify rotor fluxes of the induction machine. The next stage shown in Chapter 7, was to identify and validate the LPV model of the induction machine.

In this chapter, modelling and simulation results are discussed in detail including model verification, field orientation control, the effect of saturation and model discretization. All the simulations are carried out by employing S-Functions in Simulink, the dynamic system simulator for MATLAB from The MathWorks Inc. Details on the use of S-Functions are available elsewhere [39].

6.1 Simulation of the Induction Machine Model without Saturation

The simulation of the induction machine without saturation is carried out in Simulink with an S-Function based on the model (2-18) and (2-19). The model represents a 1-kW induction motor with parameters listed in Table 6-1 [2].

Table 6-1 Induction Machine Parameters

parameters	Values
τ_r	0.07697s
R_s	4.64191 Ω
L_s	0.14392 H
L_r	0.14392 H
L_m	0.1375 H
J_m	0.00657 Nm s^2
f_c	0.04397 Nm
f_v	0.0003383 Nms
p'	1

Note that for all simulation results presented in this thesis, the induction machine is operated with no load. From a controller perspective, the no load condition represents a more difficult control problem than is the case for a loaded machine. However, from an identification perspective, the no load condition presents an opportunity to capture the higher frequency dynamics of the induction machine.

In the S-Function, the scaled rotor flux linkages $\hat{\lambda}_r = \frac{L_m}{L_r}\lambda_r$ instead of λ_r are chosen as the last two state variables. Thus (2-18) becomes

$$\begin{bmatrix} v_{ds} \\ v_{qs} \\ 0 \\ 0 \end{bmatrix} = \begin{bmatrix} r_s + \frac{L_m^2 r_r}{L_r^2} + (L_s - \frac{L_m^2}{L_r})p & 0 & -\frac{1}{\tau_r} & -\omega_r \\ 0 & r_s + \frac{L_m^2 r_r}{L_r^2} + (L_s - \frac{L_m^2}{L_r})p & \omega_r & -\frac{1}{\tau_r} \\ -\frac{L_m^2}{\tau_r L_r} & 0 & \frac{1}{\tau_r} + p & \omega_r \\ 0 & -\frac{L_m^2}{\tau_r L_r} & -\omega_r & \frac{1}{\tau_r} + p \end{bmatrix} \begin{bmatrix} i_{ds} \\ i_{qs} \\ \hat{\lambda}_{dr} \\ \hat{\lambda}_{qr} \end{bmatrix} \qquad (6\text{-}1)$$

and (2-22) becomes

$$t_m = \tfrac{3}{2} p'(i_{qs}\hat{\lambda}_{dr} - i_{ds}\hat{\lambda}_{qr}) \qquad (6\text{-}2)$$

As an initial test of the model, we apply a three-phase voltage input to the model's stator terminals; this is often referred to in industry as a cold start. For $t \geq 0$

$$v_a = 120 * \sin(50 * 2\pi * t)$$

$$v_b = 120 * \sin(50 * 2\pi * t - 2\pi/3)$$

$$v_c = 120 * \sin(50 * 2\pi * t - 4\pi/3)$$

The three-phase voltage is transformed into a two-phase representation as in (6-1), i.e., the S-Function is written in terms of the d-q voltages. In Fig. 6-1, shown for a cold start are, (a) stator currents, (b) rotor fluxes, and (c) the rotor velocity and torque. In Fig. 6-1 (a) and (b), the lower figures are the zoomed-in variables of the q-axis. Note that the steady state values of the stator currents, rotor fluxes, rotor velocity and the torque for the cold start simulation agree with traditional steady state calculations [11].

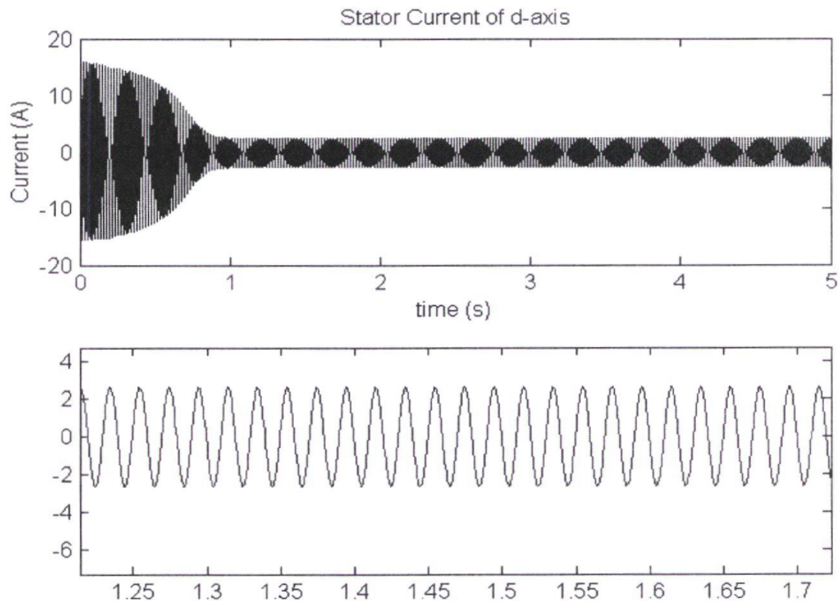

(a) stator currents

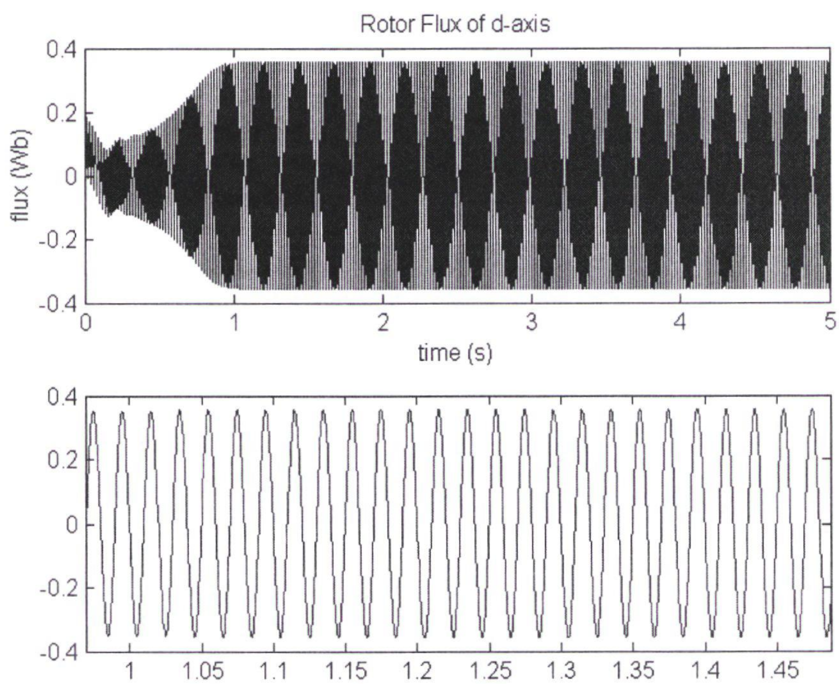

(b) rotor fluxes

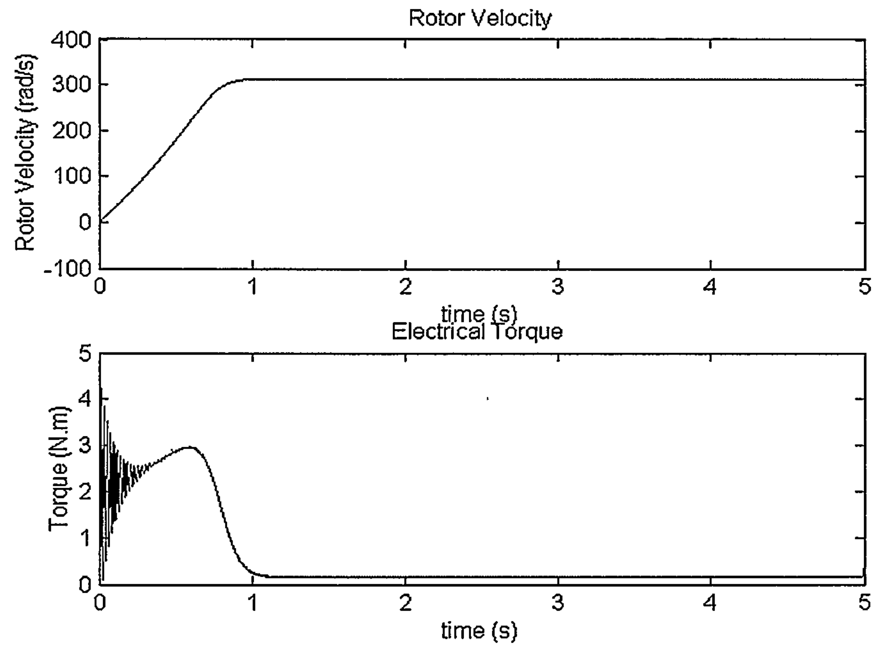

(c) rotor velocity and torque

Fig. 6-1 Cold start stator currents, rotor fluxes, rotor velocity and torque

A further test of the S-Function model is carried out by using a simulated Pulse Width Modulation (PWM) inverter to control the induction machine [23]. The method (commonly) employed to generate the output of a PWM inverter is to compare the (continuous time) input signal with a much higher frequency and slightly higher amplitude triangle wave signal. When the triangle signal is smaller than the input, the inverter outputs a positive DC voltage; when the triangle signal is larger than the input, the inverter outputs a negative DC voltage. In the actual simulation, 1 and –1 are the outputs corresponding to positive DC voltage and negative DC voltage respectively. Then DC voltage is multiplied to the result to obtain the PWM inverter output.

For our test, we generated a triangle wave signal whose amplitude was 1.1 times, and whose frequency was 10 times, that of the sinusoidal input. With this triangle signal, the PWM inverter output signal is generated as in Fig. 6.2. The resulting stator current and the corresponding torque are presented in Fig. 6.3. The large steady state torque pulsations are related to the non-sinusoidal components of the PWM voltage input.

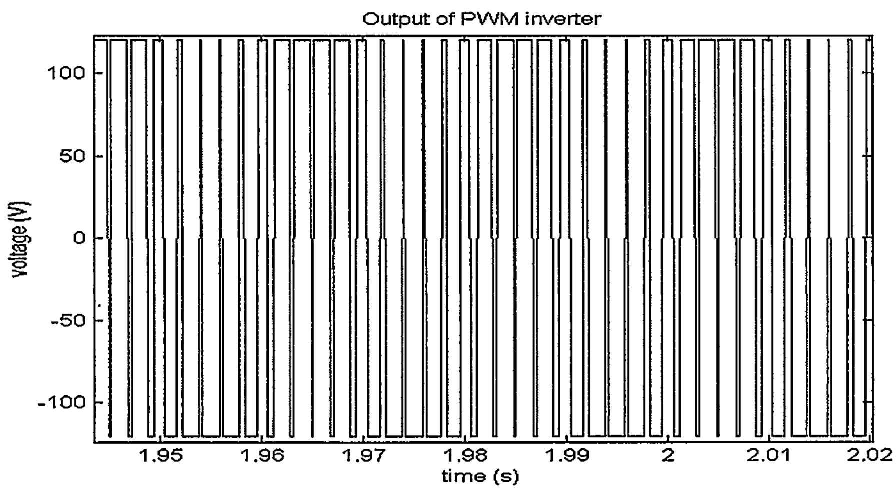

Fig. 6.2 Output signal of PWM inverter

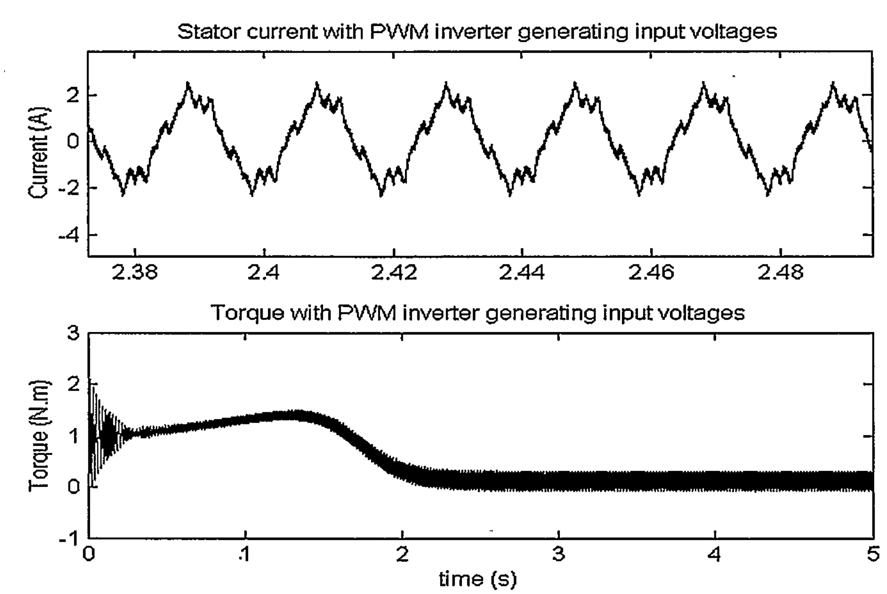

Fig. 6.3 Stator current and torque with PWM inverter as the source

From Fig. 6.3, we can tell that the PWM inverter introduces much higher frequency terms in both stator currents and the torque. Also it takes more time to reach the steady state in the PWM inverter case as shown in Fig. 6.4.

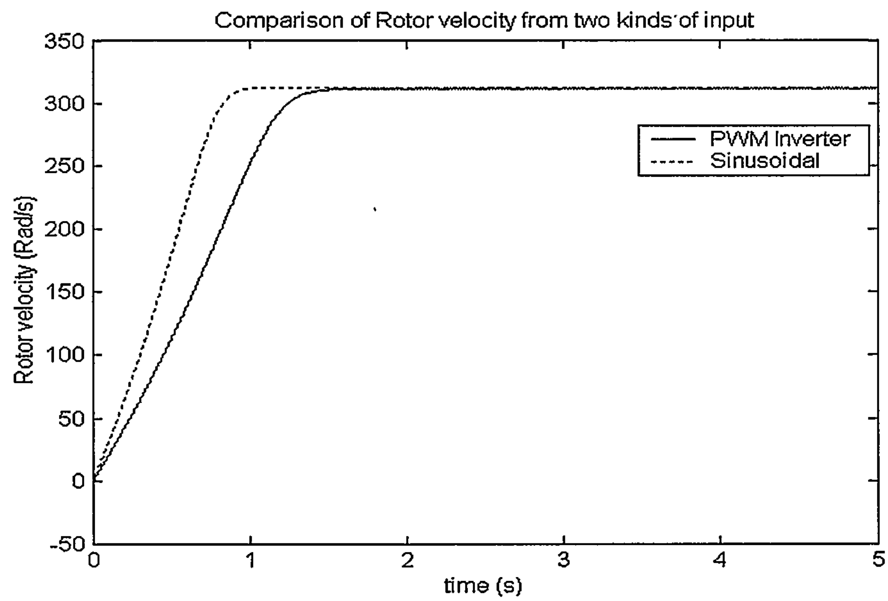

Fig. 6.4 Comparison of rotor velocity

6.2 Simulation of the Induction Machine Model with Saturation

The saturated induction machine model is simulated with equations (2-35) to (2-39). The key to introducing the saturation effect is the application of a dynamic inductance, L, and a static inductance, L_m, defined by (2-29), (2-30), respectively. According to the simplified saturation model represented by the dashed line in Fig. 2.1, the dynamic inductance L is equal to the static inductance L_m when the magnetizing current is less than that of point b. When the magnetizing current is larger than that of point b, the magnetic flux λ_m remains constant, equal to the magnetic flux at point b λ_{mb}. In this case according to (2-29) and (2-30),

$$L = 0 \tag{6-3}$$

$$L_m = \frac{\lambda_{mb}}{i_m} \tag{6-4}$$

Therefore, before simulating the saturated model, the rated magnetizing current and flux corresponding to point *b* must be obtained.

The simulated induction machine is a 1kW two pole induction machine with a rated input frequency of 50Hz. The rated torque can be calculated as follows:

$$T_{rated} = \frac{P}{\omega_r} \times p' \tag{6-5}$$

Taking the rated slip as 0.06,

$$T_{rated} = \frac{1000}{50 \times 2\pi \times 0.94} \times 1 = 3.4 \text{ N·m}$$

Applying the rated voltage with a peak value of 169.7 V and load torque 3.4 N·m, we can calculate the rated magnetizing current $i_m = 3.166$ A and the corresponding flux linkage $\lambda_{mb} = 0.4159$ Wb.

Now we apply the sinusoidal voltages with a peak value of 200V, which is larger than rated, to the models with and without saturation. By comparing the rotor fluxes from the two models in Fig. 6.5, we can see that the flux of the saturated model remains constant beyond the rated point while the flux of the model without saturation continues to increase.

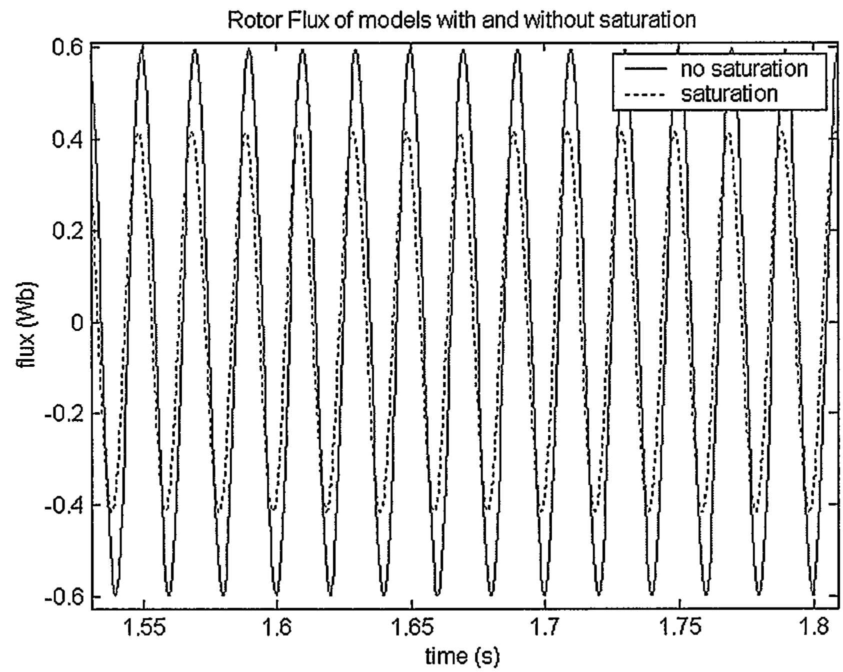

Fig. 6.5 Comparison of rotor flux with and without saturation

6.3 Simulation Results of Field Orientation Control

As indicated in Chapter 3, indirect Field Orientation Control of an induction machine is the implementation approach with which this thesis is concerned. For an open-loop control method, the reference rotor flux and torque are set to generate the command stator currents used to control the induction machine as shown in the Simulink model in Appendix B.1. If a closed-loop control method is applied, the actual rotor flux and torque are required for comparison with the reference ones to generate the stator currents that perform the control. In the simulink model shown in Appendix B.2, a closed-loop controller for rotor velocity is used and the flux control loop is kept open.

In order to compare the performance of FOC with cold start performance, the rotor flux magnitude 0.356Wb in Fig. 6.1 (b) and the rotor speed 312.7 rad/s in Fig. 6.1 (c) are set as the reference values. As shown in Fig. 6.6, the dynamic response of FOC has a much faster rising time than that of a cold start while the overshoot is a little bigger and the settling time is longer.

However the disadvantage of indirect FOC, as indicated in section 3.3.2, is the sensitivity to variations of induction machine parameters. The parameters change widely with the environmental temperature, frequency and current amplitude. We take rotor resistance as an example to investigate the impact of parameter variations on the generation of torque in FOC.

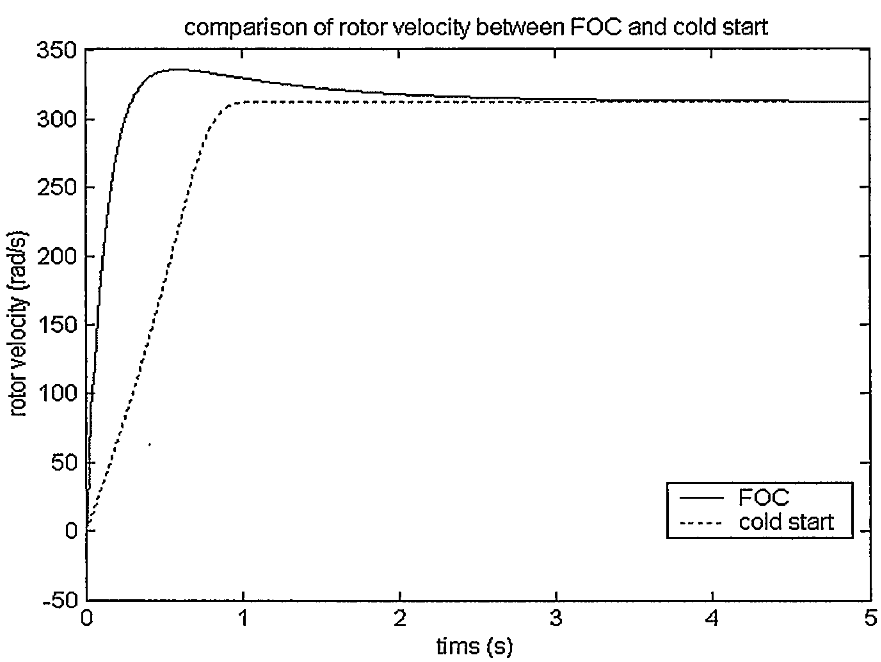

Fig. 6.6 Comparison of rotor velocity of FOC and cold start

Let R_{ra} denote the actual rotor resistance of an induction machine while R_{rn} denotes the value of rotor resistance as derived from nameplate data that is used in FOC. The ratio between the two values is

$$kr = \frac{R_{ra}}{R_{rn}} \tag{6-6}$$

The open-loop model in Appendix B.1 is used to perform the investigation. First a reference value of torque is set to 2 N·m, ie about half the rated value. Then simulations are performed with kr = 1 (i.e. $R_{ra}=R_{rn}$), kr = 2 and kr = 0.5. As shown in Fig. 6.7, the variations of rotor resistance cause considerable errors in torque generation, hence deteriorating the dynamic performance of FOC. Therefore it is essential to perform identification to alleviate the influence of induction machine parameter variations.

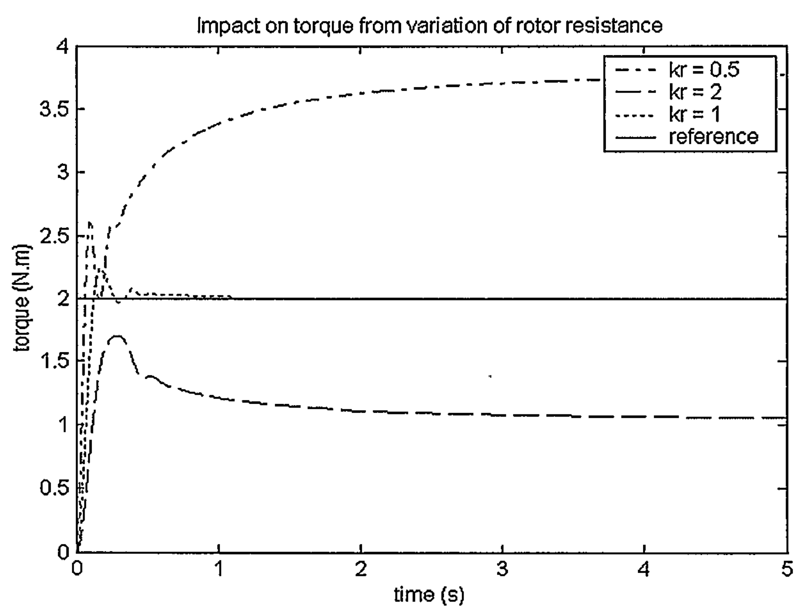

Fig. 6.7 Impact on torque from variation of rotor resistance

To make the FOC simulation more realistic, a PWM inverter is utilized to control the induction machine. Unlike the cold start case, however, the PWM signal cannot be generated through comparison between a sinusoidal signal and a triangle wave since the input stator voltages are produced instantaneously according to the reference values of torque and flux. Therefore, the principle that two voltage signals with the same value of volt-second product are equivalent is applied to generate the PWM signals, as shown in Fig. 6.8.

In Fig. 6.8, t_k, t_{k+1} are the sampling points of time. $v_s(t_k)$ is the command stator voltage at time t_k and V_{dc} is the voltage of the DC link. The idea is to find out the turn-off time t_{off} so that the areas of the two shaded rectangles are equal. That means:

$$V_{dc}(t_{off} - t_k) = v_s(t_k)(t_{k+1} - t_k) \tag{6-7}$$

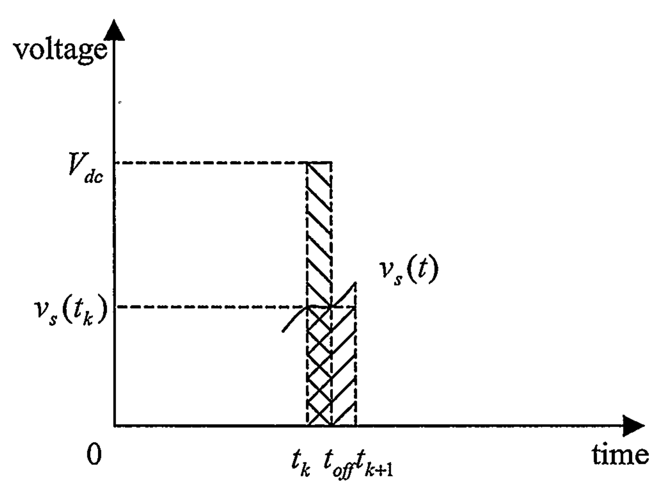

Fig. 6.8 The principle of PWM signal generation

The open-loop model in Appendix B.1 is used with the same reference values for rotor flux and rotor speed as in Fig. 6.6. Therefore we choose the switching frequency as 1kHz, i.e. the switching period is 0.001s. The simulation step is 0.00004s, i.e. 25 steps in one switching period. The DC link voltage is selected as 120V. The calculation of pulse width is carried out in the S-Function.

In Fig. 6.9, we can see that the dynamic performance of the model with a PWM inverter is a little worse than that of the model without it, such as a longer rising time and a larger overshoot. This is expected as the inverter operation introduces a delay into the system.

The width of pulses in the PWM signals varies according to the command input voltage as illustrated in Fig. 6.10. Also the line voltage between phase a and phase b is presented in Fig. 6.10. We can see that the line voltages of PWM inverters resemble sinusoidal signals more than the individual phase voltages do.

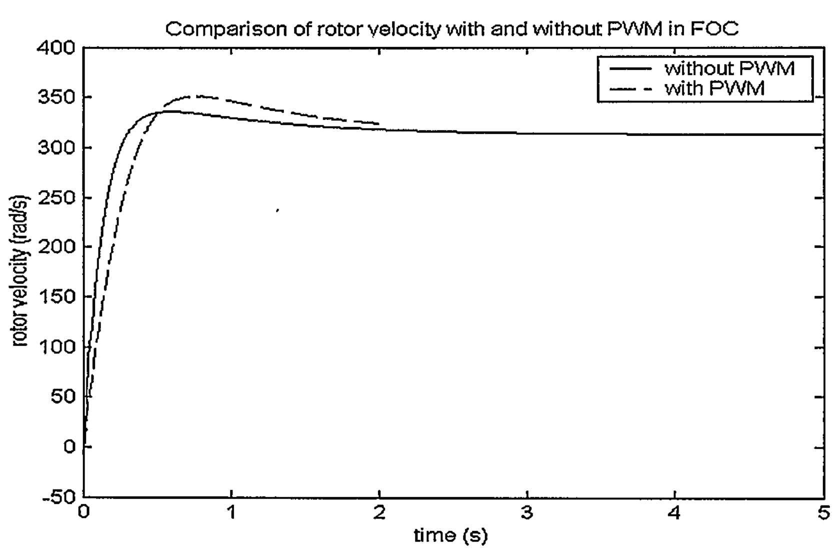

Fig. 6.9 Comparison of rotor velocity with and without PWM in FOC

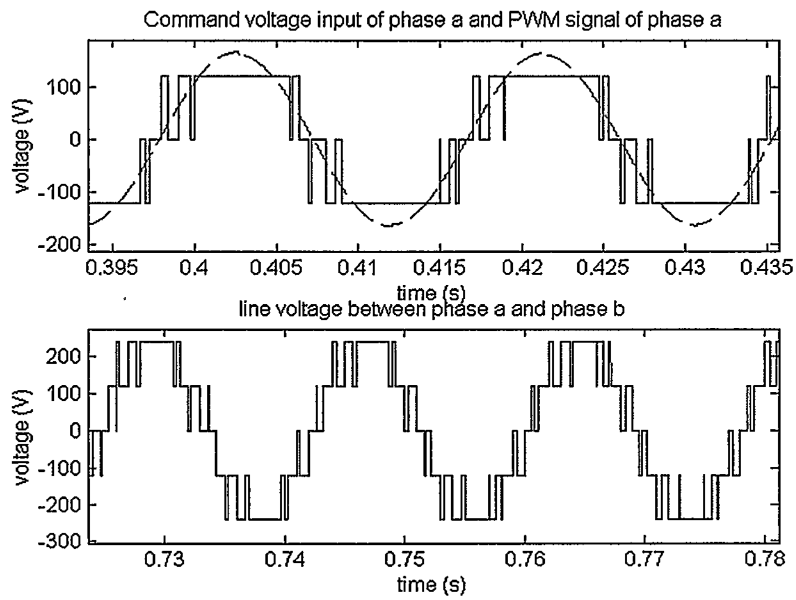

Fig. 6.10 Upper: Command voltage input of phase *a* and the corresponding PWM signal; Lower: Line voltage between phase *a* and phase *b*

6.4 Bilinear Model Simulation

As shown in Section 2.5, an induction machine can be described with a bilinear model or a linear parameter-varying (LPV) model. To verify the applicability of these models for induction machines, a bilinear Simulink model and a LPV Simulink model were designed to simulate induction machines, where the rotor velocity has been added as one of the input variables. As expected, exactly the same stator currents and rotor fluxes are obtained as with the model taking the rotor speed as a state variable. Note that taking the rotor speed as an input variable is just a technique to make the identification easier. Actually we cannot adjust the rotor speed independently for identification purposes. It can either be measured in practice or be obtained via simulation.

6.5 Simulation of Discretized Models

In the simulation of continuous models, the time step varies and is determined by Simulink according to dynamic characteristics of the simulated model. However the time step is fixed for discretized models. From the derivation of discretized models in Chapter 5, we can tell the impact of the time step on the accuracy of the simulation results. The larger the time step is, the more considerable the error introduced by discretization is.

In Fig. 6.11, a three phase sinusoidal voltage signal, i.e. same cold start input as in Section 6.2, is used as the input to the discretized model. As the time step increases, the error in rotor velocity, as compared to that from the continuous model, increases accordingly.

The simulation result of the discretized model for the saturated induction machine is represented in Fig. 6.12. A three phase sinusoidal signal with peak value of 200V is applied to excite saturation effects in the model. Due to the error from discretization, the integral of the generated torque of the simulation with a small time step, 0.1ms, is larger than that of the simulation with a larger time step, 1ms. Therefore the steady state of the rotor velocity for the simulation with small time step is a little bigger.

For the discretized LPV model, if the time step is 0.1ms, the stator currents and the rotor fluxes are almost the same as those of the continuous LPV model. Fig. 6.13 presents the comparison of d-axis stator currents for the discretized LPV model with the time step 1ms and 0.1s.

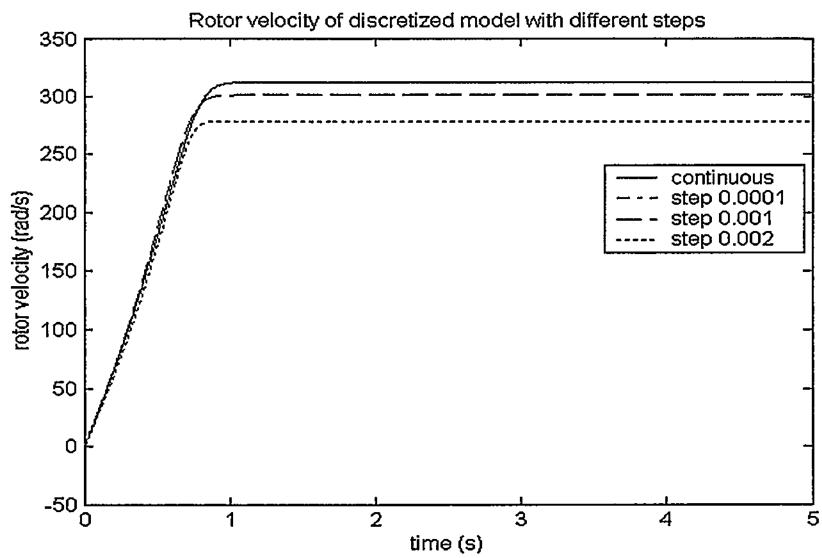

Fig. 6.11 Comparison of rotor velocity for different steps

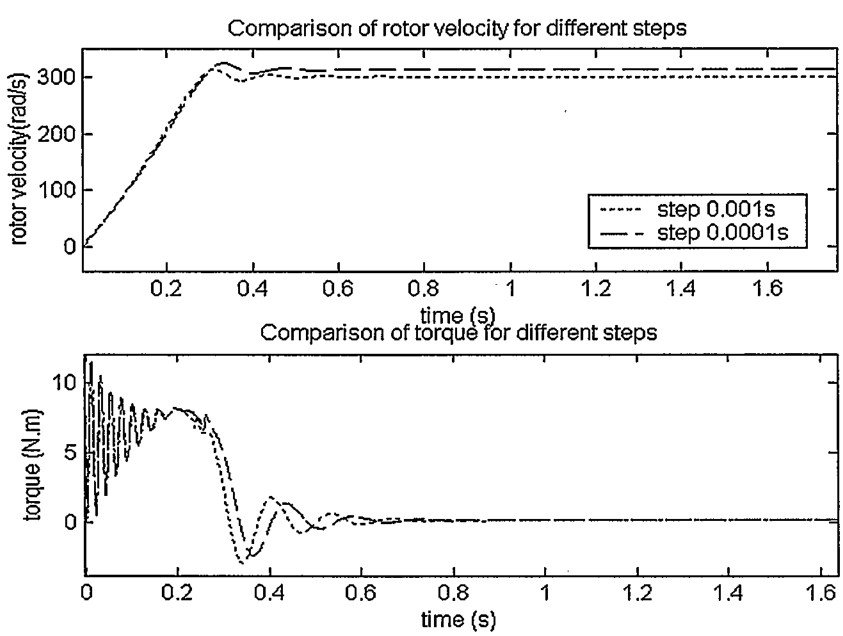

Fig. 6.12 Comparison of rotor velocity and torque for discretized saturation model with different steps

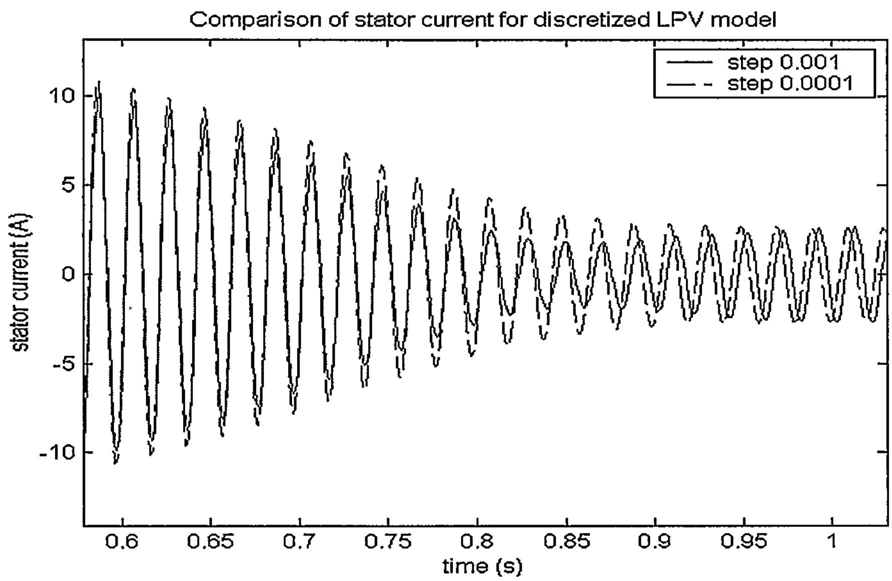

Fig. 6.13 Comparison of stator current for discretized LPV model

6.6 Chapter Summary

Chapter 6 presents some simulation results about induction machines including cold start and PWM inverter drive simulation. We have verified that a rotor resistance error in a FOC system can produce a large error in torque command tracking. The model with magnetic saturation is also simulated. Simulation results of all the discretized models with different time steps illustrate the influence of time step size in the accuracy of the discretized simulation. As a rule of thumb, we have shown that a time step of at most 1ms should be employed to achieve reasonable accuracy.

Chapter 7

Identification and Validation

In this chapter, system identification methods are applied to data obtained from the simulation models described in Chapter 6, and the results discussed. First, a linear system was created by taking the products of rotor velocity and rotor fluxes as inputs. Since the system was linear, we used the toolbox SMI2.0 [16] to identify the model. Next, an LPV description was identified using full state measurements. We then showed that the rotor fluxes could not be reliably estimated using only stator currents and rotor velocity measurements. This suggested that a new measurement should be introduced to assist with the identification of rotor fluxes. Hence we proposed the use of the time derivative of rotor velocity to obtain the optimized estimation of the rotor flux components.

7.1 Subspace Identification of an Induction Machine with the Products of Rotor Velocity and Rotor Fluxes as Inputs

Based on the algorithms presented in Section 4.2, the subspace method identification toolbox (SMI 2.0) was developed [16]. However since this toolbox is designed for linear system identification, it cannot be applied directly to identify induction machines. As indicated in Chapter 2, nonlinearity is encountered in the model of an induction machine in terms of the product of the rotor speed and the rotor fluxes. In order to make sure that the product of the rotor speed and the rotor fluxes is the only significant nonlinear component in the discretized model of induction machines, we assume for simulation purposes that this product could be measured. Although it is not practical to directly measure the products of rotor velocity and flux components, it is still very useful to employ these products in simulation to determine the significance of the rotor velocity and flux product nonlinearity. In this case, the model of the induction machine (2-54) becomes:

$$\begin{bmatrix} \dot{i}_{ds} \\ \dot{i}_{qs} \\ \dot{\lambda}_{dr} \\ \dot{\lambda}_{qr} \end{bmatrix} = \begin{bmatrix} -\dfrac{r_s + \frac{L_m^2}{L_r} r_r}{L_s - \frac{L_m^2}{L_r}} & 0 & \dfrac{\frac{L_m}{L_r \tau_r}}{L_s - \frac{L_m^2}{L_r}} & 0 \\ 0 & -\dfrac{r_s + \frac{L_m^2}{L_r} r_r}{L_s - \frac{L_m^2}{L_r}} & 0 & \dfrac{\frac{L_m}{L_r \tau_r}}{L_s - \frac{L_m^2}{L_r}} \\ \frac{L_m}{\tau_r} & 0 & -\frac{1}{\tau_r} & 0 \\ 0 & \frac{L_m}{\tau_r} & 0 & -\frac{1}{\tau_r} \end{bmatrix} \begin{bmatrix} i_{ds} \\ i_{qs} \\ \lambda_{dr} \\ \lambda_{qr} \end{bmatrix} + \mathrm{B}^*\mathrm{u} \qquad (7\text{-}1)$$

where $$B = \begin{bmatrix} \dfrac{1}{L_s - \frac{L_m^2}{L_r}} & 0 & 0 & \dfrac{\frac{L_m}{L_r}}{L_s - \frac{L_m^2}{L_r}} \\ 0 & \dfrac{1}{L_s - \frac{L_m^2}{L_r}} & -\dfrac{\frac{L_m}{L_r}}{L_s - \frac{L_m^2}{L_r}} & 0 \\ 0 & 0 & 0 & -1 \\ 0 & 0 & 1 & 0 \end{bmatrix} \text{ and } u = \begin{bmatrix} v_{ds} \\ v_{qs} \\ \omega_r \lambda_{dr} \\ \omega_r \lambda_{qr} \end{bmatrix}$$

In order to make the exciting inputs richer than sinusoidal signals, three chirp voltage signals with 120 degrees of phase difference between each other are applied as inputs to stimulate the induction machine dynamics. The frequency range of the chirp signals is from 30 Hz to 50 Hz, and the frequency ramps up over a five second period (this will likely be possible in practice by utilizing the appropriate modulating signals in a PWM inverter drive). In the simulation, the products of the rotor velocity and rotor fluxes are calculated. Using the stator voltages and the products of rotor velocity and rotor fluxes as inputs and the stator currents as outputs, we used the SMI2.0 toolbox to identify the model (7-1) and obtained the results shown in Fig. 7.1.

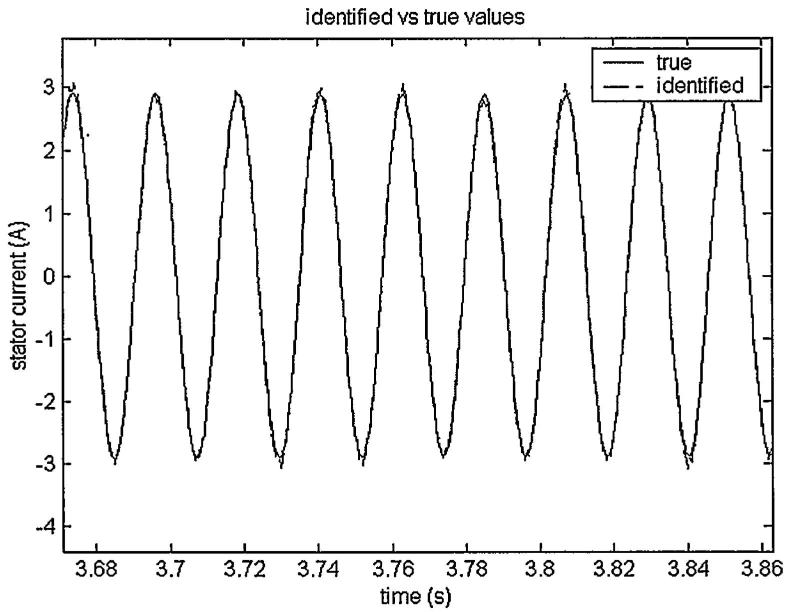

Fig. 7.1 Comparison of true stator d-axis current with the identified current

For a quantitative indication of how close the true signal and its estimate resemble each other, the Variance-Accounted-For (VAF) figure-of-merit is calculated as follows [16]:

$$VAF = 1 - \frac{\text{variance}(y - y_{est})}{\text{variance}(y)} \times 100\% \tag{7-2}$$

For the case above, the VAFs of the d-axis and q-axis stator currents are 99.7% and 99.8% respectively. Note that for validation purposes all the VAFs in this thesis were obtained through a separate data set from the one used in the identification process.

The results of identification using SMI2.0 strongly suggest that the primary nonlinearity of the induction machine model involves the products of the rotor velocity and the rotor fluxes. Therefore we can represent the induction machine model with an LPV system model, using the rotor speed as the varying parameter.

7.2 LPV System Identification with Full State Measurements

All remaining results presented in this chapter were obtained using a pre-release copy of the LPV toolbox developed by V. Verdult [42]. However, our induction motor model (c.f. section 2.5) is not suitable for standard LPV representation, therefore it was necessary to modify Dr.Verdult's toolbox, such that only a portion of the full state is employed in the update equation (4-26).

A well-designed input is essential to the success of the identification process. After trying a variety of types of inputs, the white noise signal is finally chosen as the input signal to perform identification of the induction machine. Although it does not seem practical to apply pure white noise signals to real induction machines, it is still a good choice in the simulation stage due to its property of Persistence of Excitation. However, it is possible to superimpose a noise signal on a practical input for experimental identification.

Using the white noise signals as inputs to simulate induction machine operation, we obtain results of stator currents, rotor fluxes and the rotor speed presented in Fig. 7.2.

In this section, the white noise voltages are the inputs, the rotor speed is to be measured and is used as the linear varying parameter in the LPV model of the induction machine. We also suppose that we are able to obtain the measurements of all the state variables in the LPV model, the two stator currents in d-q axis representation and the two rotor fluxes in d-q axis representation. Our ultimate goal is to identify the rotor fluxes with measurements of stator voltages as inputs and stator currents as outputs only. However identifying the LPV model of an induction machine with full state measurements is a good start.

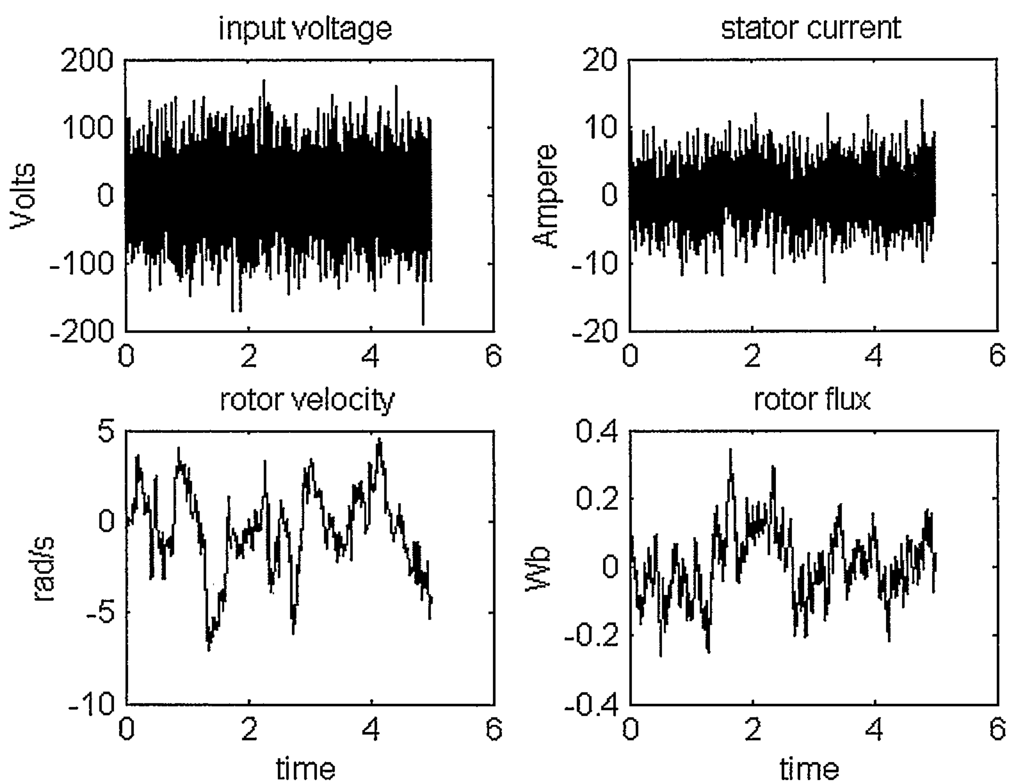

Fig. 7.2 White noise inputs and corresponding outputs

Before identifying with the full state measurements, we need to check the input signals and the output signals to make sure that they are suitable for identification.

First we observed that the values of the rotor fluxes are too small compared with the values of the stator currents. Therefore scaling was required to make sure that the identification algorithm puts equal weights on the rotor fluxes and the stator currents. Comparing the values of the two sets of quantities, we applied a multiplication factor of 40 to the rotor fluxes.

The other issue is the power-up transient. Since the system is not in the steady state, the data obtained in the power-up transient probably contains information inconsistent with that from the data in steady state. Therefore the data should be truncated to remove the transient. In our case, the first 6000 points of both the inputs and the outputs are cut off, corresponding to about ¼ second of the start-up time.

With the scaled and truncated data of inputs and outputs, the LPV nonlinear identification toolbox [42] can be used to identify the stator currents and the rotor fluxes shown in Fig. 7.3.

As presented in Fig. 7.3, the identified rotor flux fits the true rotor flux quite well. A quantitative analysis in this case gives,

$$\mathrm{VAF} = 95.4\%$$

At the same time, the VAF of the stator current estimation is also high, 84.9% (figure not shown).

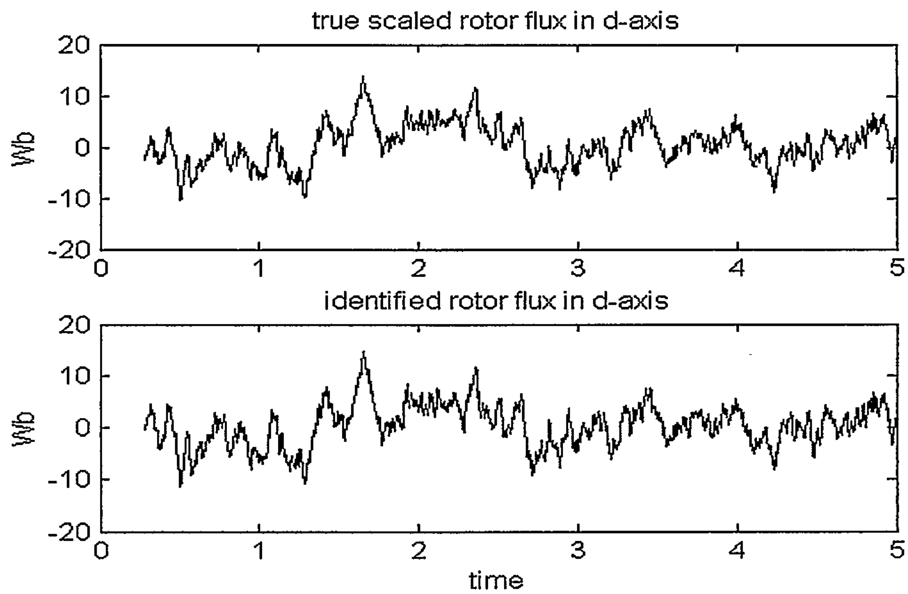

Fig. 7.3 Identified rotor flux with full state measurements

7.3 Stator Current Identification with a Second Order LPV Model

As we noticed in Fig. 7.2, the values of rotor fluxes are much smaller than the values of stator currents. This begs the question: How significant are the rotor fluxes in the evolution of the states of stator currents? In order to determine the significance of rotor fluxes, we identify the stator currents with a second order LPV model using stator currents as the inputs and stator voltages as the outputs. The result is shown in Fig. 7.4.

When designing this test, we expected that if there was a lot of correlation between stator currents and rotor fluxes, it would not be possible to identify stator currents quite well with a second order LPV model without measuring the rotor fluxes. If so, then a higher-order model could be expected to include information for the rotor fluxes in its state vector and we can identify rotor fluxes with measurements of stator currents only.

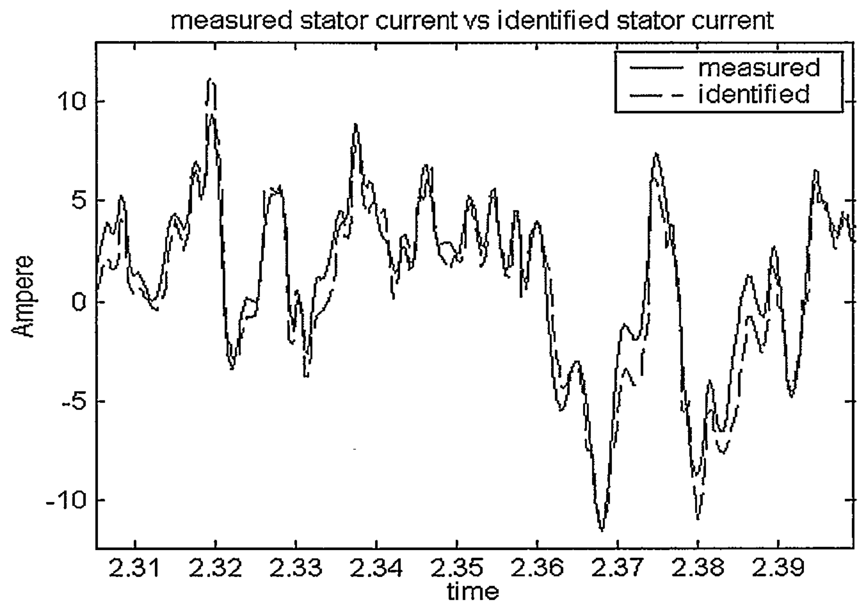

Fig. 7.4 Measured stator current and identified stator current
VAF = 88.1%

Unfortunately the stator currents identified even with the second order LPV model are quite similar to the measured values. The VAF of this estimation is 88.1%, even better than the counterpart of the identification result with a fourth order model. From the result of this test, we conclude that rotor fluxes are difficult to estimate given only stator current measurements. This indicates that more information has to be introduced to complete the flux identification task.

7.4 Identification of Rotor Fluxes with the Assistance of $\dot{\omega}$

In order to estimate rotor fluxes from the measurements of stator currents, we need to introduce another known variable to link the two together. After reviewing the induction machine model in Chapter 2 we considered that $\dot{\omega}$ might be suitable for this purpose.

The equation for $\dot{\omega}$ is obtained by substituting (2-20) to (2-23) into (2-19), or for convenience

$$\dot{\omega} = -\frac{\omega f_v}{J_m} + \frac{p'}{J_m}(\tfrac{3}{2}p'\frac{L_m}{L_r}(i_{qs}\lambda_{dr} - i_{ds}\lambda_{qr}) - f_c \operatorname{sgn}(\omega)) \tag{7-3}$$

Obviously, in practice it is difficult to measure $\dot{\omega}$ even though it is possible to calculate it from $\omega(t)$. However we still can suppose that $\dot{\omega}$ is measurable and known for identification purposes. Employing (7-3), $\dot{\omega}$ can be obtained by the simulation, and is shown in Fig. 7.5 for the white noise input data.

Here $\dot{\omega}$ is used to optimize the identified LPV model and thus provide an accurate estimation of rotor fluxes. In the LPV nonlinear identification toolbox [42], the nonlinear optimization is completed by performing a gradient search known as the Levenberg-Marquardt algorithm in the local parameter space surrounding the model estimated by the subspace identification methods [31]. Therefore to incorporate $\dot{\omega}$ into the nonlinear optimization, what is needed is to calculate the gradient of $\dot{\omega}$ with respect to the local parameter space denoted by θ_l. From (7-3), we can obtain the gradient of $\dot{\omega}$ as follows

$$\frac{\partial\dot{\omega}}{\partial\theta_l} = \frac{3}{2}\frac{p'^2}{J_m}\frac{L_m}{L_r}(i_{qs}\frac{\partial\lambda_{dr}}{\partial\theta_l} + \lambda_{dr}\frac{\partial i_{qs}}{\partial\theta_l} - i_{ds}\frac{\partial\lambda_{qr}}{\partial\theta_l} - \lambda_{qr}\frac{\partial i_{ds}}{\partial\theta_l}) \tag{7-4}$$

Taking the scaling of rotor fluxes into consideration, (7-4) becomes

$$\frac{\partial\dot{\omega}}{\partial\theta_l} = \frac{3}{2}\frac{1}{40}\frac{p'^2}{J_m}\frac{L_m}{L_r}(i_{qs}\frac{\partial\lambda_{dr}}{\partial\theta_l} + \lambda_{dr}\frac{\partial i_{qs}}{\partial\theta_l} - i_{ds}\frac{\partial\lambda_{qr}}{\partial\theta_l} - \lambda_{qr}\frac{\partial i_{ds}}{\partial\theta_l}) \tag{7-5}$$

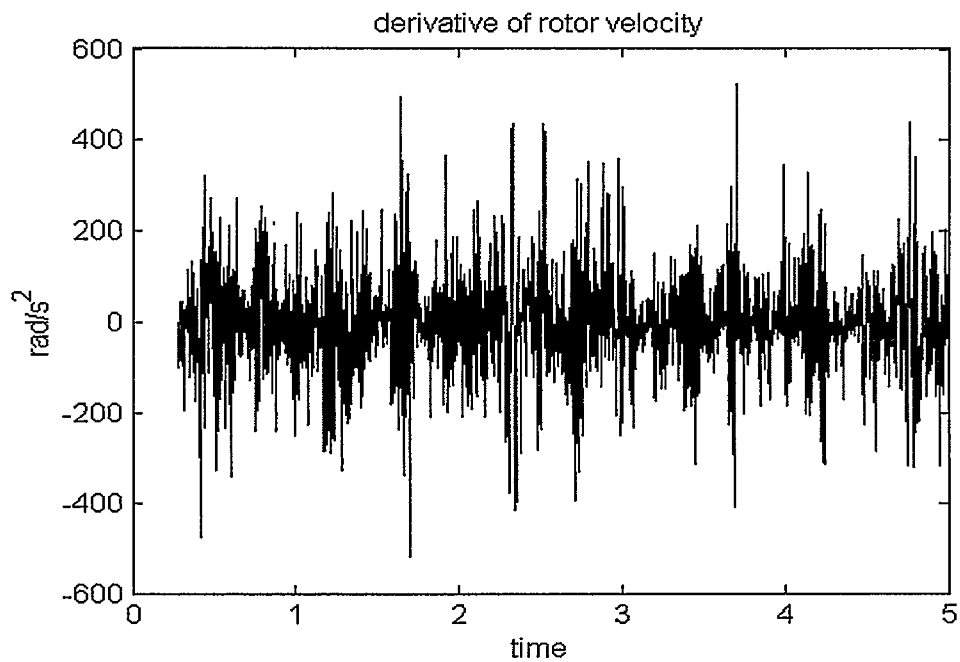

Fig. 7.5 The derivative of the rotor velocity $\dot{\omega}$

In the nonlinear optimization with a gradient search method, it is of paramount importance to obtain a good initial starting point of θ_l. Otherwise the gradient search process is easily stuck in a local minimum. In our case, the identified model obtained in section 7.2 provides a good initial starting point for optimization. After the optimization process, rotor fluxes are estimated with a relatively high accuracy as shown in Fig. 7.6. The VAF of the estimated rotor fluxes is 70.9%. Although this is a reasonably accurate result, indicating that our proposed approach has merit, it would be desirable to obtain a higher VAF.

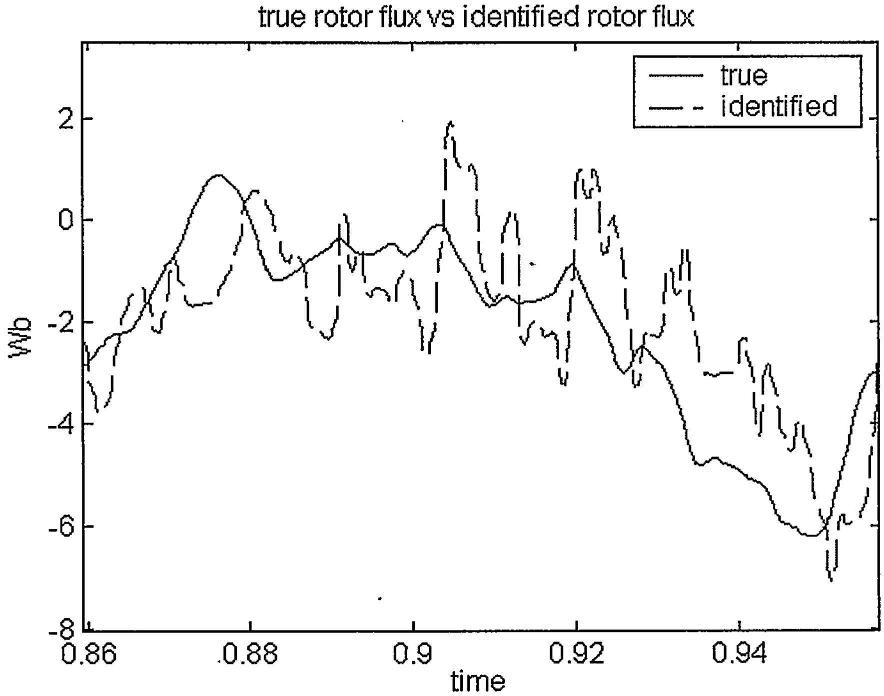

Fig. 7.6 Identified rotor flux after optimization

7.5 Chapter Summary

Identification results of rotor fluxes with the subspace identification method and nonlinear optimization are presented. Although the identification method is still premature, the positive identification results reveal the potential of the proposed use of $\dot{\omega}$ in the identification of rotor fluxes in induction machines.

Chapter 8

Conclusions and Future Work

8.1 Conclusions

The objective of this thesis is to identify a model of an induction machine that can predict its rotor flux in order to alleviate or even eliminate the impact from variations of induction machine parameters upon the performance of the field orientation motor drive system. In the process we have not only presented a proof-of-concept identification method, but we have also presented novel induction machine representations in continuous and discrete time.

To perform field orientation control, coordinate transformations are required to transform AC variables of the induction machine to DC ones in the d-q frame to be used by the controller. The resulting command inputs achieved in the controller have to be transformed back to AC variables to perform the control to the induction machine. These transformations are discussed in Chapter 3 and the sensitivity to variations of induction machine parameters is also studied. To extend the applicability of the identification algorithm, saturation effects are taken into consideration in the model of the induction machine. Basic principles of subspace identification, and a technique for LPV identification are reviewed in Chapter 4. In Chapter 5 all the models are discretized for identification purposes and to assist eventual implementation of the algorithm with a microprocessor or digital signal processor. In Chapter 6 the discretized models are presented along with preliminary simulation results to verify the accuracy of the proposed models. An LPV system model was proposed and found to be most suitable to describe the induction machine. Therefore a subspace identification method for LPV systems is chosen to identify the rotor flux by using the angular velocity ω_r as the varying parameter. The simulation results in Chapter 7 show that if the derivative of the angular velocity ω_r is known then the rotor flux can be identified with the proposed LPV system identification approach.

In summary, the original contribution of this thesis includes:

1. Proposal of a continuous time induction machine model with LPV representation (c.f. equations (2-59))
2. Discretization of different models of induction machines (Chapter 5)
3. Introduction of a novel method for estimation of rotor fluxes with subspace identification (Chapter 7)
4. Application of $\dot{\omega}$ to assist in the identification of rotor fluxes (Section 7.4)

8.2 Future Work

Some suggestions for future work are:

1) An investigation of the derivative calculation for the angular velocity to make the algorithm more practical,

2) Optimization of the identification algorithm to shorten the computation time required,
3) The application of the method in field orientation control to identify the rotor flux,
4) The physical implementation of the identification method with a digital signal processor.

References

[1] K.P. Allan, "Artificial neural network flux estimation for field oriented control", M.Sc. thesis, Dept. of Electrical Engineering, The University of Calgary, July, 1994.

[2] F. Alonge, F. D'Ippolito, F.M. Raimondi, "Least squares and genetic algorithms for parameter identification of induction motors", *Control Engineering Practice*, vol. 9, pp. 647-657, 2001.

[3] C. Attaianese, A. Damiano, G. Gatto, "Induction motor drive parameters identification", *IEEE Trans. on Power Electronics*, vol. 13, no. 6, pp. 1112-1122, Nov. 1998

[4] A.V. Balakrishnan, State space theory of systems, 2nd Ed., Optimization Software, Inc., New York, 1988.

[5] A. Behal, M. Feemster, D.M. Dawson, A. Mangal, "Partial state feedback control of induction motors with magnetic saturation: elimination of flux measurements", *Automatica,* vol. 38, pp. 191-203, 2002

[6] F. Blaschke, "A new method for the structure decoupling of AC induction machines,", *Second IFAC Symposium on Multi-Variable Technical Control Systems*, Pt. 3, pp. 11-13, Oct. 1971.

[7] J.E. Brown, K.P. Kovacs, P. Vas, "A method of including the effects of main flux path saturation in the generalized equations of A.C. machines", *IEEE Trans. on Power Apparatus and Systems*, vol. 102, no.1, pp. 96-102, Jan. 1983.

[8] C.C. Chan, H. Q. Wang, "An effective method for rotor resistance identification for high-performance induction motor vector control", *IEEE Trans. on Ind. Electron.*, vol. 37, no.6, pp. 477-482, Dec. 1990.

[9] P. Eykhoff, "System Identification – parameter and state estimation", John Wiley & Sons, London, 1974.

[10] J.M. Ferreira de Jesus, "A model for saturation in induction machines", *IEEE Trans. on Energy Conv.*, vol. 3, no. 3, pp. 682-688, Sep. 1988.

[11] A.E. Fitzgerald, C. Kingsley, S.D. Umans, "Electric Machinery", 5th Ed., McGraw-Hill, Inc., New York, 1990.

[12] A.A. Ganji, P.Guillaume, R. Pintelon, P. Lataire, "Identification of the induction motor dynamic and static inductance with regard to saturation", Power Electronics and Variable Speed Drives, pp. 42-47, Sep. 23-25, 1996.

[13] L. Garces, "Parameter adaption for the speed controlled static AC Drive with squirrel cage induction motors", *IEEE-Trans. Ind. Appl.*, vol. 16, no. 2, pp. 173-178, Mar./Apr., 1980.

[14] A. Gastli, "Identification of induction motor equivalent circuit parameters using the single-phase test", *IEEE Trans. on Energy Conv.*, vol. 14, no. 1, pp. 51-56, Mar. 1999.

[15] N.N. Hancock, "Matrix Analysis of Electrical Machinery", Oxford: Pergamon, 1974.

[16] B.R.J. Haverkamp, "State space identification-Theory and practice", Ph.D. dissertation, Faculty of Information Technology and Systems, Delft University of Technology, 2001.

[17] B. L. Ho and R. E. Kalman, "Effective construction of linear, state-variable models from input/output functions", *Regelungstechnik*, vol. 14, pp.545-548, 1966.

[18] K.S. Huang, Q.H. Wu, D.R. Turner, "Effective identification of induction motor parameters based on fewer measurements", *IEEE Trans. on Energy Conv.*, vol. 17, no.1, pp. 55-60, Mar. 2002.

[19] G. Kim, C. Yim, I. Choy, "Study on the parameter identification for induction motors", IEEE CIEP, Cuernavaca, Mexico, pp. 223-230, October 14-17 1996.

[20] R.F.F. Koning, C.T. Chou, M.H.G. Verhaegen, J.B. Klaassens, J.R. Uittenbogaart, "A novel approach on parameter identification for inverter driven induction machines", *IEEE Trans. on Control Systems Technology*, vol. 8, no. 6, pp. 873-882, Nov. 2000.

[21] R. Krishnan, A. S. Bharadwaj, "A review of parameter sensitivity and adaption in indirect vector controlled induction motor drive systems", *IEEE Trans. on Power Electronics*, vol. 6, no.4, pp. 695-703, Oct. 1991.

[22] S. K. Kung, "A new low-order approximation algorithm via singular value decomposition", *Proceedings 12th Asilomar Conference on Circuits, Systems and Computers*, pp. 705-714, 1978.

[23] Cyril W. Lander, "Power electronics", 3rd Ed., McGRAW-Hill Book Company, London, 1993.

[24] W. Leonhard, "Control of Electrical Drives", Springer-Verlag Berlin. Heidelberg, 1985.

[25] E. Levi, "A unified approach to main flux saturation modeling in D-Q axis models of induction machines", *IEEE Trans. on Energy Conv.*, vol. 10, no. 3, pp. 455-461, Sep. 1995.

[26] Lennart Ljung, "System Identification: Theory for the User", 2nd Ed., Upper Saddle River, New Jersey: Prentice-Hall, 1999.

[27] C.J.B. Macnab, G.M.T. D'Eleuterio, "Discrete time Lyapunov design for neuroadaptive control of elastic-joint robots", *Journal of Robotics Research*, vol. 19, no. 5, pp. 511-525, May 2000.

[28] H. Matsumoto, H. Takami, R. Takase, "Vector control scheme for an induction motor controlled by a voltage model-operation with current control loop", *IEEE-Trans. Ind. Appl. Annual Meeting*, vol.1, pp. 368 – 374, Oct. 1-5, 1989.

[29] T. Matsuo, T.A. Lipo, "A rotor parameter identification scheme for vector controlled induction motor drives", *IEEE-Trans. Ind. Appl. Society*, vol. IA-21, no. 4, May/Jun., pp. 624-632, 1985.

[30] S. Moon, A. Keyhani, "Estimation of induction machine parameters from standstill Time-Domain Data", *IEEE Trans. on Ind. Appl.*, vol. 30, no. 6, pp. 1609-1615, Nov./Dec. 1994.

[31] J. J. More, "The Levenberg-Marquardt algorithm: implementation and theory". Numerical Analysis, G. A. Watson (Ed.), Volume 630 of *Lecture Notes in Mathematics*, pp. 106-116, Berlin: Springer Verlag, 1978.

[32] D.W. Novotny, T.A. Lipo, "Section 2: Principles of vector control and field orientation", tutorial document, *IEEE Ind. Appl. Society Annual Meeting,* pp. 2-1 to 2-65, 1985

[33] Katsuhiko Ogata, "Discrete-time Control Systems", 2nd Ed., Prentice-Hall, Inc., Upper Saddle River, NJ, 1995.

[34] J.O. Ojo, A. Consoli, T.A. Lipo, "An improved model of saturated induction machines", *IEEE Trans. on Ind. Appl.*, vol. 26, no. 2, pp. 212-221 Mar./Apr. 1990.

[35] O. Ojo, M. Vipin, I. Bhat, "Steady-state performance evaluation of saturated field oriented induction motors", *IEEE Trans. on Ind. Appl.*, vol. 30, no. 6, pp. 1638-1647, Nov./Dec. 1994

[36] H. Pan, J. Jiang, J. Holtz, "Decoupling control and parameter identification of field-oriented induction motor with saturation", *Proceedings of the IEEE International Conference on Industrial Technology*, pp. 757-761, 1996.

[37] P.W. Sauer, "Constraints on saturation modeling in AC machines", *IEEE Trans. on Energy Conv.*, vol. 7, no. 1, pp. 161-167, Mar. 1992.

[38] C.R. Sullivan, S.R. Sanders, "Models for induction machines with magnetic saturation of the main flux path", *IEEE Trans. on Ind. Appl.*, vol. 31, no. 4, pp. 907-917, Jul./Aug. 1995.

[39] "Simulink dynamic system simulation for MATLAB, writing S-Functions", V4, The MathWorks Inc., Natick, MA, 2000.

[40] P. Vas, M. Alakula, "Field-oriented control of saturated induction machines", *IEEE Trans. on Energy Conv.*, vol. 5, no.1, pp. 218-224, Mar. 1990.

[41] P. Vas, K.E. Hallenius, J.E. Brown, "Cross-Saturation in smooth-air-gap electrical machines", *IEEE Trans. on Energy Conv.*, vol. EC-1, no. 1, pp. 103-109, Mar. 1986.

[42] V. Verdult, "Nonlinear system identification: a state-space approach", Ph.D. dissertation, Faculty of Applied Physics, University of Twente, 2002.

[43] V. Verdult, M. Verhaegen, "Identification of multivariable linear parameter-varying systems based on subspace techniques", *Conference on Decision and Control*, Sydney, pp. 1567-1572, Dec. 2000.

[44] V. Verdult, M. Verhaegen, "Subspace identification of multivariable linear parameter-varying systems", *Automatica*, 38, pp. 805-814, 2002.

[45] M. Verhaegen, P. Dewilde, "Subspace model identification part 1. The output-error state-space model identification class of algorithms", *Int. J. Control*, vol. 56, no. 5, pp. 1187-1210, 1992.

[46] M. Verhaegen, P. Dewilde, "Subspace model identification part 2. Analysis of the elementary output-error state-space model identification algorithm", *Int. J. Control*, vol. 56, no. 5, pp. 1211-1241, 1992.

[47] M. Verhaegen, "Subspace model identification part 3. Analysis of the ordinary output-error state-space model identification algorithm", *Int. J. Control*, vol. 58, no. 3, pp. 555-586, 1993.

[48] J. Zhang, "Field oriented control of induction motor speed", M.Sc. thesis, Dept. of Electrical Engineering, The University of Calgary, Aug., 1985.

Appendix A

A.1 Equivalency Proof of Saturation Models

The purpose of this appendix is to prove the equivalency of the saturation model of induction machines (2-24) from [7] and (2-35) from [25].

Expanding the model (2-35) for v_{ds}, we can obtain:

$$v_{ds} = [(L_l - \frac{L_{lr}^2}{L_{dd}})p + r_s]i_{ds} - \frac{L_{lr}^2}{L_{dq}} i_{qs} + (1 - \frac{L_{lr}}{L_{dd}})p\lambda_{dr} - \frac{L_{lr}}{L_{dq}} p\lambda_{qr} \quad \text{(A-1)}$$

We take the parameter between v_{ds} and i_{ds} in the models as an example to prove the equivalency. According to [25],

$$\frac{d\lambda_{dr}}{dt} = c_{51}\frac{di_{ds}}{dt} + c_{52}\frac{di_{dr}}{dt} + (\Lambda' - \Lambda)[\frac{i_{dm}^2}{i_m^2}\frac{di_{dm}}{dt} + \frac{i_{qm}i_{dm}}{i_m^2}\frac{di_{qm}}{dt}] \quad \text{(A-2)}$$

$$\frac{d\lambda_{qr}}{dt} = c_{51}\frac{di_{qs}}{dt} + c_{52}\frac{di_{qr}}{dt} + (\Lambda' - \Lambda)[\frac{i_{qm}^2}{i_m^2}\frac{di_{qm}}{dt} + \frac{i_{qm}i_{dm}}{i_m^2}\frac{di_{dm}}{dt}] \quad \text{(A-3)}$$

where $c_{51} = L_m$

$c_{52} = L$

$\frac{i_{dm}^2}{i_m^2} = \cos^2\delta$

$\frac{i_{dm}i_{qm}}{i_m^2} = \cos\delta\sin\delta$

For the model with the stator currents i_{ds}, i_{qs} and the rotor currents i_{dr}, i_{qr},

$\Lambda' = L$

$$\Lambda = L_m$$

Substituting (A-2) and (A-3) into (A-1), we can obtain the parameter between v_{ds} and i_{ds} as follows:

$$a_{v_{ds},i_{ds}} = [(L_l - \frac{L_{lr}^2}{L_{dd}})p + r_s] + (1 - \frac{L_{lr}}{L_{dd}})(L - L_m)\cos^2\delta - \frac{L_{lr}}{L_{dq}}(L - L_m)\cos\delta\sin\delta \quad \text{(A-4)}$$

Then substituting (2-41) to (2-43) into the above formula and rearranging, we can get

$$a_{v_{ds},i_{ds}} = r_s + L_{ls} + L\cos^2\delta + L_m\sin^2\delta \quad \text{(A-5)}$$

The parameter between v_{ds} and i_{ds} in (2-24) is the same as the parameter above. The rest parameters in the two models can be proved to be same in a similar way.

The following diagrams are the simulink models for open-loop and closed-loop field orientation control in B.1 and B.2 respecitvely.

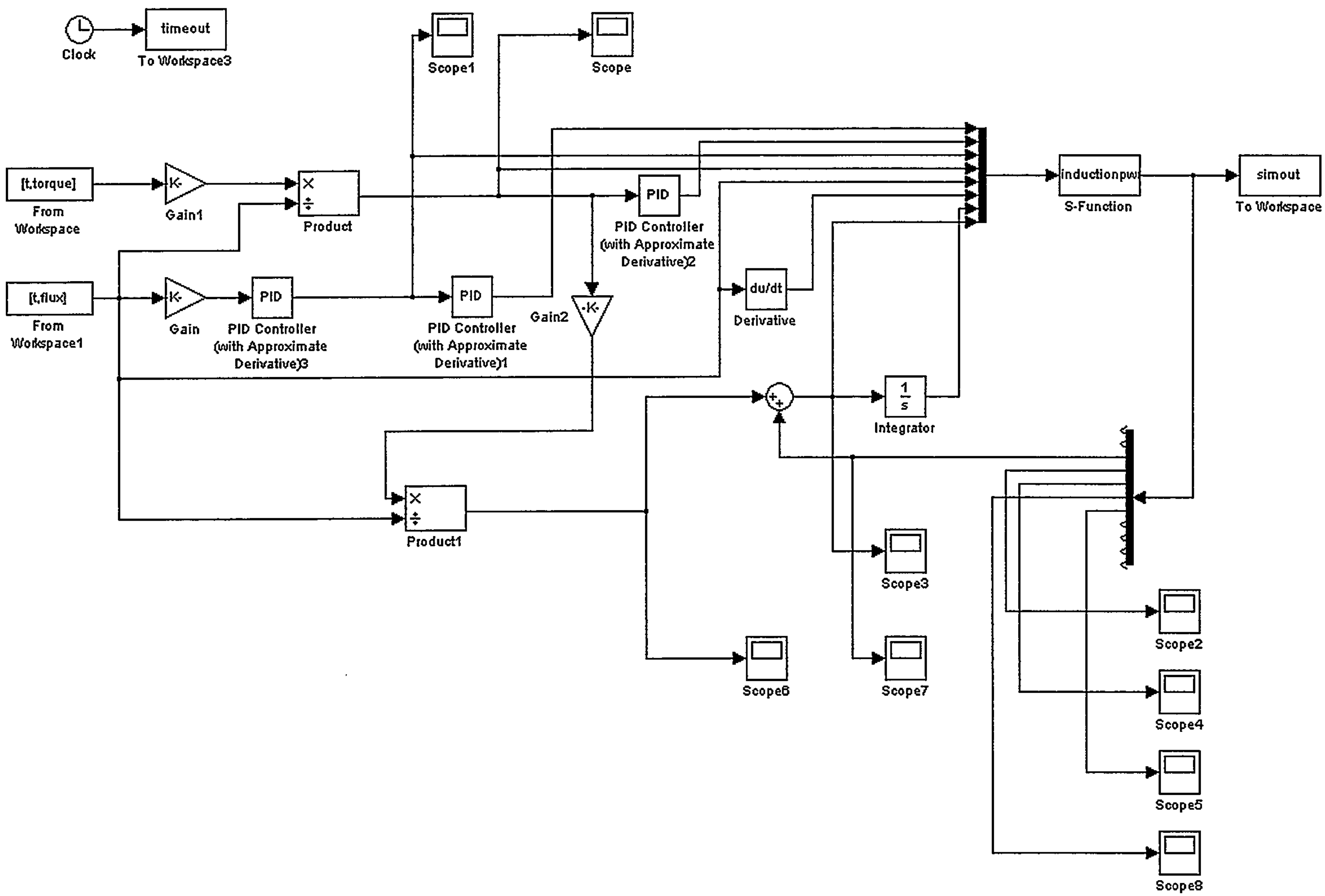

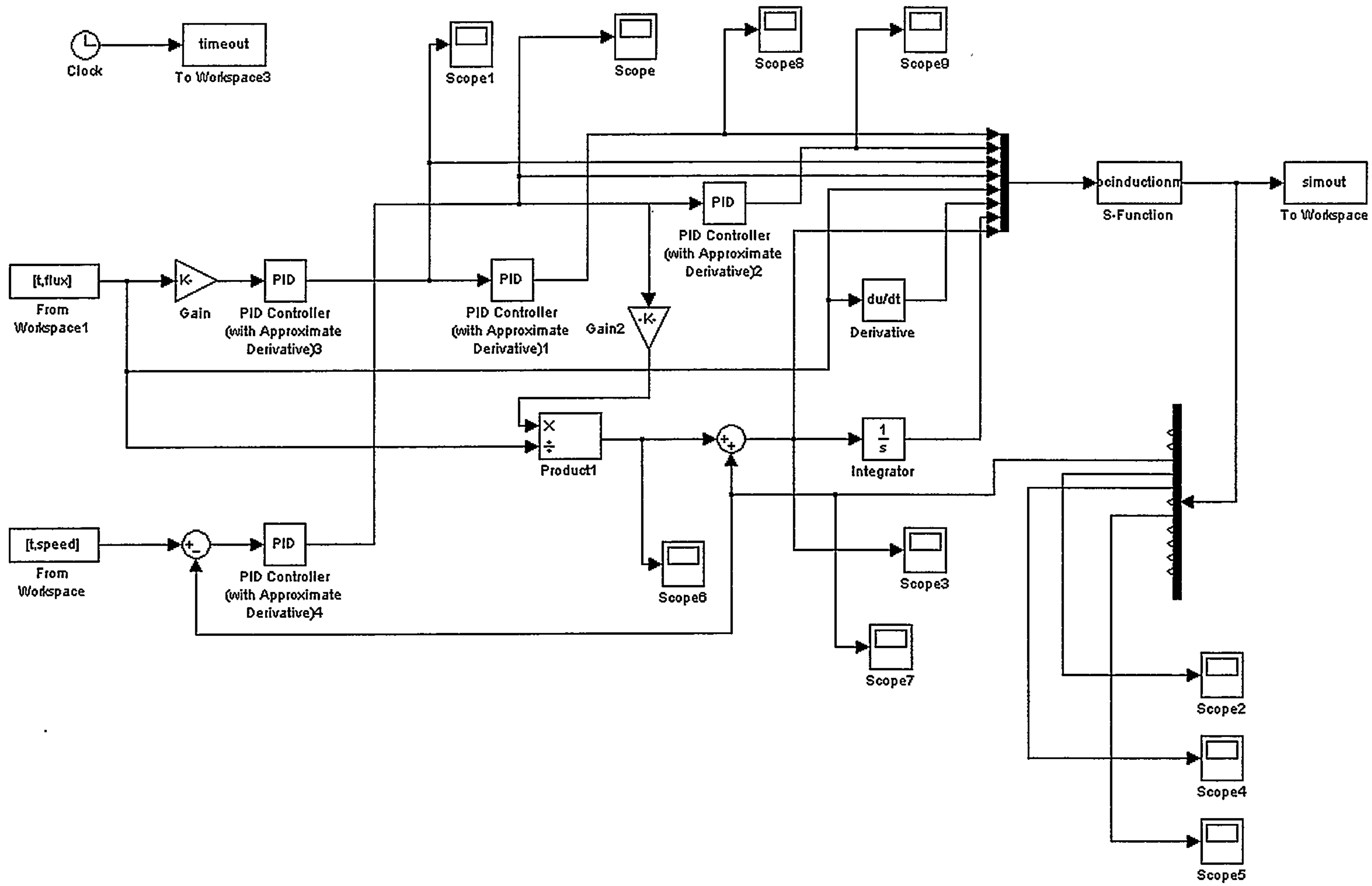
Clock
timeout
To Workspace3
Scope1
Scope
Scope8
Scope9
PID
PID Controller (with Approximate Derivative)2
cinductionm
S-Function
simout
To Workspace
[t,flux]
From Workspace1
K-
Gain
PID
PID Controller (with Approximate Derivative)3
PID
PID Controller (with Approximate Derivative)1
Gain2
-K-
du/dt
Derivative
Product1
1/s
Integrator
[t,speed]
From Workspace
PID
PID Controller (with Approximate Derivative)4
Scope6
Scope3
Scope7
Scope2
Scope4
Scope5